Aus dem

Institut für Kardiovaskuläre Physiologie und Pathophysiologie im Walter-Brendel-Zentrum für Experimentelle Medizin

Ludwig-Maximilians-Universität München

Myeloid-related protein 8/14 (MRP8/14) coordinates neutrophil recruitment through Ca^{2+} supply at LFA-1/F-actin adhesion clusters

Dissertation

zum Erwerb des Doctor of Philosophy (Ph.D.)

an der Medizinischen Fakultät der

Ludwig-Maximilians-Universität München

vorgelegt von

Matteo Napoli

aus

Rho/Italien

Jahr

2024

Mit Genehmigung der Medizinischen Fakultät der

Ludwig-Maximilians-Universität München

Erstes Gutachten: Prof. Dr. Markus Sperandio

Zweites Gutachten: Dr. Ralph Böttcher

Drittes Gutachten: Prof. Dr. Anne Krug

Viertes Gutachten: Prof. Dr. Hendrik Sager

Dekan: Prof. Dr. med. Thomas Gudermann

Tag der mündlichen Prüfung: 03.05.2024

Table of content

Acknowledgements

I would like to express my deepest gratitude to those who have contributed to the completion of this Ph.D. thesis. This journey has been challenging and rewarding, and I am sincerely thankful for the support and encouragement I have received along the way.

Above all, I am immensely grateful to **Prof. Dr. med. Markus Sperandio** for his constant scientific and personal support throughout the entire research process. You were always open for a chat or a discussion and your presence gave me confidence and relief to conduct experiments and complete this work.

At the same time, I would like to thank **Moni**. You were the person getting me onboard in the lab; to me we were immediately a match since the first moment we met outside of the building for my interview. If I joined this lab is mostly because of what you transmitted me on that day, the passion for the job and for the people you care about, the dedication and perseverance but also the fun and light-hearted behavior, together with the laughing and your funny Italian accent. You were my supervisor but to me you always have been much more than that, you were a mom and a friend, and your guidance and mentorship was determinant to steer the project navigating throughout difficult moments. It was quite a journey, and I would not be here telling it without you on my side. GRAZIE!

I extend my profound thanks to the members of my dissertation committee, **Prof. Dr. Joerg Renkawitz** and **Dr. Ralph Boettcher** for their insightful feedback and constructive criticism. Their expertise has played a crucial role in shaping the direction of this research.

I want to acknowledge the collaboration and assistance of my colleagues and fellow researchers at the Biomedical Center, LMU Munich. I believe that the factor that played a critical role in this achievement is the working environment, which has always been a safe place filled with very nice and friendly people on which I could lean on for support and discussions, their input has been fundamental for my personal and scientific growth.

- **Sergi & Lou**. Among all the others, I have to especially thank you 2 guys, and despite being an amazing trio I would like to spend few words for each of you. **Sergi** (Maldi'), you have been the second reason I joined the lab (Moni being the first). When I think of Munich, your face is the first thing that comes to my mind. Indeed, after I joined you became my best friend inside and outside the lab; you helped me settling down in a new city always being available for a chat, a drink or some ranting. We shared amazing moments, happy or sad but especially drunk ones. We had some fights too, but we always were there for each other. Thanks for the help in the lab whenever it was necessary and especially for always being there for me. **Lou** (Mama), you arrived during COVID when socializing was hard and you brought an amazing energy with you, which me as much as everyone else needed. You were always like a mom to both of us but especially to me since I am the clumsiest one. You were always there to share a joy, with beer of course, to cheer me up, to discuss any important or bullshit topic and but most importantly you were always a shoulder to lean on and a safe haven to me. We also shared a lot together, drinking, nights out, parties, friends and I have to thank you for always keeping an eye on me and looking after me in the lab but also outside in my everyday life. I don't have enough space and time to thank both of you enough, together we created this timeless friendships, which will last forever, independently of where we are and how often we will see each other. I love being with both of you, just as I love being with each of you.
- **Roland**. My lab experience started with your passionate talking about the lab and the projects and your knowledge and skills shaped my way up until today. Thanks for the

Abstract

Neutrophils are the first immune cells invading the inflamed or damaged tissue from the systemic circulation to restore tissue homeostasis. They are the most abundant immune cell type in humans and therefore their functions must be tightly controlled in order to avoid poor immune response on one side and persistent inflammation with overwhelming inflammatory burden leading to autoimmune and chronic inflammatory diseases on the other side.

MRP8/14 (S100A8/A9 or Calprotectin) is a small heterodimeric protein with an alarmin-like function that is only expressed by neutrophils, monocytes and during the early stages of macrophage differentiation. Once released, it enhances immune cell recruitment at the inflammatory sites through an autocrine activation loop signaling through TLR4 and activating β_2 integrins in neutrophils. Moreover, it is a reliable biomarker in the clinical field for several acute and chronic inflammatory disorders including rheumatoid arthritis, Morbus Crohn, and COVID-19.

Despite solid knowledge about the function of extracellular MRP8/14, the role of cytosolic MRP8/14 in neutrophils is still elusive.

This work investigated the function of cytosolic MRP8/14 during acute inflammation employing a wide range of experimental settings. First, we could detect abundant levels of intracellular MRP8/14 in stimulated neutrophils, indicating that only a small amount of protein leaves the cell during inflammation. The lack of cytosolic MRP8/14 led to reduced neutrophil adhesion *in vivo* and *in vitro* under flow conditions, without affecting neutrophil rolling behavior. Surprisingly, we found that the observed adhesion defect was independent of the lack of extracellular MRP8/14, since mutMRP8/14 injection did not rescue the adhesion defect in MRP8/14 deficient neutrophils neither *in vivo* nor *in vitro*. In line, defective extravasation of neutrophils, but not other leukocyte subset, was observed in the absence of intracellular MRP8/14. However, no difference in surface adhesion marker expression was detected between WT and *Mrp14*^{-/-} neutrophils. In addition, neutrophil β_2 integrin activation under static conditions by chemokine CXCL1 was completely normal in MRP8/14 deficient neutrophils. However, intracellular MRP8/14 was shown to be indispensable for postarrest modifications such as cell polarization, cell shape change and neutrophil crawling under flow. Furthermore, MRP8/14 deficient neutrophils showed decreased phosphorylation of cytoskeletal adapter proteins, indicative of defective postarrest modifications.

In fact, at higher shear stress, MRP8/14 deficient neutrophils detached easier compared to WT neutrophils, both *in vivo* and *in vitro*. Finally, we investigated Ca^{2+} signaling in neutrophils. We found impaired Ca^{2+} signaling of MRP8/14 deficient neutrophils with lower cytosolic Ca^{2+} levels and faster Ca^{2+} flickers in activated neutrophils. Particularly, this was caused by defective subcellular Ca^{2+} supply at the LFA-1 nanocluster/F-actin focal spots in *Mrp14*$^{-/-}$ neutrophils, which led to lower Ca^{2+} levels at the cluster sites, inducing less LFA-1 cluster formation and F-actin polymerization. These findings imply a critical role of MRP8/14 in Ca^{2+} signaling.

List of figures

List of tables

Abbreviation list

2-APB	2-aminoethoxydiphenyl borate
BAPTA	1,2-bis(o-aminophenoxy)ethane-N,N,N′,N′-tetraacetic acid
Ca^{2+}	Calcium ion
CaBP	Ca^{2+} binding protein
CAD	CARC activation domain
calbidin D9K	S100G
CaM	Calmodulin
CaMKID	Calmoduline kinase ID
CD	Chron's disease
CD11/CD18	β_2 integrins
CD11c	Integrin α-X
CD16	FcγRIIB
CD18	β subunit
CD182	CXCR2
CD32	FcγRIIA
CD35/CR1	Complement receptor 1
CD62E	E-selectin
CD62L	L-selectin
CD62P	P-selectin
Cdc42	Cell division control protein
CF	Cystic fibrosis
Cftr	Cystic fibrosis transmembrane conductance regulator
CMP	Common myeloid progenitor
CR3	Complement receptor 3
CRAC	Calcium release-activated channel
CRACR2A	Calcium release-activated channel regulator 2A
CREB1	CAMP responsive element binding protein 1
CRP	C-reactive protein
DAG	Diacylglycerol
DAMPs	Danger associated molecular patterns
Dpc	Days postcoitum
E-FABP	Epidermal type fatty acid-binding protein
ELISA	Enzyme-linked immunosorbent assay
ER	Endoplasmic reticulum
ESAM	Endothelial cell-selective adhesion molecule
ESL-1	E-selectin ligand-1
ESR	Erythrocyte sedimentation rate
FACS	Fluorescence activated cell sorting

FAK	Focal adhesion kinase
FLIM	Fluorescence lifetime imaging microscopy
FOV	Field of view
FPR	formyl peptide receptor
G-CSF	Granulocyte-colony stimulation factor
GPCRs	G protein coupled receptors
GSDMD	Gasdermin D
HIV	Human immunodeficiency virus
HSCs	Hematopoietic stem cells
i.p.	intraperitoneal
i.s.	intrascrotal
i.v.	Intravenous
IBD	Inflammatory bowel disease
ICAM-1	Intercellular adhesion molecule-1
Id3	Inhibitor of differentiation 3
IL-1b	Interleukin 1b
IL-8	Interleukin-8
IP3/InsP3	Inositol-1,4,5 triphosphate
IP3R	Inositol-1,4,5 triphosphate receptor
IVM	Intravital microscopy
JAMs	Junctional adhesion molecules
K$^+$	Potassium
LAD	Leukocyte adhesion deficiency
LFA-1	Lymphocyte function-associated antigen-1
LPS	Lipopolysaccharide
mAbp1	Mammalian actin-binding protein 1
Mac-1	Macrophage-1 antigen
MAPK	p38 mitogen-activated protein kinase
MDSCs	Myeloid derived suppressor cells
MFI	Mean fluorescence index
MIF	Macrophage migration inhibitory factor
Mn^{2+}	Manganese ion
MPO	Myeloperoxidase
MRP14	Myeloid related protein 14
MRP8	Myeloid related protein 8
MRP8/14	Myeloid related protein 8/14
MST1	Mammalian sterile 20-like kinase 1
NADPH	Nicotinamide adenine dinucleotide phosphate oxidase
NE	Neutrophil elastase

NET	Neutrophil extracellular traps
NF-kB	Nuclear factor kappa B
NLR	Nucleotide-binding domain, leucine-rich–containing family
NLRP3	NLR pyrin domain–containing-3
NLRs	NOD-like receptors
NNEA	Non-essential amino acids
NO	Nitric oxide
NO$_2$	Nitrogen dioxide
NOD	Nucleotide oligomerization domain
NOS	Nitric oxide synthase
O2$^-$	Superoxide anion
OH	Hydroxyl radical
ON	Over night
PECAM-1	Platelet endothelial cell adhesion molecule-1
PFA	paraformaldehyde
PI3K	Phosphoinositide-3-kinase
PIP2	Phosphatidylinositol 4,5 biphosphate
PLCγ	Phospholipase Cγ
PMA	Phorbol-12-Myristate-13-Acetate
PMNs	Polymorphonuclear leukocytes
PRRs	Pattern recognition receptors
PSGL1	P-selectin glycoprotein ligand-1
PVR	Poliovirus receptor
Pyk2	Protein tyrosine kinase 2
RA	Rheumatoid arthritis
Rac1	Ras-related C3 botulinum toxin substrate 1
RAGE	Receptor for advanced glycosylated end products
Rm	Recombinant murine
ROI	Region of interest
ROS	Reactive oxygen species
RT	Room temperature
SDF-1	Earlier stromal cell-derived factor 1
SFK	Src-family kinases
SOCE	Store operated calcium entry
STAT3	Signal transducer and activator of transcription 3
STIM1/2	Stromal interaction molecule ½
Syk	Spleen tyrosine kinase
TEM	Transendothelial migration
TF	Transcription factor

TIR	Toll/interleukin-1 receptor
TIRF	Total internal reflection fluorescence
TLR4	Toll-like receptor 4
TRCPs	Transient receptor potential channels
TRIAL	TNF-α-related apoptosis-inducing ligand
TRIF	TIR domain-containing adapter-inducing interferon-β
TRPV5/TRPV6	Transient receptor potential channel
UC	Ulcerative colitis
VCAM-1	Vascular cell adhesion molecule-1
VSOP/Hv1	Voltage-gated proton channel
WBC	White blood cell count
WT	Wildtype

1. Introduction

1.1 Myeloid Related Protein 8/14

Myeloid related protein 8 (MRP8) and myeloid related protein 14 (MRP14) are two Ca^{2+} binding proteins and part of the S100 protein family [1]. Initially, these proteins were shown to form heterocomplexes (MRP8/14) only in humans [2], representing the physiological and most stable form of the protein [1, 3, 4]. In mice, both MRP8 and MRP14 were found in progenitor myeloid cells in the developing liver at 11.5 days postcoitum (dpc) [5], and only MRP8 but not MRP14 expression could be detected in extraembryonic tissue at 6.5 to 7.5 dpc [6]. MRP8 null mutation is embryonically lethal and causes embryo resorption between day 9.5 and 13.5 dpc in 100% of homozygous null embryos due to abnormal transplacental leukocyte infiltration of maternal origin [6]. Embryo implantation is detected as a form of acute inflammation and MRP8 shows immune-regulatory modulation in fetal-maternal interactions [6, 7]. On the contrary, mice with genetic loss of MRP14 are viable and do not show any obvious phenotypic, developmental or differentiation defect [8]. In addition, although MRP14 null mice have normal MRP8 mRNA expression, no MRP8 protein is detected in the absence of MRP14, suggesting that either inefficient translation of MRP8 mRNA or MRP8 instability in the absence of MRP14 occurs, demonstrating that MRP8/14 heterodimer is the predominant protein form in the murine system [8, 9].

1.1.1 Nomenclature

MRP8 is also known as p8, L1 light chain of the cystic fibrosis (CF) antigen, Calgranulin A or S100A8 while MRP14 is known as p14, L1 heavy chain, Calgranulin B or S100A9. The heterocomplex (MRP8/14, S100A8/A9) is often referred to as calprotectin [1, 10-13]. MRP8 was originally called the CF antigen because of its elevated serum levels in CF affected individuals [14]. However, the discovery of the cystic fibrosis transmembrane conductance regulator (*cftr*) gene by Dorin et al. in 1987 [15] and the absence of MRP8 in adult and fetal CF lung tissue [16] suggested a reconsideration of its name. In 1988, Andersson et al. described that MRP8 and MRP14 were sequentially identical to the leukocyte L1 protein and were also named L1 light chain and L1 heavy chain, respectively [13]. The terms Calgranulin A and Calgranulin B were introduced for MRP8 and MRP14 because of their Ca^{2+} binding ability [1] and the presence of the proteins in granulocytes, but did not reflect their entire distribution and therefore were also abandoned [3, 17].

1.1.1.1 S100 protein family

In 1965, Moore described for the first time the presence of a protein in brain tissue of different species that was soluble in saturated ammonium sulfate solution, naming it the "S-100 protein" [18]. Thereafter, S100A8 and S100A9 were widely used as synonyms for MRP8 and MRP14, due to their Ca^{2+} binding ability, the small molecular masses in addition to the EF-hand motif in the

structure (which will be discussed in the next section), and the ability to form multimers [3, 19-21]. S100A8 and S100A9 inhibit the casein kinase activity and once secreted can regulate cell growth [20], in addition S100A8/A9 acts in a cytokine-like fashion and mediate pro-inflammatory signals [19]. To date, more than 20 members of this well conserved protein family are described with different functions ranging from cell growth, contraction, motility, transcription, differentiation and secretion [19]. S100B, the first S100 protein identified together with S100A1, prevents hypertrophic responses post myocardial infarction through inhibition of a β-PKC phosphorylation and also blocks p53 phosphorylation [22]. S100A1 is mainly expressed in the myocardium and associates with membranes of the sarcoplasmic reticulum and together with S100B regulates cell division and cell morphology through Ca^{2+} dependent regulation of *Ndr* nuclear serine/threonine protein kinase [22, 23]. S100A3, mainly found in the inner root of hair cuticles, is overexpressed in different tumor types [24, 25]. Different studies show an association between S100A4 and metastasis formation through alteration of cell motility and invasiveness [24, 26]. S100A13 triggers the release of FGF-1 and p40 synaptotagmin-1 upon temperature stress [24, 27]. S100A10 is known for being involved in trafficking of the Transient Receptor Potential Channels (TRPV5 and TRPV6) to the plasma membrane enhancing Ca^{2+} currents [23, 28]. S100A16, one of the latest S100 proteins identified, shows a potential role in gene silencing or cell cycle progression [23, 29]. Contrarily to S100A4, S100A2 shows tumor suppressor functions in mammary carcinoma patients [22, 30]. S100A11 presents a function in contact inhibition of cell growth, also suppressing tumor activity [22, 30]. S100A7 is highly expressed in human keratinocytes of psoriatic patients and interacts with the epidermal type fatty acid-binding protein (E-FABP) [31] but does not correlate with familial psoriasis susceptibility [22, 32].

1.1.2 Structure: monomers, homodimers, heterodimers and heterotetramers

MRP8 and MRP14 belong to the low molecular weight Ca^{2+} binding protein (CaBP) family, with a molecular mass of 10.8kDa (but shows electrophoretic mobility of an 8kDa protein) and 93 amino acids, and 14kDa, and 114 amino acids, respectively [3, 10]. They are part of the largest subgroup within the EF-hand protein family, the S100 proteins, together with troponin-C, parvalbumin, calmodulin and myosin light chains [33]. Human MRP8 and MRP14 genes are located in a gene cluster on chromosome 1q21, along with most of the S100 proteins, showing conservative structure [1, 23]. They carry two distinct EF-hand motifs with different Ca^{2+} affinities flanked by hydrophobic α-helices, resulting in a helix-loop-helix structure, involved in Ca^{2+} coordination [3, 24]. The *C*-terminal is referred to as canonical Ca^2 binding loop (site II) and consists of 12 amino acids with the residues Asp58-Glu70 for MRP8 and Asp67-Glu78 for MRP14 as Ca^2 binding sites [3, 24, 34]. The *N*-terminal extended binding loop (site I) consisting of 14 amino acids is specific for S100 proteins and shows lower affinity for Ca^{2+}, with the residues Ser20-Asp33 for MRP8 and Ser23-Glu37 for MRP14 as Ca^2 binding sites [3, 24, 34]. *N* and *C*-terminal sequences are

hydrophobic for both MRP8 and MRP14 with MRP14 *C*-terminus being the longest within the S100 family. Variations in Ca^{2+} binding affinity for the two sequences explains their multiple functions in different cell types and tissues [3, 35]. The central hinge region separates the two EF-hands and confers biological function [19, 34, 36]. Moreover, MRP14 translocates from the cytosolic to the cortical cytoskeleton and membrane area upon being phosphorylated in a Ca^{2+} dependent manner at Thr133 by p38 mitogen-activated protein kinase (MAPK) [37-39].
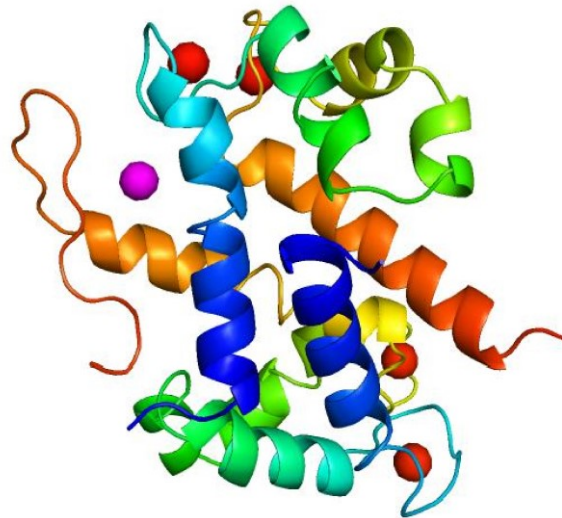
Figure 1.1: S100A8/A9 (MRP8/14) heterodimer with bound metal ions. The crystalized structure of the heterodimer shows S100A8 in blue (Helice I) interacting with S100A9 in orange (Helice IV) to form a hydrophobic cleft. In green Helices II and III of each respective subunit are visible. Bound Ca^{2+} ions are shown as red spheres while Mn^{2+} appears as a purple sphere. Figure from Pruenster, Vogl, Roth and Sperandio, 2016.

1.1.2.1   MRP8 and MRP14 Monomers

The existence of S100 monomers, including MRP8 and MRP14, *in vivo* and *in vitro* has always been questioned, except for S100G (calbindin D9K) [22]. Both MRP8 and MRP14 monomers contain four helices (helix I, II, III, and IV) of two helix-loop-helix motifs and they are oriented in an antiparallel way forming noncovalent homodimers [40]. MRP8 and MRP14 monomers can bind two Ca^{2+} ions and their structural similarity induces their hetero-dimerization rather than homo-dimerization [41].

1.1.2.2   MRP8 and MRP14 Homodimers

MRP8 and MRP14 tend to form noncovalent homodimers aligning in an antiparallel fashion. Their thermal stability dramatically increases upon Ca^{2+} binding [3]. MRP8 homodimer act as a potent chemotactic agent for leukocytes [7, 42, 43] and together with MRP14 homodimer, they show pro-inflammatory and cytokine-inducing activities in different disease models [3, 44].

1.1.2.3   MRP8/14 heterodimer

Both human and murine MRP8 and MRP14 preferentially form MRP8/14 heterodimers compared to homodimers *in vitro* and *in vivo* [1, 2, 45, 46]. Indeed, Hunter and Chazin showed that

homodimers are formed in solutions containing only MRP8 or MRP14 monomers but in protein mixtures the heterodimer is highly preferred (10:1 ratio) [46]. Initially MRP8/14 heterodimer formation was thought to happen in a Ca^{2+} dependent manner [41, 46] but subsequent research showed it was Ca^{2+} independent [36, 47]. The heterodimeric protein, 22kDa in size, exhibits a polar nature due to the positively charged MRP8 and negatively charged MRP14 and can bind up to 4 Ca^{2+} ions [41]. In addition, MRP14 is considered the regulatory unit of the complex since its phosphorylation triggers its translocation to the cytoskeleton, as reported earlier. Moreover, the heterodimer regulates myeloid cell differentiation and function through phosphorylation of topoisomerase I and RNA polymerases I and II via casein kinase I and II modulation [48]. Finally, MRP8/14 heterodimers and homodimers might co-exist, but there is currently no method to discriminate between their effects if they are present simultaneously [3].

1.1.2.4   (MRP8/14)$_2$ tetramer

MRP8/14 heterodimerization is fundamental for (MRP8/14)$_2$ tetramer formation [3]. In addition, while Ca^{2+} is dispensable for heterodimer assembly, it is indispensable for tetramer formation [49, 50] and the heterotetramer can bind up to 8 Ca^{2+} ions. The tetramer formation, other than being Ca^{2+} dependent, also relies on the EF-hand II of MRP14 and is caused by increased burial of solvent accessible surface areas of both heterodimers [1, 3, 51]. Ca^{2+} induces conformational change of the MRP8/14 heterodimer during heterotetramer formation, exposes a hydrophobic cleft of the hinge region necessary for protein interaction [19]. Other than Ca^{2+} MRP8/14 also binds Zn^{2+} and Mn^{2+}, both essential for bacterial growth, therefore exhibiting antimicrobial activity [52]. However, only the heterodimer and the heterotetramer showed antimicrobial activity but not MRP8 or MRP14 homodimers [3]. In addition, tetramerisation of MRP8/14 is crucial for some of the biological functions of (MRP8/14)$_2$ including tubulin polymerization in resting phagocytes [39, 53].

1.1.3 MRP8/14 expression

MRP8 and MRP14 were initially isolated from peripheral blood leukocytes, using a monoclonal antibody against the human macrophage migration inhibitory factor (MIF) [11]. They are crucial for myelomonocytic differentiation, since their increase correlates with development of myeloid lineage and they are abundantly expressed in granulocytes and monocytes but absent in lymphocytes [5, 11, 54]. Human MRP8/14 is highly expressed in inflammatory mononuclear and polymorphnuclear leukocytes (PMNs), representing roughly 45% and 1-5% of the cytosolic protein content, in neutrophils and monocytes, respectively [1, 10]. In addition, murine MRP8/14 shares 59% homology to its human counterparts and it has been described to be functionally equivalent, despite the low degree of sequence identity [5, 8, 55]. While both proteins are highly expressed in inflammatory neutrophils and monocytes, they are completely absent in terminally differentiated and mature tissue-resident macrophages [5, 56]. However, in acute inflammatory tissue infiltrates, MRP14 but not MRP8 could be expressed by certain macrophage subsets [57]. On the contrary, granulocyte expression of MRP8 and MRP14 is not altered during maturation

[56]. Additionally to myeloid cells, MRP8/14 is present in chronically inflamed epithelial cells like intestinal mucosal or squamous epithelium and keratinocytes [58-61].

1.1.4 Extracellular vs intracellular MRP8/14 functions

1.1.4.1   Extracellular functions

Extracellular MRP8 (S100A8) and MRP14 (S100A9) are endogenous danger associated molecular pattern (DAMP) molecules in neutrophils and together with S100A12 (human-only), they are pro-inflammatory factors mediating innate immune responses [36]. Activated or damaged cells release DAMPs such as S100A8/A9 [36]. The way MRP8/14 is released by activated neutrophils and monocytes has been the focus of extensive research since the discovery of the protein. It was already known that the heterodimer is released independently from the classical Golgi-route, since the blockade of vesicular trafficking between the endoplasmic reticulum (ER) and Golgi did not affect MRP8/14 release [62]. However, the exact release mechanism has been an unsolved question until recently as outlined below. Concerning S100A8/A9 receptors, the multiligand receptor for advanced glycation end products (RAGE) was first identified and described as receptor for MRP8/14 in addition to other S100 proteins [19]. Later, Vogl et al. discovered that MRP8/14 is an endogenous activator of Toll-like receptor 4 (TLR4) in monocytes and critical for survival during septic shock [44]. In addition, monocytes were also shown to actively release MRP8/14 upon contact with inflamed endothelium. This was preceded by an increase in intracellular Ca^{2+} levels [63]. Pruenster et al. showed in 2015 that this mechanism is conserved in neutrophils, too, defining E-selectin-PSGL1 interaction in mice to be critical for MRP8/14 release during neutrophil rolling over the inflamed endothelium *in vivo* [12]. In addition, they showed that MRP8/14 binds to TLR4 on the neutrophil surface in an autocrine fashion activating a Rap1-GTPase-dependent pathway of rapid β_2 integrin activation mediating neutrophil adhesion and enhancing neutrophil recruitment under inflammatory circumstances [12]. Only recently, Pruenster et al. discovered that neutrophils rolling along the inflamed endothelium release MRP8/14 through E-selectin mediated gasdermin D (GSDMD) transient pore formation, via a nucleotide-binding domain, leucine-rich–containing family, pyrin domain–containing-3 (NLRP3) inflammasome dependent process [64]. Interestingly, neutrophils did not undergo pyroptosis as usually in the canonical NLRP3 inflammasome activation pathway in monocytes. Instead, they showed that a repair mechanism took place via the ESCRT-III machinery, which was recruited to gasdermin D pores in the plasma membrane to remove them [64]. Once released, MRP8/14 mediates inflammatory responses and recruits immune cells to sites of inflammation signaling through different pattern recognition receptors (PRRs), but mainly TLR4 [12, 36, 44]. Importantly, it has been shown that upon MRP8/14 release where the environment changes from a low intracellular Ca^{2+} milieu (~100nM) to a high extracellular Ca^{2+} concentration (~2mM), the heterocomplexes form tetramers that cannot bind anymore to TLR4. This process restricts its biological functions to the mostly locally confined environment, which reduces

undesirable systemic inflammatory effects [65]. In addition, MRP8/14 release is independent from de novo synthesis and associated with mRNA down-regulation of both genes [36].

An important extracellular function of MRP8/14 is the antimicrobial activity of the heterocomplex [1], as shown by McNamara et al. and described as a "substance released from dying neutrophils, which inhibits candida growth into the surrounding tissues" [66]. Later, Steinbakk et al. confirmed those findings describing MRP8/14 as calprotectin because of the calcium-binding property of such protein with antimicrobial activity against *Candida* spp and bacteria *in vitro* [67]. As mentioned before, only MRP8/14 heterodimer, but not MRP8 or MRP14 alone, contains a Zn^{2+}-binding site leading to inhibition of bacterial growth because of Zn^{2+} removal [3, 68]. Maximal pathogen inhibition requires Mn^{2+} deprivation. This is achieved by MRP8/14 unique Mn^{2+} binding, which sequesters this metal ion [52]. Indeed, MRP8/14 is found in *Staphylococcus aureus* abscesses where it prevents bacterial growth and diminishes its virulence by inhibiting the Mn^{2+} dependent superoxide dismutase [69]. It is also protective against *Helicobacter pylori* [70], *Candida albicans* [71], *Acinetobacter baumannii* [72] and *Klebsiella pneumoniae* [73]. MRP8/14 binding affinity for Zn^{2+} and Mn^{2+} is tightly connected to its antimicrobial properties as removal starves bacteria from those nutrients [1, 69].
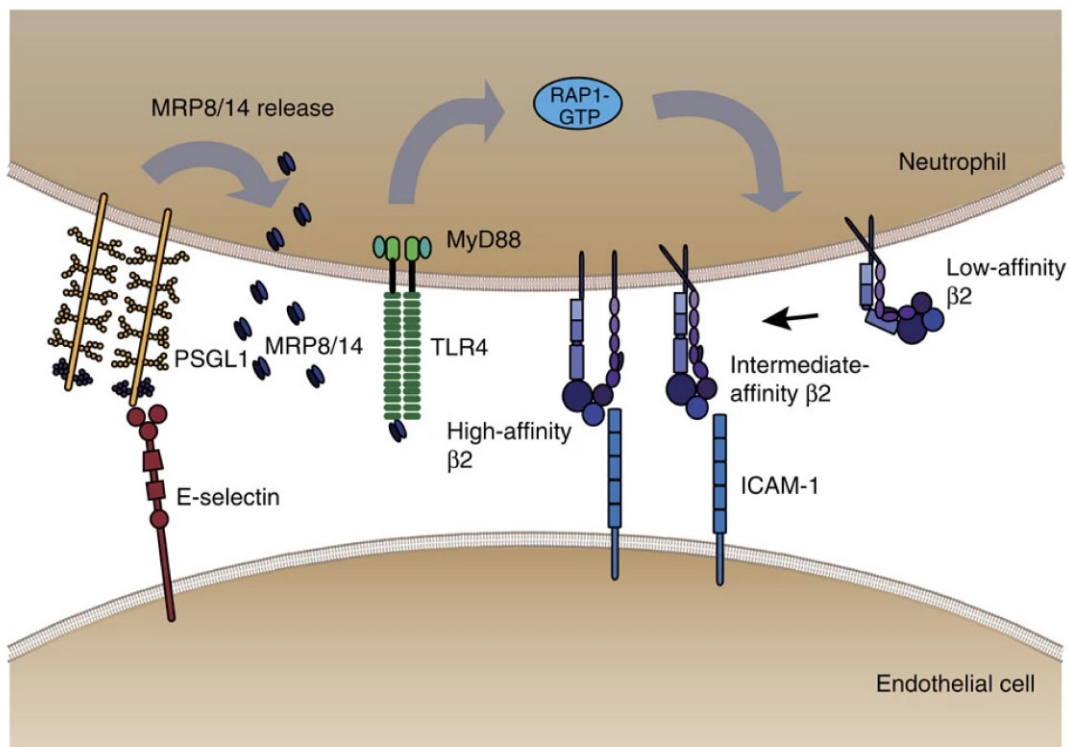
Figure 1.2: Role of extracellular MRP8/14 in leukocyte recruitment. MRP8/14 is released from neutrophils during rolling along the inflamed endothelium, in an E-selectin dependent fashion. After being released, MRP8/14 binds to TLR4 on the neutrophil surface in an autocrine way and triggers β_2 integrin activation via the MyD88 pathway resulting in neutrophil adhesion. Figure from Pruenster, Kurz et al., 2015.

1.1.4.2   Intracellular functions

The property of MRP8/14 to bind Ca^{2+} was one of the first described features of the heterocomplex and intensive research has been conducted on calcium dependent functions of the protein in myeloid cells, without being able to completely decipher its intracellular role, yet [10]. First, Edgeworth et al. thought that MRP8/14 could act either as a calcium buffer tightly regulating intracellular Ca^{2+} levels preventing immune cell hyper-activation and protecting them from prolonged Ca^{2+} overload or locally control Ca^{2+} flux in specific cellular regions triggering directed responses only in such regions associated with cell activation [10]. However, McNeill et al. did not detect any role of MRP8/14 in buffering free intracellular Ca^{2+} in neutrophils, although they observed altered responses of *Mrp14*$^{-/-}$ cells to inflammatory stimuli, but G protein signaling and Ca^{2+} release from intracellular stores were completely unaffected [74]. Although it was speculated that MRP8/14 plays a central role in Ca^{2+} dependent interactions between the actin cytoskeleton and the plasma membrane, concrete functional evidence is still missing [1, 4]. In unstimulated neutrophils, MRP8/14 associates with cortical F-actin and upon fMLP stimulation it localizes at the lamellipodia and associates with plasma membrane and secretory vesicles in a p38 MAPK dependent manner [75]. MRP8/14 was found to bind vimentin in monocytes in an yet unanswered direct or indirect way, showing a Ca^{2+} dependent correlation of the protein to cytoskeletal units [56]. Furthermore, MRP8/14 heterodimer induced microtubule polymerization in resting phagocytes, which was reversed during inflammation where the concomitant p38 MAPK activation and the rise in intracellular Ca^{2+} triggered conformational changes-dependent MRP14 phosphorylation by p38, reversing MRP8/14 stabilizing effects on microtubules and inducing migration through Ras-related C3 botulinum toxin substrate 1 (Rac1) and cell division control protein (Cdc42) activation [39]. Stabilizing effect on microtubules was dependent on (MRP8/14)$_2$ tetramer formation, relying on Ca^{2+} binding through cross-link and bundling of individual tubulin filaments [53]. In addition, MRP8/14 was shown to influence keratin assembly and disassembly in monocytes [76]. Further, MRP8/14 heterocomplexes but not monomers are involved in intracellular signaling events, inhibiting casein kinase I and II activity in vitro [48, 77]. In differentiating keratinocytes or during inflammation, MRP8/14 heterodimers but not monomers act as transporters of polyunsaturated fatty acids, showing high affinity and reversible binding to arachidonic acid or γ-linoleic in a calcium dependent manner [78]. However, it was then demonstrated that the calcium levels necessary to achieve such an interaction were not within the physiological range [1, 8]. On the other hand, MRP8/14 potentiates the redox component of the nicotinamide adenine dinucleotide phosphate oxidase (NADPH) in neutrophils and supports its activation. This is related to binding to the cytosolic phox proteins p67phox, p47phox and Rac2 [1, 79]. In psoriatic epidermis, MRP8/14 could be found at the nuclear level of keratinocytes interacting with and remodeling chromatin, supporting complement C3 transcription through histone and nucleosome interaction and induction of epigenetic changes in gene expression [80]. However, MRP8/14 nuclear localization has not been reported in neutrophils yet, and further research will be needed [47].

1.1.5 Clinical relevance

MRP8/14 has been extensively described as reliable biomarker for inflammatory disease activity, being more sensitive and specific in inflammatory bowel disease than other conventional markers such as erythrocyte sedimentation rate (ESR) or C-reactive protein (CRP) [63]. Over the last 30 years, MRP8/14 has been adopted as a biomarker for a wide range of acute and chronic inflammatory diseases [3]. Because of its local secretion at the site of inflammation, MRP8/14 serum levels reflect neutrophil activity in rheumatoid or juvenile idiopathic arthritis [81, 82], inflammatory bowel disease [83], vasculitis [84], dermatitis [85] and acute lung inflammation [86]. In addition, MRP8/14 serum levels correlate with disease activity in autoimmune diseases such as systemic lupus erythematosus [87] and dermatomyositis [88], or has strong implications in systemic sclerosis [89], renal allograft rejection [90], sepsis [91] or sterile inflammation [92] as well as cardiovascular diseases like acute coronary syndrome and myocardial infarction [3, 93, 94]. Methotrexate has been proposed as good candidate for innate immune system suppression to treat juvenile idiopathic arthritis in patients with high serum levels of MRP8/14 [95]. Moreover, Nordal et al. and Keskitalo et al. determined that MRP8/14 levels had the strongest association with assessment of disease activity, preventing patient exposure to harmful drugs' side effects [96, 97]. In addition, urinary MRP8/14 is a potent diagnostic tool to differentiate between pre-renal kidney injury and acute kidney injury [98]. Contrarily, following renal allograft acute rejection, high MRP8/14 levels from infiltrating cells correlate with favorable chronic allograft nephropathy prognosis, enhancing tissue repair mechanisms and inhibiting fibroblast proliferation [99]. In patients with acute Kawasaki disease, intravenous (i.v.) immunoglobulin treatment is effective in rapidly reducing the inflammation outcome and the incidence of coronary artery lesions leading to suppression of MRP/14 gene expression [100]. Importantly, faecal MRP8/14 levels are useful 1) to monitor response to therapy in inflammatory bowel disease (IBD) patients, 2) to predict colectomy in patients with acute severe ulcerative colitis (UC), 3) to predict relapse in patients with IBD, UC or Chron's disease (CD) and 4) to decide on withdrawal of treatment [101]. Reumatoid arthritis (RA) patients, responders to adalimumab, infliximab or rituximab showed a decrease by 40% to 70% of MRP8/14 levels, which correlates with disease progression [82]. In atherosclerosis-free arteries no MRP8/14 expression could be detected, and MRP14 was discovered to alter phospholipid binding to calcium, promoting blood vessel calcification [102]. Furthermore, at high concentration, MRP8/14 induces tumor cell apoptosis while at low concentration it promotes tumor cell growth and migration via RAGE and p38 MAPK dependent nuclear factor kappa B (NF-κB) activation [103-106]. Moreover, it has been shown that MRP8/14 induces myeloid derived suppressor cells (MDSCs) from which it is secreted in addition to tumor cells, hindering tumor immunity and contributing to cancer progression blocking active T-cell and NK-cell immunotherapy [107, 108]. Further, aberrant MRP8/14 expression leading to non-resolving inflammation triggers colorectal tumorigenesis via inhibitor of differentiation 3 (Id3) activation [109]. Also, MRP8/14 promotes prostate cancer invasion and metastasis through TLR4 and NF-κB mediated β_1 integrin/focal adhesion kinase (FAK) activation [110]. In breast cancer, MRP8/14 in the presence of Ca^{2+} conferred an invasive phenotype to the MCF10A breast cancer

line while MRP14 alone induced growth repression in infiltrating ductal carcinoma of the breast in MCF-7 cells, through binding of oncostatin-activated signal transducer and activator of transcription 3 (STAT3) to the MRP14 promoter in MCF-7 breast cancer cells [102]. Quinoline-3-carboxamides have been demonstrated to downregulate the inflammatory activity of MRP8/14 via binding to MRP14, limiting its interaction with RAGE, TLR4 and arachidonic acid. Further, they have been positively tested in patients with metastatic prostate cancer in a phase II clinical trial, based on their anti-angiogenic properties [102, 111]. However, the specificity of quinolone-3-carboxamides for MRP14 has been discussed controversially [112].

1.2 The role of neutrophils in inflammatory responses

Innate immune cells are involved in early and late stages of immune responses; they comprise a subset of bone-marrow-derived cells of myeloid origin including professional phagocytes like neutrophils, and monocytes, macrophages and dendritic cells [113]. Neutrophils are the most abundant leukocyte subset in human blood, making up 50% to 70% of all circulating leukocytes [114], while in mice they are second only to lymphocytes and make up 20% to 30% of all circulating leukocytes [115]. Due to their abundance, neutrophils are critical for the innate immune system representing the first line of defense against various infectious pathogens like bacteria, fungi and protozoa [114, 116-118]. Neutrophils are terminally differentiated cells that behave as sentinels of our innate immune system with a function in patrolling, surveying and eliminating threats through different effector functions, which need to be tightly regulated in order to avoid unwanted inflammatory processes and autoimmune reactions [119].

1.2.1 Neutrophil production and development

Already in the mid-1960s, neutrophils have been reported to have a short half-life and high turnover rate in peripheral blood [113]. Cartwright, Athens and Wintrobe were the first to describe the half-life of granulocytes to be approximatively 7.2h *in vivo* or 6.8h *in vitro*, in 1964 [120]. Neutrophils originate from the hematopoietic stem cells (HSCs) in the bone marrow, which is a highly proliferative organ, where only 30 stem cells are enough to replenish the entire cellular compartment [121]. About 55% to 60% of all cells produced in the bone marrow are neutrophils, which are generated at a rate of 10^{11} per day per kilogram of body weight under homeostatic conditions, but the production can be increased up to 10^{12} during infections [114, 122]. Development of neutrophils from HSCs to common myeloid progenitor (CMP) cells towards mature neutrophils happens over more than 10 days in which the cell nucleus condensates and takes up the multilobular shape together with the appearance of cell type-specific primary, secondary and tertiary intracellular granules [118, 122]. Recent studies show that the neutrophil lifespan is normally 8-12h in the circulation and up to 24h in the tissue with an increase in inflammatory environments [114]. Interestingly, some have reported that in humans, neutrophil lifespan under homeostatic conditions increases to up to more than 5 days in the circulation while

murine neutrophils have shorter half-lives [123]. An inhibitory feedback loop was described to regulate granulopoiesis upon phagocytosis of apoptotic neutrophils in the tissue by macrophages and dendritic cells. Indeed, phagocytosis of those phagocytes causes downregulation of IL-23 production, with reduced IL-17 production by unconventional T cells which in turn decreases granulocyte colony-stimulating factor (G-CSF) release and leads to diminished neutrophil production in the bone marrow [122, 124]. During inflammatory bursts, the increasing neutrophil demand needs an efficient granulopoiesis and mobilization, which are both achieved through G-CSF [125]. G-CSF is mainly produced by stromal cells in the bone marrow via the neutrophil-mass sensing, a process not completely defined yet. In fact, it was shown that Gr-1 antibody-mediated neutrophil depletion is enough to trigger an increase of G-CSF serum levels without any additional inflammatory cytokine [126]. It has been hypothesized that TLR4 and Toll/interleukin-1 receptor (TIR) domain-containing adapter-inducing interferon-β (TRIF) regulates this signaling pathway, since neutrophil depletion in *TLR4*$^{-/-}$ or *TRIF*$^{-/-}$ mice does not increase G-CSF production [114, 127]. In the bone marrow, CXCL12 is constitutively expressed and provides a key retention signal for neutrophils by signaling through CXCR4 [118, 128]. CXCL12 is antagonized by CXCL8 in human or CXCL1 and CXCL2 in mice signaling through CXCR2 and triggering neutrophil egress from the bone marrow [128]. G-CSF balances and regulates neutrophil mobilization from the bone marrow through downregulation of CXCR4 and upregulation of CXCR2 [117, 118]. Recently, it has been shown that G-CSF induced neutrophil mobilization requires mammalian sterile 20-like kinase 1 (MST1), which in turn activates STAT3 upregulating CXCR2 expression on bone marrow neutrophils [117]. In addition, due to its unique function in neutrophil mobilization, recombinant G-CSF has been used as standard therapy for most neutropenic disorders [122]. Concerning neutrophil clearance, the bone marrow has been described as major site together with the spleen and the liver [129], which altogether account for 30% of neutrophil clearing from the circulation under homeostatic conditions [130, 131]. Upon senescence, neutrophils downregulate CXCR2 expression and upregulate CXCR4 expression in order to home back to the bone marrow mediated by CXCL12 [130]. Finally, the CXCL12/CXCR4 interaction promotes neutrophil apoptosis via the upregulation of the TNF-α-related apoptosis-inducing ligand (TRIAL) [132], promoting neutrophil phagocytosis by resident macrophages [131].

1.2.2 Neutrophil recruitment cascade

Billions of neutrophils enter the circulation every day to patrol and monitor the entire organism. Their presence is key to initiate an inflammatory process, which is essential to re-establish tissue homeostasis after injury. Free-flowing neutrophils in the bloodstream enter inflamed tissue through a multi-step mechanism that requires changes in neutrophil and endothelial cell surface molecule expression in a tightly organized manner. First, *in vitro* studies revealed that cultured vascular endothelial cells treated with inflammatory stimuli like TNF-α, lipopolysaccharide (LPS) or interleukin-1β (IL-1β) triggered adhesion of leukocytes [133]. In 1991, Butcher described leukocyte-endothelial cell recognition as an active process that requires initial transient and reversible adhesion events as first step, followed by leukocyte activation by chemoattractants or

cell contact-mediated signals as second step leading to strong and sustained attachment [134]. Intravital microscopy (IVM) has been adopted as a tool to study postcapillary venules and neutrophil recruitment [135].
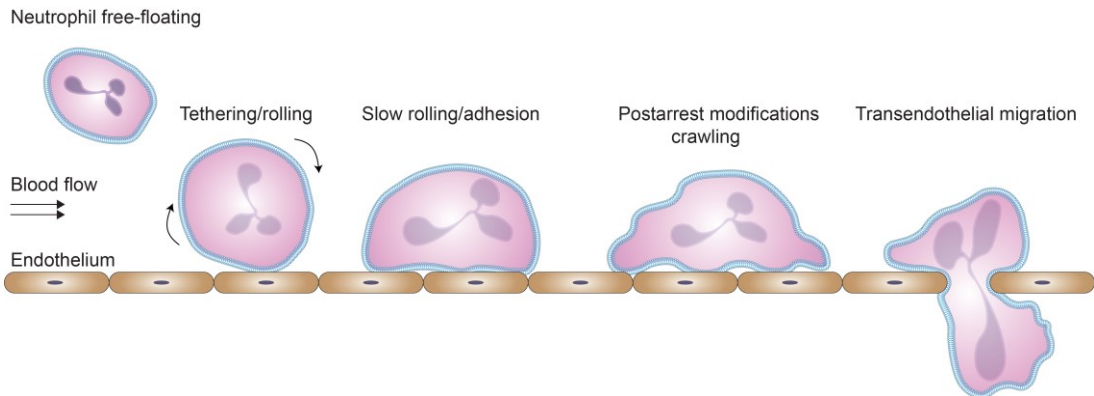
Figure 1.3: Neutrophil recruitment cascade. Free-floating neutrophils in the bloodstream reach the inflammation sites where they interact with the inflamed endothelium. First they roll, then they adhere, polarize, crawl and finally transmigrate into inflamed tissue.

1.2.2.1   Capture and rolling

The first steps of the neutrophil recruitment cascade is the capture, or tethering, of free-flowing neutrophils and the subsequent rolling, which are mediated by three C-type lectins, named selectins, expressed on inflamed endothelial cells or on the leukocyte surface. Selectins bind to their cognate ligands expressed on neutrophils or endothelial cells [136-138]. Selectins are type-I cell-surface glycoproteins and include L-selectin (CD62L), P-selectin (CD62P) and E-selectin (CD62E). They bind specific fucosylated and sialylated carbohydrates determinants [137, 139, 140]. L-selectin is the only selectin constitutively expressed on leukocytes and critical for lymphocyte rolling on lymph node high endothelial venules. L-selectin can be shed upon cell stimulation in order to regulate neutrophil recruitment [138, 141] and it has been shown to drive leukocyte interstitial migration [142]. In addition to the classical tethering, L-selectin also mediates secondary tethering, which is the binding of free-flowing leukocytes to already adherent ones on the inflamed vessel wall [143]. P-selectin can be found in endothelial cells and platelets where mild inflammation triggers its fast relocation to the cell surface from Weibel-Palade bodies and α-granules, respectively [138, 140]. It has been shown that mild trauma, induced by surgical exteriorization of the murine cremaster muscle, triggers P-selectin mediated leukocyte rolling in postcapillary venules [144]. Contrarily to P-selectin, E-selectin is not pre-stored in endothelial cells but newly synthetized upon stimulation with proinflammatory cytokines like TNF-α or IL-1β and its expression is controlled by NF-κB and by translational mechanisms [140, 145, 146]. O note, in skin and bone marrow microvessels E-selectin is constitutively expressed [138]. While the average leukocyte rolling velocity on P-selectin is 15-20μm/s, E-selectin mediates a slower rolling behavior with rolling velocities around 3-7μm/s [138, 147, 148]. P-selectin glycoprotein ligand-1 (PSGL-1) has been described as the main selectin ligand that can bind to all three selectins in an inflammatory milieu *in vivo* [138, 145] and *in vitro* [140], and localizes at the tips of microvilli [149]. PSGL-1 is the predominant, if not only relevant P-selectin ligand during inflammation [150]. PSGL-

1 binding to L-selectin mediates leukocyte-leukocyte interaction also known as secondary tethering, as mentioned above [151]. Furthermore, PSGL1 is an important capture ligand for E-selectin but dispensable for E-selectin mediated leukocyte slow rolling [152, 153], which is mediated by other E-selectin ligands such as E-selectin ligand-1 (ESL-1) and CD44 [138, 154]. Selectin selectin-ligand interactions show catch bond behavior under physiological shear stress conditions [155, 156] and requires coordinated formation (on-rates) and breakage (off-rates) of adhesive bonds to allow leukocyte rolling [155, 157].

1.2.2.2   Slow rolling and adhesion

Tethering and rolling mediated by low affinity adhesive contacts of selectins and their ligands slow down neutrophil rolling velocity and expose neutrophils to pro-inflammatory stimuli like chemokines or DAMPS, expressed on the inflamed endothelium or released by macrophages and other leukocytes [138, 158]. Chemokine binding to appropriate G-protein-coupled receptors (GPCRs) activate integrins on the neutrophil surface by triggering a complex intracellular signaling network [136]. Integrins are ubiquitously expressed cell surface receptors made of transmembrane heterodimers with an α-subunit and a noncovalently bound β-subunit. As different α and β subunits exist various integrin heterodimers are formed that can bind multiple cell matrix and cell surface proteins [138, 157, 159]. The β_2 integrins (CD11/CD18) are leukocyte adhesion receptors with a common β subunit (CD18) that in neutrophils form heterodimers including lymphocyte function-associated antigen-1 (LFA-1; $\alpha_L\beta_2$; CD11a/CD18) and macrophage antigen-1 (Mac-1; αMβ2; CD11b/CD18) [160]. Integrins are able to shift between different conformational states, which influence their affinity towards their ligands. They can transmit bidirectional signals inside or outside the cell across the cell membrane [138, 161]. On resting neutrophils, β_2 integrins adopt the bent conformation with low ligand binding affinity (low affinity αI domain); but upon E-selectin engagement, integrin activation occurs (inside-out signaling) with β_2 integrins adopting an extended conformation with intermediate binding affinity (low/intermediate affinity αI domain) [160]. The intermediate affinity LFA-1 further slows down neutrophil rolling velocity (slow rolling) by transiently interacting with intercellular adhesion molecule-1 (ICAM-1) on endothelial cells [162]. ICAM-1 is a transmembrane immunoglobulin protein, which is constitutively expressed on endothelial cells and upregulated during inflammation. ICAM-1 is the main β_2 integrin ligand during neutrophil recruitment [136, 163]. However, it has been shown that during neutrophil recruitment β_2 integrins can also bind to ICAM-2 or RAGE [164, 165].

During neutrophil slow rolling, chemokine-mediated GPCR signaling induces LFA-1 extended conformation with high binding affinity, quickly triggering neutrophil arrest on ICAM-1 or vascular cell adhesion molecule-1 (VCAM-1) [136, 138, 160]. Interestingly, Fan and colleagues discovered an additional conformation for β_2 integrins, showing that not extended but high affinity β_2 integrins face each other to form oriented nanocluster that bind ICAM-1 in cis, preventing interactions and having anti-inflammatory potential [166]. In addition to the classical GPCR-mediated β_2 integrin activation, Pruenster described a parallel pathway that leads to β_2 integrin activation in mice via E-selectin-PSGL1 interaction leading to NLRP3 inflammasome dependent MRP8/14 release,

which in turn binds to TLR4 triggering downstream signaling [12, 64]. MRP8/14 release has also been reported in humans, with MRP8/14 release triggered by L-selectin-E-selectin interactions [167]. Moreover, talin-1 and kindling-3 are two actin-binding proteins that act as β_2 integrin adaptor molecules [161].

1.2.2.3 Postarrest modifications, crawling and transendothelial migration

While β_2 integrin inside-out signaling regulates ligand-binding affinity triggering neutrophil slow rolling and firm arrest [160], β_2 integrin clustering and allosteric conformational changes contribute to the initiation of outside-in signaling, orchestrating the fine-tuning of cytoskeletal rearrangements required to withstand adhesion under shear stress conditions and inducing neutrophil spreading and intraluminal crawling [136, 160]. β_2 integrin outside-in signaling triggers tyrosine phosphorylation of the Src-family kinases (SFK) like Hck, Fgr, and Lyn and of the spleen tyrosine kinase (Syk) on adherent neutrophils. This in turn activate phospholipase C γ (PLCγ) and Vav-family molecules [168]. In addition, the mammalian actin-binding protein 1 (mAbp1) has also been demonstrated to be phosphorylated downstream of Src and Syk, acting as a scaffold protein and translocating from the cytoplasm to the plasma membrane to locally activate Cdc42 and colocalize with cortical actin [169]. β_2 integrin outside-in signaling triggers changes in integrin conformation and cell surface distribution [170] and defective outside-in signaling has been shown to accelerate neutrophil detachment under shear stress conditions dampening extravasation [171]. A recent study by Klapproth and colleagues showed that podosomes can form independent of paxillin family members and that kindlin-3, although dispensable for the initial step of the talin-1, vinculin and paxillin-enriched adhesion patches assembly, is necessary to recruit leupaxin to the adhesion complexes and trigger paxillin phosphorylation to further regulate podosome turnover and lifetime in myeloid cells [172]. Further, the focal adhesion kinase (FAK) and the protein tyrosine kinase 2 (Pyk2), along with many others, have been shown to interact with paxillin and talin-1 upon phosphorylation regulating adhesion turnover, Rho-family GTPase activation and cell migration [173, 174]. After adhesion strengthening, neutrophils perform postarrest modifications in order to change their shape and flatten over the endothelial layer, which is a prerequisite for successful intraluminal crawling along the endothelial wall to find a proper spot for extravasation [136]. While neutrophil adhesion is mainly mediated by LFA-1, intraluminal crawling mostly relies on Mac-1 binding to ICAM-1 and ICAM-2 expressed by the inflamed endothelial surface [164]. When neutrophil find exit cues, they start breaching the endothelial layer performing transendothelial cell migration (TEM), which mainly occurs via the paracellular route (~70%–90%) and to a lower extent through the body of the endothelium (transcellular TEM) [136, 175]. During leukocyte adhesion events, clustering of endothelial ICAM-1 and concomitant recruitment of vascular cell adhesion molecule-1 (VCAM-1, CD106) provides a stable platform for leukocyte firm arrest and TEM [176]. In addition, it was shown that this adhesion platform apart from ICAM-1 and VCAM-1 contains also activated moesin and ezrin, clustered in those endothelial actin-rich docking structures [177]. At this point, firmly adherent leukocyte trigger the

paracellular opening through various signaling mechanisms consequently leading to diapedesis that involves a series of different endothelial cell adhesion molecules, such as platelet endothelial cell adhesion molecule 1 (PECAM1), junctional adhesion molecules (JAMs), endothelial cell-selective adhesion molecules (ESAM), CD99 and poliovirus receptor (PVR) [178]. Crossing the endothelial layer is a rapid process for leukocytes (2-5min). However, passing the underlying basement membrane takes longer (5-15min) [136]. The basement membrane is composed of a network of laminins and collagen type IV interconnected through many other different glycoproteins [179]. The migration mechanism of leukocytes through this complex structure is still under debate. However, in 2020 Rohwedder and colleagues showed that SFK was indispensable to trigger Rab27a-dependent surface mobilization of neutrophil elastase (NE), integrin VLA-3 and VLA-6-containing vesicles, which in turn results in effective basement membrane penetration [171]. In addition, leukocytes preferentially migrate at low-expression sites for collagen IV and gaps in the discontinuous pericyte sheath [136, 180]. Finally, neutrophil migration in inflamed tissue is mostly integrin independent mainly relying on protrusive F-actin flow and cell squeezing that transiently deforms the pericellular environment without causing collateral damage [181].

1.2.3 Neutrophil effector functions

The ultimate reason for neutrophils to extravasate into tissue is to resolve infections or tissue damages adopting a repertoire of mechanisms that they have at their disposal [182]. One of those mechanisms is phagocytosis of invading microorganisms and foreign agents, which is carried out by two different classes of receptors: FcγReceptors [FcγRIIA (CD32) and FcγRIIB (CD16)] and complement receptors [CR1 (CD35) and CR3 (Mac-1)] [183]. IgG-coated targets are ingested after phosphorylation of cytoplasmic immunoreceptor tyrosine-based activation motifs (ITAMS) triggered by SFK activation [183]. Indeed, SFK deficient mice show delayed phagocytic activity [184]. Phosphorylated SFK triggers the activation of phosphoinositide-3-kinase (PI3K) and RhoA, which is dispensable for FcR-mediated phagocytosis [185] but essential for the formation of the phagocytic cup via F-actin recruitment [186]. Then, Cdc42 regulates membrane extension over the foreign insult edges and Rac1, in concert with PI3K, finalizes the phagocytic process by membrane integration and closure [187]. Contrarily to FcγR-mediated phagocytosis, CR3-mediated phagocytosis does not occur through membrane pseudopods but via sinking of C3bi-opsonized targets into the cell [183]. In addition, CR3-mediated phagocytosis does not involve either Rac1 nor Cdc42 [185] and is independent from the rise in cytosolic free Ca^{2+} [188]. Another difference is that in FcγR-mediated phagocytosis the activation of respiratory burst and cytokine production are critical events while they are dispensable in CR3-dependent uptake. [189]. Further, neutrophils from CD18-deficient [leukocyte adhesion deficiency-I (LAD-I)] patients displayed defective antibody-dependent phagocytosis due to the loss of CR3 (Mac-1) [190].

Another neutrophil self-defense mechanism that contributes to tissue homeostasis but must be tightly controlled is degranulation. Degranulation is the secretion of proinflammatory substances and mediators, which are derived from intracellular granules [191]. Neutrophil granules contain

microbicidial molecules, which are released upon cell activation, and are classified in four types [183]. Primary or azurophilic granules contain the most toxic mediators including myeloperoxidase, serine proteases and defensins and are mobilized upon phagocytosis [192]. Secondary granules contain lactoferrin, collagenase and lipocalin whereas tertiary granules contain matrix metalloprotease 9 [193, 194]. In addition, secretory vesicles represent the last type of granules, with a proposed endocytic origin since they contain plasma proteins like albumin [183]. Sengelov et al. showed that rise in intracellular free Ca^{2+} triggers degranulation or exocytosis depending on the grade of stimulation, of secretory vesicles first, tertiary and secondary granules thereafter and finally azurophilic granules [195]. Upon receptor stimulation and intracellular Ca^{2+} increase, granules translocate to the plasma membrane to release their content through actin cytoskeleton remodeling and microtubule assembly [196], followed by vesicles tethering and docking, granule priming and then formation of a transitory vesicle pore structure [191].

Once stimulated, neutrophils assemble two types of responses, the already described release of antimicrobial proteins stored in their granules (non-oxygen-dependent pathway), and the oxidative burst, which relies on NADPH-oxidase activation and radical oxygen species (ROS) production [183]. In addition, with the myeloperoxidase (MPO) pathway, neutrophil create different kind of reactive oxidants [197]. Upon cell activation, MPO release occurs amplifying H_2O_2 through generated reactive intermediates [198]. MPO has been shown to be fundamental for endotoxemia protection, since its blockade or genetic deletion increased mortality in LPS challenged mice [199]. In addition, the amount of free radicals in neutrophils can be increased by the production of nitric oxide (NO) from the nitric oxide synthase (NOS) enzyme [200], which then can react with oxygen to produce even stronger oxidants like nitrogen dioxide (NO_2) [183]. Although in urinary tract infections neutrophils displayed a marked increase in NOS activity, the enzyme has been shown to contribute to host defense only against certain pathogens like *Mycobacterium tuberculosis* and *Leishmania major*, as shown in $NOS^{-/-}$ mice [201]. Furthermore, it was demonstrated that NO and NOS play a crucial role in neutrophil apoptosis via activating the mitochondrial death pathway and boosting ROS production [202].

Another mechanism that neutrophils adopt to clear pathogens from the extracellular environment is NETosis, a type of regulated cell death in which net-like structures of decondensed chromatin and proteases form neutrophil extracellular traps (NET) that are released by granulocytes [203]. NETs are crucial for pathogen clearance. They interact with endothelial and epithelial cells inducing cytotoxic effects, mainly through histones and peptides [204]. While phagocytosis and degranulation are rather fast events that happen in the minutes range, NETosis has been described to take a few hours in human neutrophils and up to nearly a day in murine neutrophils [205]. Indeed, murine NETs take longer to form and have a more compact appearance compared to human NETs [206].

1.3   Calcium signaling regulation in neutrophils

Neutrophils are short living cells, which often need to adapt to changing environments through signaling events that come from messengers whose concentrations vary with time, like Ca^{2+} [207], an evolutionary conserved signaling molecule that plays a key role in many different biological processes [208]. Free cytosolic Ca^{2+} concentration rises rapidly and transiently upon neutrophil activation leading to many downstream cellular events like phagocytosis and ROS production, exocytosis, secretion and degranulation, integrin avidity and clustering, cytoskeletal rearrangements and migration [209, 210]. Since Ca^{2+} is able to precipitate phosphate and an overload of Ca^{2+} can be detrimental and dangerous for cell homeostasis, neutrophils, among other cells, have evolved ways to control it through compartmentalization or chelation which helps to buffer or lower cytosolic Ca^{2+} levels [207].

1.3.1 Ca^{2+} store release and store operated Ca^{2+} entry (SOCE) in neutrophils

Cytosolic Ca^{2+} influx in neutrophils, or in immune cells in general, is a two-step process that begins with Ca^{2+} release from intracellular stores upon stimulation and continues with Ca^{2+} influx from the extracellular space across Ca^{2+} channels on the plasma membrane [211]. Ligand-receptor interaction including GPCRs or FcγRs, $β_2$ integrin activation [212, 213] or E-selectin–PSGL1/L-selectin binding triggers downstream activation of PLC [210]. PLC activation in turn converts phosphatidylinositol 4,5 biphosphate (PIP_2) into diacylglycerol (DAG) and inositol-1,4,5 triphosphate (IP_3 or InsP3), the latter binds to the IP_3 receptor (IP_3R) localized on the ER membrane triggering depletion of intracellular Ca^{2+} stores [210, 214]. ER store depletion is sensed by stromal interaction molecule 1 and 2 (STIM1 and STIM2), two transmembrane proteins which undergo conformational changes upon store depletion enabling them to translocate to the ER-plasma membrane contacts where they form large clusters, called puncta, into which ORAI1 is recruited and bound [211]. STIM1-dependent ORAI1 channel recruitment causes localized high Ca^{2+} influx with a marked increase in cytosolic $[Ca^{2+}]$, a process named store-operated Ca^{2+} entry (SOCE) [215]. STIM1 was shown to be the main player as its deficiency strongly reduces SOCE in immune cells, while STIM2 seems to be important only for prolonged Ca^{2+} influx [216]. Among many other proteins, calcium release-activated channel regulator 2A (CRACR2A) was also proposed to associate with ORAI1 and to bind to STIM1, stabilizing and sustaining SOCE in activated cells [217]. Both human and murine neutrophils express ORAI2 and ORAI3, which represent the dominant isoforms in resting bone marrow neutrophils, while ORAI1 is the main ORAI channel in activated neutrophils [218]. In addition, it was demonstrated that transient receptor potential channels (TRPCs) contribute to SOCE in murine neutrophils, particularly TRPC1 and TRPC6 [218, 219]. Ca^{2+} influx in immune cells critically relies on potassium (K^+) efflux, preserving the electrochemical gradient to maintain and enhance Ca^{2+} entry [211]. Although this role was attributed to the calcium-activated potassium channel $K_{Ca}3.1$ [220], recent work by Immler and colleagues showed that in neutrophils voltage-gated potassium channel $K_v1.3$ is

responsible for depolarization –mediated K^+ efflux, upon rise in intracellular Ca^{2+}, which in turn regulates membrane potential [116]. Furthermore, ATP-gated purinergic nonselective cation channels, P2X1R and P2X7R are expressed in human and mouse neutrophils. It was shown that P2X7R activation via binding of extracellular ATP, mediates K^+ efflux [221]. Neutrophil SOCE is not a standardized mechanism but rather a complex and diversified one, in which different ligand-receptor interactions initiate different range, amplitude and duration of calcium fluxes in activating neutrophils requiring tight and specific regulation [208].
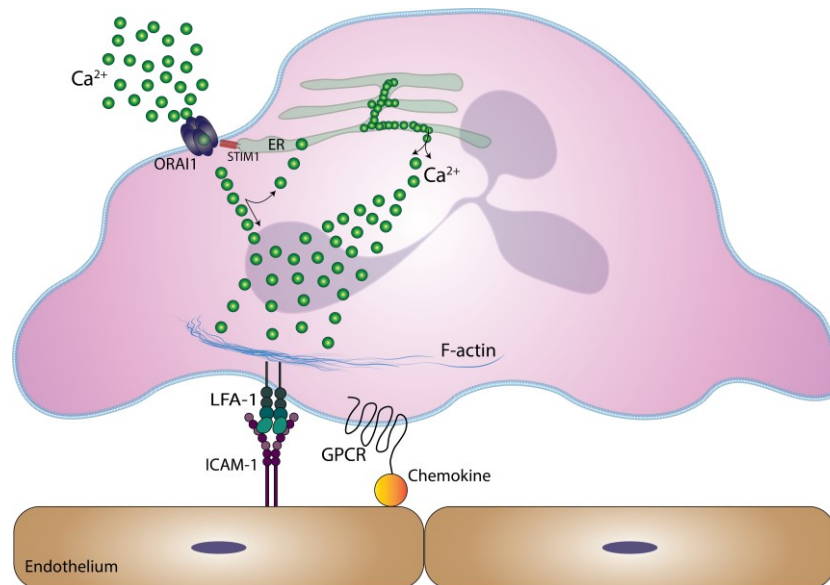
Figure 1.4: Ca^{2+} store release and SOCE in neutrophils. During neutrophil activation by stimuli f.e. expressed on the inflamed endothelium, a concert of different signaling pathways trigger Ca^{2+} release and Ca^{2+} entry in neutrophils. Upon GPCRs activation, the G_α subunit dissociates from the $G_{\beta\gamma}$ subunits causing PLC_β activation. In the meantime, β_2 integrins are activated and activate PLC_γ via Syk. Then, both PLCs convert PIP_2 into DAG and IP_3, which activates IP_3R inducing Ca^{2+} store release out of the ER. Finally, Ca^{2+} store depletion induces STIM1 translocation to the ORAI1 channels where it triggers extracellular Ca^{2+} entry (SOCE).

1.3.2 Ca^{2+} signaling during neutrophil recruitment

Previous work has been demonstrated that both tethering and rolling of neutrophils along the inflamed endothelium and their exposure to physiological shear stress are important co-factors to activate intracellular calcium signaling in those cells [222]. Indeed, stimulation of rolling human neutrophils with interleukine-8 (IL-8) triggers a 10-fold higher Ca^{2+} influx as compared to IL-8 stimulation in the absence of shear stress or adhesive contacts [212]. In addition, it was shown that in the absence of chemokine–mediated signaling, neutrophil rolling on E-selectin was sufficient to trigger a small but significant increase in intracellular Ca^{2+} [212], although this needs to be confirmed.

Among the CRAC family ORAI1 is the principal channel that coordinates neutrophil transition from rolling to arrest in concert with IP_3 gated channels [223] and TRP channels, mediating Ca^{2+} entry in neutrophils [224]. During the transition from rolling to slow rolling and adhesion, tensile forces build up on LFA-1/ICAM-1 bonds in neutrophils [225], which trigger cell arrest together with β_2

integrin outside-in signaling sustaining cell spreading and polarization, crawling and migration and finally extravasation [210, 226]. Tensile forces applied on LFA-1/ICAM-1 bonds through shear stress also affect Ca^{2+} influx [212]. This goes along with ORAI1 colocalizing with high-affinity LFA-1 at the focal adhesion plane triggering Ca^{2+}release from cytosolic Ca^{2+} stores and sustaining localized Ca^{2+} influx. This mediates LFA-1 cluster assembly and F-actin polymerization at the leading edge of polarized PMNs [227]. In fact, treatment of human neutrophils with 2-aminoethoxydiphenyl borate (2-APB), a selective inhibitor of ORAI1 –mediated SOCE but not Ca^{2+} store-release [228], dampened IL-8 mediated β_2 integrin activation and neutrophil arrest [212]. Further, chelation of intracellular Ca^{2+} with 1,2-bis(o-aminophenoxy)ethane-N,N,N′,N′-tetraacetic acid (BAPTA), SOCE blockade through 2-APB or knockdown of ORAI1 in PMNs reduced LFA-1 clustering resulting in defective adhesion strengthening at shear stress higher than 4dyne cm^{-2} [229]. Interestingly, β_2 integrin activation and kindlin-3 dependent LFA-1 clustering [229] is tightly regulated by the rate of SOCE at the focal adhesion spots rather than a global increase in cytoplasmic Ca^{2+}, since treatment with 2-APB impairs integrin activation and neutrophil arrest without completely blocking intracellular Ca^{2+} [212]. ORAI1 initiates Ca^{2+} entry when ~100 LFA-1 molecules transit to high-affinity bonds, forming submicron focal microclusters, further inducing the formation of micron sized LFA-1 macroclusters [229]. Therefore, a positive feedback loop between LFA-1 cluster formation and ORAI1 mediated Ca^{2+} entry generates a large local transient burst of intracellular Ca^{2+} necessary to sustain neutrophil postarrest modifications that finally lead to extravasation into the inflamed tissue [230].

1.4   Aim of the thesis

Neutrophil recruitment is a multi-step process enabling free-flowing neutrophils to interact with the inflamed endothelium, prime them through proinflammatory mediators in order to let them stop at adhesion sites, polarize and then crawl along the luminal vessel wall to find appropriate spots to extravasate into inflamed tissue.

Both inadequate and exacerbated immune responses are detrimental for tissue homeostasis. Therefore, the number of neutrophils that transmigrate into inflamed tissue and the way they do it must be tightly controlled.

Ca^{2+} is a fundamental player in regulating neutrophil functions. The ability to control and buffer intracellular Ca^{2+} levels allows neutrophils to differentially modulate the recruitment process.

MRP8/14 is an alarmin and DAMP molecule with high Ca^{2+} binding affinity and passively or actively secreted by activated neutrophils. MRP8/14 triggers cell arrest through high-affinity β_2 integrin activation enhancing immune cell recruitment to inflammation sites. Despite a well-established role of extracellular MRP8/14 in the context of inflammation, the role of cytosolic MRP8/14 is still rather unexplored.

Accordingly, this work aims to elucidate a hypothetical role of cytosolic MRP8/14 as Ca^{2+} modulator of neutrophil postarrest recruitment steps during the inflammatory response.

2.   Materials

2.1   Animals

C57BL/6 wildtype (WT) mice were purchased from Charles River Laboratories (Sulzfeld, Germany) and Janvier Labs (Saint Berthevin, France). *Mrp14*^{-/-} (functional double MRP8 and MRP14 ko aimals) were kindly provided by Johannes Roth (Institute for Immunology, Muenster, Germany). *B6;129S6-Polr2atm1(CAG-GCaMP5g-tdTomato)* crossbred with *Lyz2*[Cre] (*GCaMP5xWT*) were kindly provided by Konstantin Stark (LMU, Munich, Germany) and crossbred in-house with *Mrp14*^{-/-} mice (*GCaMP5xMrp14*^{-/-}). All mice were housed at the Biomedical Center, LMU Munich, Planegg-Martinsried, Germany. Male and/or female mice (8–25 weeks old) were used for experiments. Animal experiments were approved by the Regierung von Oberbayern (AZ.: ROB-55.2-2532.Vet_02-17-102 and ROB-55.2-2532.Vet_02-18-22) and carried out in accordance with the guidelines from Directive 2010/63/EU.

2.1.1   Genotyping

Table 2.1: Genotyping

Genotype	Primer	5'-3'
Mrp14	WT primer	CCATATCCCAGTGTTGGTGAC
Mrp14	WT-KO primer	GTCTTTAACCAGGGACTAGG
Mrp14	KO primer	CGCCTTCTATCGCCTTCTTGA
Lyz2[Cre]	oIMR3066 mutant	CCCAGAAATGCCAGATTACG
Lyz2[Cre]	oIMR3066 common	CTTGGGCTGCCAGAATTTCTC
Lyz2[Cre]	oIMR3066 wildtype	TTACAGTCGGCCAGGCTGAC
B6;129S6-Polr2atm1(GCaMP5)	19854 common forward	TAGACACATGCCACCAAACC
B6;129S6-Polr2atm1(GCaMP5)	19855 WT reverse	TCTCTCCAGCACCATAACTCC
B6;129S6-Polr2atm1(GCaMP5)	19856 Mutant reverse	GATCGATAAAACACATGCGTCA

All primers were provided by Metabion (Planegg, Germany)

2.1.1.1   Genotyping protocol

Mrp14	35x
Initial Denaturation	3min 95°C
Denaturation	15 sec 95°C
Annealing	15 sec 58,5°C

Extension	15 sec 72°C
Final Extension	7 min 72°C
Lyz2^{Cre}	**38x**
Initial Denaturation	3min 95°C
Denaturation	15 sec 95°C
Annealing	15 sec 62°C
Extension	15 sec 72°C
Final Extension	7 min 72°C
B6;129S6-Polr2atm1(GCaMP5)	
Initial Denaturation	3min 95°C
	10x (-0.5°C/cycle)
Denaturation	15 sec 95 °C
Annealing	15 sec 65 °C
Extension	10 sec 72°C
	28 x
Denaturation	15 sec 95 °C
Annealing	15 sec 60 °C
Extension	10 sec 72°C
Final Extension	7 min 72 °C

Table 2.2: Genotyping protocol

2.2 Cell lines

Mouse myelomonocytic leukemia cell line WEHI-3B was generously provided by the Walzog group (BMC, LMU, Planegg-Martinsried, Germany). WEHI-3B supernatant containing IL-3 was used at 20% in RPMI 1640 medium to prime bone marrow-derived neutrophils.

2.3 Substances

2.3.1 Recombinant proteins

Table 2.3: Recombinant proteins

Name	Supplier
Mutant murine MRP8/14 (S100A8/A9, aa exchange N70A and E79A)	Thomas Vogl, University of Muenster (DE)
rm TNF-α	R&D Systems
rm E-selectin/Fc	R&D Systems
rm ICAM-1/Fc	R&D Systems
rm CXCL1	Peprotech

2.3.2 Other substances, chemicals and reagents

Table 2.4: Other substances, chemicals and reagents

Name	Supplier
2-Mercaptoethanol	Sigma-Aldrich
2-Propanol	Sigma-Aldrich
Accutase® Cell Detachment Solution	Corning
Acrylamide	Applichem
Agarose	Nippon Genetics Europe
Ammonium Chloride (NH4Cl)	Merck
Ammonium Peroxodisulfate (APS)	Applichem
Aqua	Braun
Bepanthen®	Bayer
Bromophenol Blue	Sigma-Aldrich
BSA	Capricorn Scientific
Casein	Sigma-Aldrich
Catheter tubes	Smith medical
Chamaleon® Duo Pre-stained Protein Ladder	LI-COR
Count Bright TM Absolute Counting Beads	Invitrogen
DAPI	Invitrogen
DNA Ladder 100pb	perQLab
Dymethil Sulfoxyde (DMSO)	Sigma-Aldrich

eBioscience Fixable Viability Dye eFluor™780	Invitrogen/Thermo Fisher Scientific
EDTA	Merck
Ethylenediaminetetraacetic Acid (EDTA)	Merck
Eukitt	Sigma-Aldrich
FCS	Invitrogen
Fluoresbrite® YG Microspheres 0.20µm	Biotrend
Giemsa	Merck
Glass capillaries (0.04x0.4)	CM Scientific
Glutagro	Corning®
Glycerol	Roth
Glycin	Bernd Kraft
Hanks Solution	Apotheke Klinikum der Uni Muenchen
Heparin	Sigma-Aldrich
Hepes	Sigma-Aldrich
Indo-1 AM	Invitrogen™
Ketaset (Ketamine)	Zoetis
Lysing solution	BD
MEM NEAA (100X)	Thermo Fisher Scientific
Methanol	AppliChem
NaCl 0.9%	Fresenius Kabi
Novalgin® (Metamizol)	Sanofi
Object slides (removable)	Ibidi
Odyssey® Blocking Buffer (TBS)	LI-COR
Oregon Green™ 488 BAPTA-1, AM	Invitrogen™
Paraformaldehdye	Applichem
Penicillin	Invitrogen
Percoll®	Sigma-Aldrich
Phosphate-Buffered Solution (PBS)	Apotheke Klinikum der Uni Muenchen
Poly-L-lysine solution	Sigma-Aldrich
ProLong Antifade	Thermo Fisher Scientific
Protease/Phosphatase Inhibitor Cocktail 100X	Cell Signalling
PVDF membranes	Immobilon

Rompun 2% (Xylazine)	Bayer
RPMI-1640	Sigma-Aldrich
Sodium Bicarbonate (NaHCO3)	Merck
Sodium Deodecyl Sulfate (SDS)	Roth
Sodium Hydroxide (NaOH)	Merck
Strptomycine	Invitrogen
TEMED	AppliChem
Tris-HCL	Merck
Triton X-100	Applichem
Trypsin-EDTA	Sigma-Aldrich
Türks solution	Merck
Tween® 20	Merck
UltraComp BeadsTM	Invitrogen
VECTASHIELD® PLUS Antifade Mounting Medium	Vector Laboratories

2.4 Buffers and solutions

Table 2.5: Buffers and solutions

Flow cytometry		
PBS-BSA 1%	BSA	1g
	PBS	up to 100mL
		pH 7.4
HBSS	BSA	250mg
	HEPES	250mg
	Hanks solution	up to 100mL
Erytrocyte Lysis Buffer	NH_4CL	8.02g
	$NaHCO_3$	0.84g
	EDTA	0.37g
	H_2O	up to 100mL
Western blotting		
Running buffer 10x		
Tris	250mM	30.3g
Glycine	1.9M	144g
SDS	1%	10g

H$_2$O		up to 1L
Running buffer 1x		
Running buffer 10x	10%	100mL
H$_2$O		up to 1L
Blotting buffer 10x		
Tris	250mM	30.3g
Glycine	1.9M	144g
H$_2$O		up to 1L
Blotting buffer 1x		
Blotting buffer 10x	10%	100mL]
Methanol	2.5%	25mL
H$_2$O		up to 1L
Tris 0.5M pH6.8		
Tris	0.5M	60.57g
H$_2$O		up to1L
		pH 6.8
Tris 1.5M pH8.8		
Tris	1.5M	181.71g
H$_2$O		up to 1L
		pH 8.8
TBS 10x		
Tris	200mM	24.4g
NaCl	1.1M	80g
H$_2$O		up to1L
		pH 7.4
TBST		
TBS 10x	10%	100mL
Tween		500µL
Modified RIPA		
Tris HCl	50mM	8.3mL
NaCl 5M	150mM	7.5mL
Triton X-100	0.1%	250µL
SDS 10%	0.5%	12.5mL
EDTA 0.5M	2mM	1mL
H$_2$O		up to 250mL
Laemmli buffer		
Tris HCl		15mL
SDS		5g

		25mL
Glycerol		25mL
β-mercaptoethanol		10mL
Bromophenol blue		125mg
Lysis buffer		
Modified RIPA		8mL
Laemmli buffer 5x		2mL
Protease/Phosphatase inhibitor cocktail		40µL
Others		
Anaesthesia		
Ketamine	125mg kg^{-1}	100µL
Rompun 2% (Xylazine)	25mg kg^{-1}	100µL
NaCl		800µL
Neutrophil isolation recommended medium		
FCS		2mL
EDTA 0.5M		200µL
PBS		up to 100mL

2.5 Antibodies

2.5.1 Antibodies for flow cytometry

Table 2.6: Antibodies for flow cytometry

Antibody	Conjugate	Host	Isotype	Clone	Company
CD18	FITC	Rat	IgG2a k	C71/16	Pharmigen
CD11a (LFA-1)	APC	Rat	IgG2a	M17/4	eBioscience
CD11b (Mac-1)	BV510	Rat	IgG2b k	M1/70	BioLegend
CD62L (L-Selectin)	FITC	Rat	IgG2a k	MEL-14	BioLegend
CD162 (PSGL1)	PE	Rat	IgG1	2PH1	Pharmigen
CD182 (CXCR2)	APC	Rat	IgG2a	242216	R&D Systems
CD44	BV570	Rat	IgG2b k	IM7	BioLegend
IgG Fc	Biotin	Goat	IgG	Polyclonal	eBioscience
Streptavidin	PerCP-Cy5.5				BioLegend
Ly6G	APC	Rat	IgG2a k	1A8	BioLegend
Ly6G	PB	Rat	IgG2a k	1A8	BioLegend

2.5.2 Isotype antibodies for flow cytometry

Table 2.7: Isotype antibodies for flow cytometry

Antibody	Conjugate	Host	Isotype	Clone	Company
IgG2a	FITC	Rat	IgG2a	RTK2759	BioLegend
IgG2a	APC	Rat	IgG2a	RTK2758	BioLegend
IgG2b	BV510	Rat	IgG2b	RTK4530	BioLegend
IgG1	PE	Rat	IgG1	eBRG1	eBioscience
IgG2b	BV570	Rat	IgG2b	RTK4530	BioLegend
IgG2a k	PB	Rat	IgG2a k	RTK2758	BioLegend
IgG2a k	APC	Rat	IgG2a k	RTK2758	BioLegend

2.5.3 Antibodies for western blot

Table 2.8: Antibodies for western blot

Primary antibodies			
Antibody	**Host**	**Clone**	**Company**
β-Actin	Rabbit	13E5	Cell Signaling
Calmodulin	Rabbit	Polyclonal	Cell Signaling
CREB-1	Rabbit	48H2	Cell Signaling
GAPDH	Mouse	6C5	Merck Millipore
p38 MAPK	Rabbit	Polyclonal	Cell Signaling
Paxillin	Rabbit	Polyclonal	Cell Signaling
Pyk2	Rabbit	Polyclonal	Cell Signaling
Phospho CREB-1 (Ser133)	Rabbit	87G3	Cell Signaling
Phospho p38 MAPK (Thr180/Tyr182)	Rabbit	Polyclonal	Cell Signaling
Phospho paxillin (Tyr118)	Rabbit	Polyclonal	Cell Signaling
Phospho pyk2 (Tyr402)	Rabbit	Polyclonal	Cell Signaling
Secondary antibodies			
Antibody	**Host**		**Company**
α-mouse IRDye 680CW	Goat		LI-COR
α-rabbit IRDye 800CW	Goat		LI-COR

2.5.4 Antibodies for IVM and confocal microscopy

Table 2.9: Antibodies for IVM and confocal microscopy

Antibody	Conjugate	Host	Isotype	Clone	Company
S100A9	Cy5.5	Rabbit		322	Provided by Thomas Vogl
CD62E (E-selectin)		Rat	IgG1	9A9	InVivo
CD11a (LFA-1)	In-house AF647 Kit	Rat	IgG2a,κ	2D7	BD Pharmigen

2.6 Kits

Table 2.10: Kits

Kit	Company
EasySepTM Mouse Neutrophil Enrichment Kit	STEMCELL Technologies
pHrodo™ Green *E. coli* BioParticles™ Phagocytosis Kit for Flow Cytometry	Invitrogen
Alexa Fluor™ 647 Antibody Labeling Kit	Invitrogen
Cytoskeleton Kit (SiR-Actin And SiR-Tubulin)	Cytoskeleton

2.7 Equipment and consumables

Table 2.11: Equipment and consumables

Equipment	Company
5427R Centrifuge	Eppendorf
572 Precision Balance	Analytik Jena
CKX41 Inverted Microscope	Olympus
CytoFLEX S Flow Cytometer	Beckman Coulter
Digital Camera C4742-80	Hamamatsu
FlowSafe® Flow Hood	Brenner
Galaxy® 170 S CO2 Incubator	New Brunswick
Gallios Flow Cytometer	Beckman Coulter
HERAfreezeTM HFU T Series Ultra-Low Temperature Freezer	Thermo Fisher Scientific
High precision syringe pump	Harvard Apparatus

LSRFortessaTM Flow Cytometer	BD
Mastercycler® Thermocycler	Eppendorf
MegafugeTM 8 Centrifuge	Thermo Fisher Scientific
Mini-PROTEAN® Tetra Handcast System	BIO-RAD
MP220 pH Meter	Mettler Toledo
MultifugeTM X3R Centrifuge	Thermo Fisher Scientific
NanoDropTM 2000	Thermo Fisher Scientific
Neubauer Chamber	
Odyssey® CLx Imaging System	LI-COR
PowerPacTM Power Supply	BIO-RAD
ProCyte Dx Hematology Analyser	IDEXX
Rotina 420R Centrifuge	Hettich Zentrifugen
SBC 32 Analytical Balance	Scaltec
Spark® Microplate Reader	TECAN
TCS SP8 X White Light Laser Confocal Microscope	Leica
TCS SP8 SMD White Light Laser Confocal Microscope for FCS, FLIM and FLCS	Leica
SP8 FALCON confocal and MP microscope	Leica
DM2500 optical microscope	Leica
Wet/Tank Blotting Systems	BIO-RAD
Consumables	**Company**
Cell Culture Dishes (60, 100mm)	Corning, Falcon
Centrifuge Tubes (15, 50ml)	Corning, Falcon
CryotubeTM Vials	Thermo Fisher Scientific
DiscarditTM II Syringes (2, 5, 10, 20ml)	BD
EASYstrainerTM Cell strainer 40µm	Greiner
Eppendorf Tubes® (1.5, 2, 5ml)	Eppendorf
Flasks (75cm2)	Corning, Falcon
Immobiolion®-E PVDF Membrane	Merck Millipore
Inject®-F Fine-dose Syringes	B. Braun
Microcapillary Pipettes (15µl)	Drummond Scientific

MicrolanceTM Needles (several sizes)	BD
Microtainer® Blood Collection Tubes	BD
Omnican® Insulin Syringes	B. Braun
Parafilm	Bemis
Polythene Tubing 0.40mm	SIMS PORTEX
Round Bottom Tubes (5ml)	Corning, Falcon
Serological Pipettes (25ml)	Greiner Bio-One
Sterican® Needles (several sizes)	B. Braun
Stripette® Serological Pipettes (5, 10ml)	Costar
TipOne® Pippete Tips (10, 200, 1000µl)	STARLAB
Vasco® Nitril Soft Blue	B. Braun

2.8   Software

Table 2.12: Software

Software	Company
Adobe Illustrator	Adobe
Excel	Microsoft
Fiji	ImageJ
FlowJo Analysis Software	BD
GraphPad Prism 9	GraphPad software
ImageStudio ™ Lite	LI-COR
Kaluza	Beckman Coulter
Leica Application Suites	Leica

3. Methods

3.1 Biological sample harvesting

3.1.1 Bone marrow harvesting

Animal termination was carried out by cervical disarticulation. Bones from legs, hips and arms were sampled using scissors and tweezers. Bone ends were cut-open after cleaning the residual muscular and fat tissue and the bone marrow was flushed out with ice cold PBS using a 23G needle. Afterwards, the cell mixture was filtered through a 40µm cell strainer and collected in 50mL falcon tubes for further processing.

3.1.2 Peripheral blood collection

Anesthesia was performed with a combination of 125mg kg^{-1} ketamine and 12.5mg kg^{-1} xylazine via intraperitoneal injection. After testing the mouse carpal and metacarpal reflexes, retro-orbital blood collection was executed using 10µL glass capillaries and blood collected into EDTA-coated tubes for further processing.

3.2 Neutrophil isolation

The EasySep™ Mouse Neutrophil Enrichment Kit was used, following the manufacturer instructions, to obtain murine neutrophils from the bone marrow/blood cell suspension by negative selection. All cells apart from neutrophils were labelled with biotinylated antibodies and streptavidin-coated magnetic particles were added to the biotinylated cells. Ultimatey, with the use of a magnet, the undesired cells were separated from the pure neutrophil population.

3.3 Cell culture and neutrophil priming

Mouse myelomonocytic leukemia cell line WEHI-3B was cultured in RPMI 1640 growth medium, supplemented with 10% FCS, 1% penicillin/streptomycin, 1% non-essential aminoacids (NNEA) and 1% glutamine at 37°C and 5% CO_2 changing the medium regularly and splitting the cells 1:4 to 1:10 when the confluence was reached. These cells were used to produce IL-3 enriched supernatant, which was sterile filtered and added to the cell culture medium in which neutrophils were incubated over night to prime them for further experiments.

3.4 MRP8/14 ELISA

MRP8/14 *in vitro* release was conducted as described earlier [231]. First, WT mice were sacrificed, bone marrow harvested and neutrophils isolated through negative selection as described above. Then, 24 well-plates were coated with recombinant murine (rm) E-selectin (rmCD62E-Fc chimera, 10µg mL^{-1}, R&D Systems) or PBS/0.1% BSA at 4°C overnight, blocked with PBS/5% casein and washed twice with PBS. Isolated neutrophils (5x10^5) were resuspended in complete HBSS buffer, seeded on the coated slides and incubated for 10min at 37°C and 5%CO$_2$. To determine the total S100A8/A9 intracellular levels, cells were lysed with 2% Triton X-100. Ultimately, frozen cell supernatants and lysates were shipped to Muenster where Thomas Vogl analyzed them by Enzyme-Linked Immonosorbent Assay (ELISA) for the quantification of the intracellular S100A8/A9 concentrations.

3.5 Intravital microscopy of the murine cremaster muscle

Intravital microscopy (IVM) of the murine cremaster muscle was conducted as previously described [116]. Shortly, male mice were anaesthetized by a combined intraperitoneal (i.p.) injection of 125mg kg^{-1} ketamine and 12.5mg kg^{-1} xylazine and after checking carpal and metacarpal reflexes the mouse skin was cut open at the trachea level, and the trachea was first cannulated to ensure a better ventilation to the mouse during the experiment and video recording. Afterwards, the right carotid artery was first separated from the right vagus nerve and then cannulated with a plastic catheter (outer and inner tube diameter: OD=0.61mm, ID=0.28mm) for later blood sampling as well as antibody injection. The cremaster muscle was dissected, mounted and constantly superfused with a bicarbonate buffer [232] at a physiological temperature of 37°C during the whole experiment. IVM was carried out on an OlympusBX51 WI or a ZEISS Axio Examiner microscope, both equipped with a 40x objective (Olympus, 0.8NA, water immersion objective) and a CCD camera (KAPPACF8HS). Postcapillary venules were distinguished from arteries thanks to their wavy borders and thinner endothelial cell layer, and they were recorded using VirtualDub or ZEISS pro. Blood velocity was determined either directly through a dual photodiode (Circusoft Instrumentation) or via fluorescent microspheres (BioTrend) and later analyzed with MTrackJ (Fiji). Movies were later analyzed off-line on Fiji [233]. Different models were employed to study leukocyte recruitment *in vivo*.
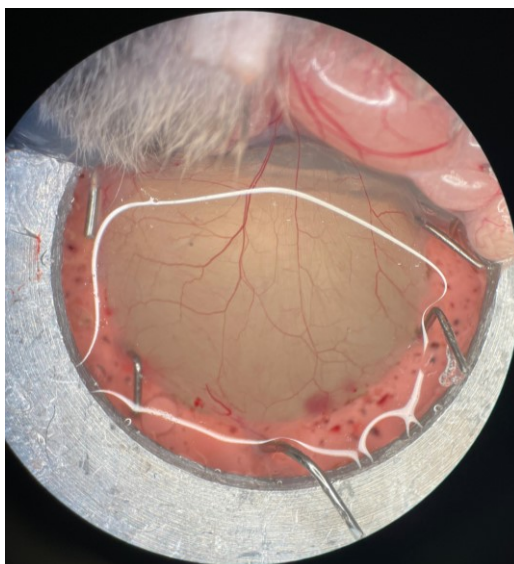
Figure 3.1: Murine cremaster muscle preparation. Picture showing the exteriorized murine cremaster muscle fixed on the stage and ready to be imaged by IVM while being continuously perfused with a bicarbonate buffer solution. The muscle is cut open and flatten out, eventual bleeding of big vessels is stopped by cauterization and the testicles are moved to the side without pinning them down to prevent the blood flow to drop.

3.5.1 TNF-α induced inflammation

TNF-α treatment leads to acute inflammation and triggers transcriptional activity on the endothelial cell layer and the expression of pro-inflammatory adhesion markers like E-selectin and ICAM-1 [234]. TNF-α (500ng) was administered via intrascrotal injection (i.s.) to WT and *Mrp14−/−* mice, 2h later the cremaster was exteriorized, and IVM performed. To confirm E-selectin dependent leukocyte rolling upon TNF-α injection in WT mice, E-selectin-blocking antibody was applied through the carotid catheter during the experiment (anti-E-selectin: clone 9A9, 30μg).

3.5.2 MRP8/14 rescue in TNF-α induced inflammation

Mrp14−/− mice not only lack cytosolic S100A8/A9 but also the ability to release it and therefore they miss the activation effect that extracellular S100A8/A9 has on neutrophil β_2 integrins via TLR-4 [12]. To take this into account, after TNF-α treatment and cremaster dissection of WT and *Mrp14−/−* mice, one postcapillary vessel was selected and recorded continuously while mutS100A8/A9 (S100A8/A9N70AE79A, 50μg mouse $^{-1}$ in 100μL, provided by Thomas Vogl, University of Muenster, Germany) was injected via the carotid catheter. The time of injection was noted to compare parameters before and after injection in both WT and *Mrp14−/−* mice.

3.5.3 MRP8/14 rescue in trauma induced inflammation

TNF-α induced inflammation results in E-selectin upregulation on the inflamed endothelium which triggers S100A8/A9 release via NLRP3-mediated and GSDMD-dependent rapid pore formation at the plasma membrane, a process rapidly reversed by the ESCRT III machinery [64]. To avoid this, we adopted the trauma induced inflammation model of the cremaster muscle where the surgical procedure alone is enough to trigger P-selectin release from the Weibel-Palade bodies

[235] and subsequent P-selectin dependent leukocyte rolling, without causing S100A8/A9 release [12]. Then, after cremaster dissection of WT and *Mrp14⁻/⁻* mice, one postcapillary vessel was selected and recorded continuously while mutS100A8/A9 was injected via the carotid catheter. The time of injection was noted to compare parameters before and after injection in both WT and *Mrp14⁻/⁻* mice.

3.5.4 Giemsa staining of TNF-α stimulated cremaster muscles

Directly after TNF-α IVM experiments, murine cremaster muscles were separated and transferred in 4% paraformaldehyde (PFA) to fix them. After Giemsa application, tissues were differentiated in acetic acid, washed at increasing ethanol concentrations and finally mounted (Eukitt) to examine extravasation of different leukocyte subsets. For the analysis, conducted at the core facility Bioimaging of the Biomedical Center (BMC), it was adopted a Leica DM2500 microscope, equipped with a 100x objective (Leica, 1.4NA, oil immersion) and a Leica DMC2900 CMOS camera.
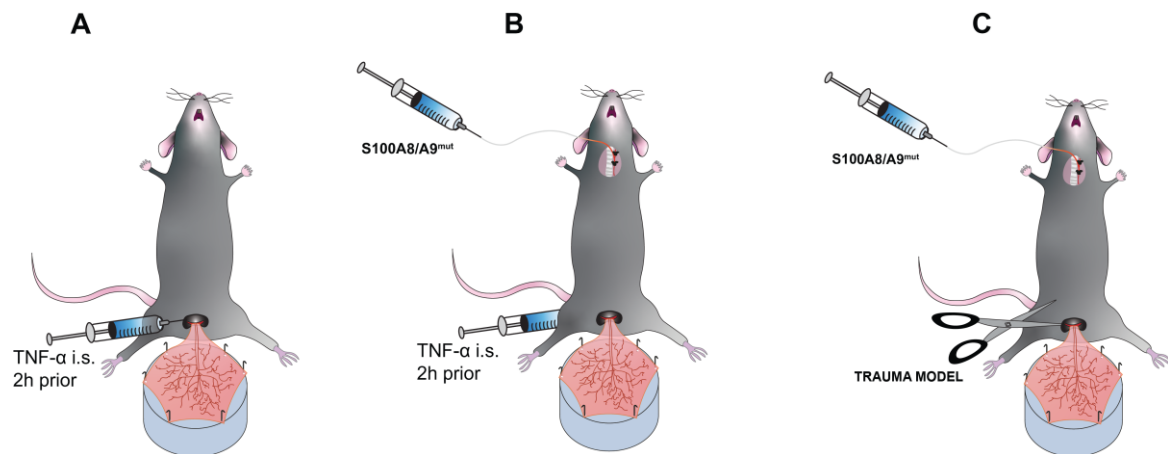
Figure 3.2: Different cremaster muscle models. Depending on the different research questions multiple cremaster models were adopted. (**A**) Simple leukocyte recruitment in an inflammatory setting, TNF-α was injected i.s. 2h prior exteriorizing the cremaster muscle for IVM. (**B**) Contribution of mutS100A8/A9 on the recruitment of WT and *Mrp14⁻/⁻* neutrophils. (**C**) Contribution of mutS100A8/A9 on the recruitment of WT and *Mrp14⁻/⁻* neutrophils, avoiding the autocrine S100A8/A9-TLR4 loop in WT neutrophils.

3.6   Intracellular MRP8/14 staining

3.6.1 *Ex vivo* staining

Cremaster muscle tissues from WT mice, previously treated with TNF-α, were removed and fixed in 4% PFA solution. Subsequently, immunofluorescence staining for PECAM-1 (5µg mL⁻¹, MEC13.3, BioLegend) and S100A9 (5µg mL⁻¹, clone 322, provided by Thomas Vogl, University of Muenster, Germany) was performed and slides mounted (Vectashield). Then, samples were imaged by confocal microscopy at the core facility Bioimaging of the BMC with an upright Leica SP8X WLL microscope, equipped with a HC PL APO 40x objective (Leica, 1.3NA, oil immersion).

Single cell analysis was performed with Fiji software, using macros (https://github.com/Napo93/AG-Sperandio-MACROS/blob/main/MACRO_MRP8_14%20intr%20levels%20upon%20%20transmigration%20cremaster%20tissues.ijm) generated to segment neutrophils and measure S100A9 mean fluorescence intensity (MFI) between intravascular and extravasated WT neutrophils.

3.6.2 *In vitro* staining

Removable glass slides (Ibidi) were coated with poly-L-lysine, E-selectin or E-selectin, ICAM-1 and CXCL1. Then, bone marrow derived WT neutrophils were isolated as described earlier, seeded on the coated slides and incubated for 10min at 37°C and 5% CO_2. Subsequently, cells were fixed in 4% PFA, immunofluorescence staining for S100A9 was performed and slides mounted (Vectashield). Samples were imaged by confocal microscopy at the core facility Bioimaging of the BMC with an upright Leica SP8X WLL microscope, equipped with a HC PL APO 40x objective (Leica, 1.3NA, oil immersion).

3.7 Flow chamber experiments

In order to distinguish and extrapolate the different steps of the leukocyte recruitment cascade, flow chamber assays were conducted on either 15µ-Slide VI 0.1 (Ibidi) or through self-assembly of small rectangular borosilicate glass capillaries (microflow chambers). The devices were coated with adhesion molecules involved in the recruitment process, mimicking an inflamed endothelial layer [116]. The coating was carried out for 3h at room temperature (RT) and flow chambers were successively blocked with 5% Casein/PBS over night (ON). Experiments were performed at an OlympusBX51 WI microscope, equipped with a 20x objective (Olympus, 0.95NA, water immersion objective) and a CCD camera (KAPPA CF 8 HS) or at a Zeiss Axioskop2 microscope, equipped with a 20x objective (Zeiss, 0.5NA, water immersion objective) and a Hitachi KP-M1AP camera and VirtualDub. Leukocyte rolling, leukocyte adhesion, rolling velocities, neutrophil spreading and neutrophil crawling were then analyzed on the recorded movies using Fiji.

3.7.1 *Ex vivo* flow chambers

Microflow chambers (0.04 x 0.4 mm) were coated with a combination of E-selectin, ICAM-1 and CXCL1. Then, WT and *Mrp14-/-* arterial blood was directly perfused into the flow chambers through the carotid artery and leukocyte slow rolling and adhesion was investigated.
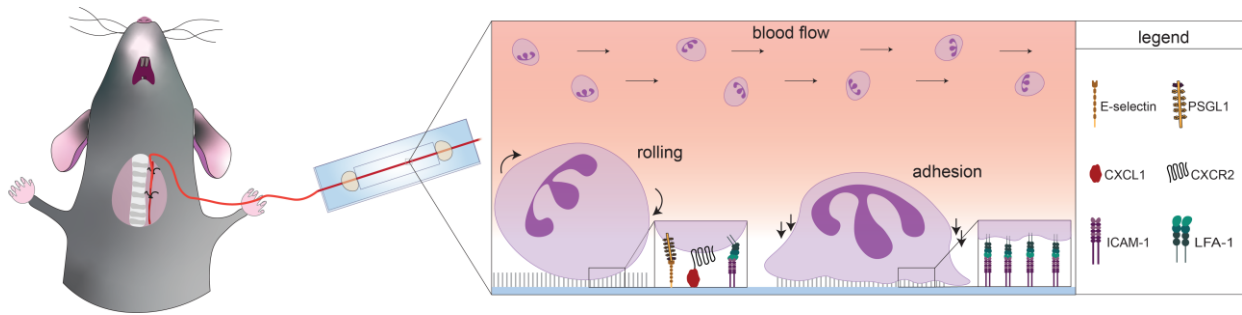
Figure 3.3: Ex vivo flow chambers. State-of-the-art technique developed in the lab to study leukocyte rolling and adhesion in a simplified environment without interfering with the system since murine whole blood will be perfused directly into rectangular borosilicate glass capillaries (Microflow chambers) coated with E-selectin, ICAM-1 and CXCL1 [236].

3.7.2 *In vitro* flow chambers

15μ-Slide VI 0.1 flow chambers (Ibidi) were coated with a combination of E-selectin, ICAM-1, CXCL1 and with or without S100A8/A9. Then, whole blood was harvested from WT and *Mrp14$^{-/-}$* mice, collected into heparinized tubes and perfused into the flow chambers at a constant shear stress level of 2dyne cm^{-2} using a high precision syringe pump (Harvard Apparatus) and leukocyte slow rolling and adhesion was studied.

3.7.3 *In vitro* spreading, crawling and detachment assays

For spreading and crawling assays, borosilicate glass capillaries (0.04 x 0.4 mm) were coated with a combination of E-selectin, ICAM-1 and CXCL1. Then, bone marrow derived WT and *Mrp14$^{-/-}$* neutrophils were isolated and incubated ON at 37°C and 5% CO$_2$ with WEHI-3B supernatant to prime them. The next day, neutrophils were seeded into the coated flow chambers, allowed to settle down for 3min and constant flow of 2dyne cm^{-2} was applied using a high precision syringe pump. Time-lapse movies were recorded for 20min at 5sec frame^{-1} and later analyzed for cell shape changes such as cell area, perimeter, circularity ($4\pi \frac{Area}{Perimeter^2}$) and solidity ($\frac{Area}{Convex\ Area}$) or for crawling velocity, distance and directionality using Fiji and the MTrackJ plugin or the ChemotaxisTool plugin (Ibidi).

For detachment assays, WT and *Mrp14$^{-/-}$* whole blood was directly perfused into the flow chambers through the carotid artery where neutrophils were allowed to settle down for 3min. Subsequently, flow was applied using a high precision syringe pump and detachment assays performed over 10min with increasing shear rates (34-272dyne cm^{-2}). Time-lapse movies were recorded and number of adherent cells was counted at the end of each step.

3.8   Static adhesion assay

Neutrophil static adhesion assay was performed as previously described [237]. Briefly, 96-well plates were coated with rmICAM-1 ($3\mu g\ mL^{-1}$) over night at 4°C and washed with PBS. Neutrophils were resuspended in complete HBSS and seeded at 1×10^5 cells per well. Cells were allowed to settle for 5min at 37°C and stimulated with 10nM rmCXCL1 or PBS (control) for 10min at 37°C. Using a standard curve, adherent neutrophils were assessed as percentage of total cells added. A standard curve was prepared by adding decreasing amount of the cell suspension on poly-L-lysine coated wells ($100\mu g\ mL^{-1}$) in triplicates. After a washing step, cells were fixed with 1% glutaraldehyde and stained with 0.1% crystal violet solution (Sigma-Aldrich). Cells were lysed with 10% acetic acid solution and absorption measured at 590nm with a microplate reader, as previously described [238].

3.9   Fluorescence activated cell sorting (FACS)

3.9.1   Neutrophil surface markers

Basal expression levels of neutrophil surface markers, critical for adhesion processes, were analyzed by flow cytometry [239]. For that, whole blood was collected from WT and $Mrp14^{-/-}$ mice by retro-orbital puncture and stained with specific monoclonal antibodies against CD18, CD11a (LFA-1), CD11b (Mac-1), CD62L (L-selectin), CD162 (PSGL1), CXCR2 and CD44 (listed in section 2.5.1) and respective isotype controls (listed in section 2.5.2). Neutrophils were defined as Ly6G ($5\mu g/\mu l$, clone1A8) positive cells. FACS lysing solution was used to lyse red blood cells and fix the samples, which were then acquired by flow cytometry with a Beckman Coulter Gallios and later analyzed with Kaluza analysis Software.

3.9.2   Soluble ICAM-1 binding assay

A soluble ICAM-1 binding assay was adopted to determine β_2 integrin activation, as recently described [162]. Shortly, ICAM-1 ($40\mu g/mL$, with a human IgG1 part) was incubated for 10min at RT with α-human Fc gamma-biotin and PerCP-Cy5.5 labelled streptavidin to form an ICAM-1 complex that was then incubated with the cells ($1.5\ 10^6$/sample) for 3min at 37°C together with CXCL1 (10nM). After 3min, the reaction was stopped by adding ice-cold FACS lysing solution. Ly6G antibody was used to identify the neutrophil population, as described before. Samples were acquired by flow cytometry with a CytoFlex S and later analyzed with FlowJo analysis software.
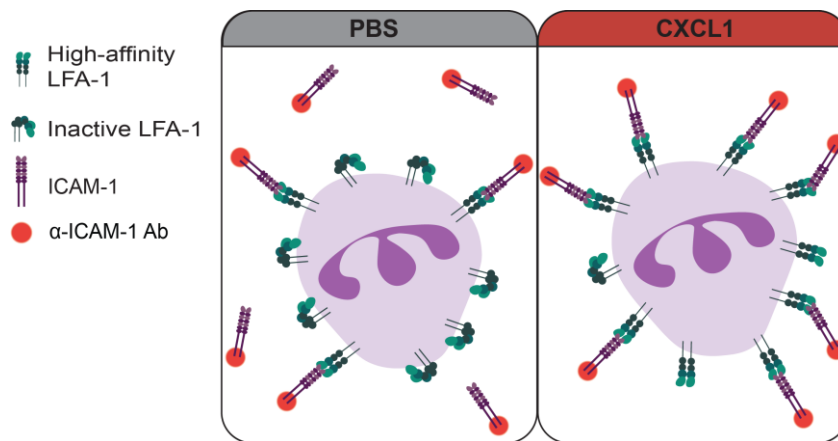
Figure 3.4.: Soluble ICAM-1 binding assay. Representative cartoon image showing the principle of the soluble ICAM-1 binding assay through which we measured the activation of β2 integrins on the neutrophil surface upon CXCL1 stimulation by indirectly measuring the amount of labelled ICAM-1 bound by neutrophils.

3.9.3 Intracellular Ca^{2+}

Intracellular Ca^{2+} levels were investigated with an adapted protocol [240]. Shortly, neutrophils isolated from the bone marrow of WT and *Mrp14*^{-/-} mice (2.5×10^6 mL^{-1}) were stained with 3µM Indo-1 AM in PBS for 45min at 37°C and 5% CO_2. Afterwards, cells were washed and stained with an APC labelled α-Ly6G and the Fixable Viability Dye eFluor™ 780 (1:1000; eBioscience™). Then, cells (2×10^5) were placed in new FACS tubes and a CXCL1 drop (10nM) was placed on the side of the tube in a 2µL volume. Samples were recorded for 45 seconds to establish baseline. Afterwards, CXCL1 stimulation was initiated by tapping the tube with subsequent fall of the drop into the cell suspension while continuously recording Indo-1 AM signals from neutrophils over time. Experiments were recorded at the flow cytometry core facility of the BMC with a BD LSRFortessa™ flow cytometer. Data were analyzed using FlowJo software. Calcium levels were expressed as relative ratios of fluorescence emission at 375nm/525nm (calcium bound/calcium unbound) and Ca^{2+} signatures quantified as AUC of kinetic averages. To measure Ca^{2+} store release only, Ca^{2+} free medium was used.

3.9.4 Phagocytosis assay

Neutrophil phagocytosis was investigated with the pHrodo™ Green *E. coli* Bioparticles™ kit as described earlier [116]. Whole blood was harvested via retro-orbital puncture from WT and *Mrp14*^{-/-} mice and collected into heparinized tubes. Then, the blood was transferred into FACS tubes and incubated with *E. coli* bioparticles either on ice (negative control) or at 37°C and 5% CO_2 for 30min. Afterwards, phagocytosis was blocked with FACS lysis solution. Neutrophils were labelled with an APC labelled α-Ly6G and the amount of *E. coli* bioparticles in neutrophils determined with a Beckman Coulter Gallios flow cytometer and Kaluza Flow analysis Software. To obtain confocal pictures, WT and *Mrp14*^{-/-} neutrophils were isolated and seeded on poly-L-lysine coated slides (Ibidi), fixed with 4% PFA, washed and counterstained with DAPI for 5min at RT. Finally, slides were embedded in ProLong Diamond Antifade mounting medium. Samples were acquired at the

core facility Bioimaging of the BMC with a Leica TSC SP8 microscope, equipped with a HC PL APO 40x (1.30NA, oil immersion objective). Images were processed (including removal of outliers and background subtraction) using FIJI software.

3.10 Confocal microscopy

3.10.1 Basal Ca^{2+} levels

WT ^{Lyz2xGCaMP5} and $Mrp14^{-/-Lyz2xGCaMP5}$ neutrophils were isolated as described above and seeded on poly-L-lysine coated slides (Ibidi). Cells were segmented through the $Lyz2$ channel and basal cytosolic Ca^{2+} levels measured at the core facility Bioimaging of the BMC with an inverted Leica SP8X WLL microscope, equipped with a HC PL APO 40x (Leica, 1.30NA oil immersion objective). Movies of 3min were recorded and Ca^{2+} MFI analyzed with Fiji.

3.10.2 Overall Ca^{2+} levels and F-actin polymerization

15µ-Slide VI 0.1 flow chambers (Ibidi) were coated with a combination of E-selectin, ICAM-1, and CXCL1. Then, bone marrow derived WT ^{Lyz2xGCaMP5} and $Mrp14^{-/-Lyz2xGCaMP5}$ neutrophils were isolated and incubated ON at 37°C and 5% CO_2 with WEHI-3B supernatant to prime them, together with SiR-actin dye to stain F-actin filaments. The next day, neutrophils were seeded into the coated flow chambers and allowed to settle down for 3min. Then, constant flow of 2dyne cm^{-2} was applied using a high precision syringe pump. Samples were imaged at the core facility Bioimaging of the BMC with an inverted Leica SP8X WLL microscope, equipped with a HC PL APO 40x (Leica, 1.30NA oil immersion objective). Movies were recorded at a scan speed of 2sec frame^{-1} for 10min. Automated single cell analysis was performed using macros with Fiji software (https://github.com/Napo93/AG-Sperandio-MACROS/blob/main/FINAL%20MACRO_Factin%20and%20tot%20Ca2%20analysis.ijm), for minute 0-1, minute 5-6 and minute 9-10, cells were segmented through the $Lyz2$ channel and overall cytosolic Ca^{2+} levels and F-actin levels measured.

3.10.3 Overall Ca^{2+} levels fluorescence lifetime imaging microscopy (FLIM)

15µ-Slide VI 0.1 flow chambers (Ibidi) were coated with a combination of E-selectin, ICAM-1, CXCL1. Then, bone marrow derived WT and $Mrp14^{-/-}$ neutrophils were isolated and incubated ON at 37°C and 5% CO_2 with WEHI-3B supernatant to prime them. The next day, neutrophils were incubated with Oregon Green™ 488 BAPTA-1 AM for 30min, seeded into the coated flow chambers and allowed to settle down for 3min. Then, constant flow of 2dyne cm^{-2} was applied using a high precision syringe pump. Samples were imaged at the core facility Bioimaging of the BMC with an upright Leica SP8 Falcon (fast lifetime contrast) microscope, equipped with a HC PL APO 40x (Leica, 1.30NA oil immersion objective). Movies were recorded at a scan speed of 2frames sec^{-1} for 5min. Automated single cell analysis was performed using macros with Fiji

software. For every recorded minute, cells were segmented through the BAPTA-1 intensity channel using Fiji. Lifetime measurements were back calculated via the LASX software through the FLIM plugin extension.

3.10.4 Subcellular LFA-1 and Ca^{2+} measurements

15µ-Slide VI 0.1 flow chambers (Ibidi) were coated with a combination of E-selectin, ICAM-1, and CXCL1. Then, bone marrow derived WT ^{Lyz2xGCaMP5} and $Mrp14^{-/-Lyz2xGCaMP5}$ neutrophils were isolated and incubated ON at 37°C and 5% CO_2 with WEHI-3B supernatant to prime them. The next day, neutrophils were stained with AF647 in-house labelled α-LFA-1 (2D7, BD Pharmigen) 1min before they were seeded into the coated flow chambers and allowed to settle down for 3min. Then, constant flow of 2dyne cm^{-2} was applied using a high precision syringe pump. Samples were imaged at the core facility Bioimaging of the BMC with an inverted Leica SP8X WLL microscope, equipped with a HC PL APO 40x (Leica, 1.30NA oil immersion objective). Movies were recorded at a scan speed of 2sec frame^{-1} for 10min. Automated single cell analysis was performed using macros with Fiji software (https://github.com/Napo93/AG-Sperandio-MACROS/blob/main/FINAL%20MACRO_LFA1%20and%20Ca2%20analysis.ijm), for minute 0-1, minute 5-6 and minute 9-10 of each recording. For the LFA-1 nanocluster analysis, the LFA-1 channel was automatically segmented and ROIs of a minimum size of 0.15µm^2 were considered as LFA-1 nanosclusters, as reported earlier [241]. The number of clusters was averaged for each analyzed time point (min 0-1, min 5-6 and min 9-10). For the subcellular Ca^{2+} analysis at the LFA-1 cluster sites, the LFA-1 segmented channel was applied to the Ca^{2+} channel and Ca^{2+} events in the selected ROIs were determined, normalized to the LFA-1 areas, and averaged over each minute of analysis. For the Ca^{2+} analysis in the negative LFA-1 area, we again adopted semi-automated single cell analysis and subtracted the LFA-1 mask from the $Lyz2$ mask in order to obtain "LFA-1 cluster negative masks". Later, the "LFA-1 cluster negative masks" were applied to the Ca^{2+} channel and Ca^{2+} intensities were measured, normalized to the "LFA-1 cluster negative masks" and averaged over each minute of analysis using macros (https://github.com/Napo93/AG-Sperandio-MACROS/blob/main/Negative%20LFA1%20mask%20(Ca2%2B%20levels%20outside%20LFA1%20clusters).ijm).

3.11 Western blot

3.11.1 Cytoskeletal rearrangements

In order to study neutrophil cytoskeletal rearrangements, the phosphorylation of cytoskeletal adapter proteins like paxillin and pyk2 was investigated as reported earlier [116]. Bone marrow derived WT and $Mrp14^{-/-}$ neutrophils were isolated and seeded on rmICAM-1 coated wells (15µg mL^{-1}) for 5min and stimulated with rmCXCL1 (10nM) for 5min at 37°C. Cells were then lysed with lysis buffer, resolved by SDS–PAGE and electrophoretically transferred onto PVDF membranes.

Membranes were then blocked (LI-COR blocking solution /TBS 1:1) and incubated with the following antibodies for later detection and analysis using the Odyssey® CLx Imaging System and Image Studio software: rabbit α-mouse phospho-Paxillin (Tyr118) or rabbit α-mouse Paxillin and rabbit α-mouse phospho-Pyk2 (Tyr402) or rabbit α-mouse Pyk2. Goat-α-mouse IRDye 800RD was used as secondary antibody (Licor).

3.11.2 Intracellular protein levels

For CREB-1 and p38 analysis, western blot was conducted as described above but from WT and $Mrp14^{-/-}$ isolated and lysed neutrophils. Membranes were then incubated with the following antibodies: rabbit α-mouse phospho-CREB-1 (Ser133) or rabbit α-mouse CREB-1 and rabbit α-mouse phospho- p38 MAPK (Thr180/Tyr182) or rabbit α-mouse p38 MAPK. Goat-α-mouse IRDye 800RD was used as secondary antibody (Licor).

For Calmodulin quantification, western blot was conducted on WT ^{Lyz2xGCaMP5} and $Mrp14^{-/- \, Lyz2xGCaMP5}$ isolated and lysed neutrophils. Membranes were then incubated with rabbit α-mouse Calmodulin and mouse α-mouse GAPDH. Goat-α-rabbit IRDye 800RD and Goat-α-mouse IRDye 680RD were used as secondary antibodies.

For β-actin levels assessment, western blot was conducted from WT ^{Lyz2xGCaMP5} and $Mrp14^{-/- \, Lyz2xGCaMP5}$ isolated and lysed neutrophils. Membranes were then incubated with rabbit α-mouse β-Actin. Goat-α-rabbit IRDye 800RD was used as secondary antibody.

4. Results

4.1 Cytosolic MRP8/14 mediates adhesion during leukocyte recruitment, independent from extracellular MRP8/14

4.1.1 Intracellular MRP8/14 levels remain high under inflammatory conditions *in vitro* and *in vivo*

To assess intracellular MRP8/14 levels upon activation, neutrophils from WT mice were isolated, stimulated with rmE-selectin or lysed with Triton-X100 and ELISA to detect amount of released MRP8/14 was performed. Indeed, it has been shown from our group that MRP8/14 is secreted during E-selectin – PSGL1 mediated rolling and binds to neutrophil TLR4 in an autocrine fashion, promoting β_2 integrin activation mediating leukocyte slow rolling and adhesion [12]. E-selectin induced MRP8/14 release accounted for only 1-2% of the total intracellular MRP8/14 content as confirmed by Triton-X100 induced cell lysis (Fig.4.1-A). Next, to validate these findings *in vivo*, TNF-α stimulated WT mouse cremaster muscles were fixed, stained against MRP8/14 and PECAM-1 for immune fluorescence (IF) (Fig.4.1-B) in order to compare the MRP8/14 signal in adherent neutrophils within vessels with the MRP8/14 signal from outside the vessels. MRP8/14 signal from neutrophils did not differ between intravascular and extravascular neutrophils (Fig.4.1-C). Finally, to further confirm those results, neutrophils from WT mice were isolated and fluorescently labelled for MRP8/14 before seeding them on poly-L-lysine, rmE-selectin, and rmE-selectin, rmICAM-1 and rmCXCL1 (Fig.4.1-D). No difference in intracellular MRP8/14 levels was observed between the groups (Fig.4.1-E). Taken together, intracellular MRP8/14 levels decrease at a very low rate in E-selectin stimulated neutrophils.
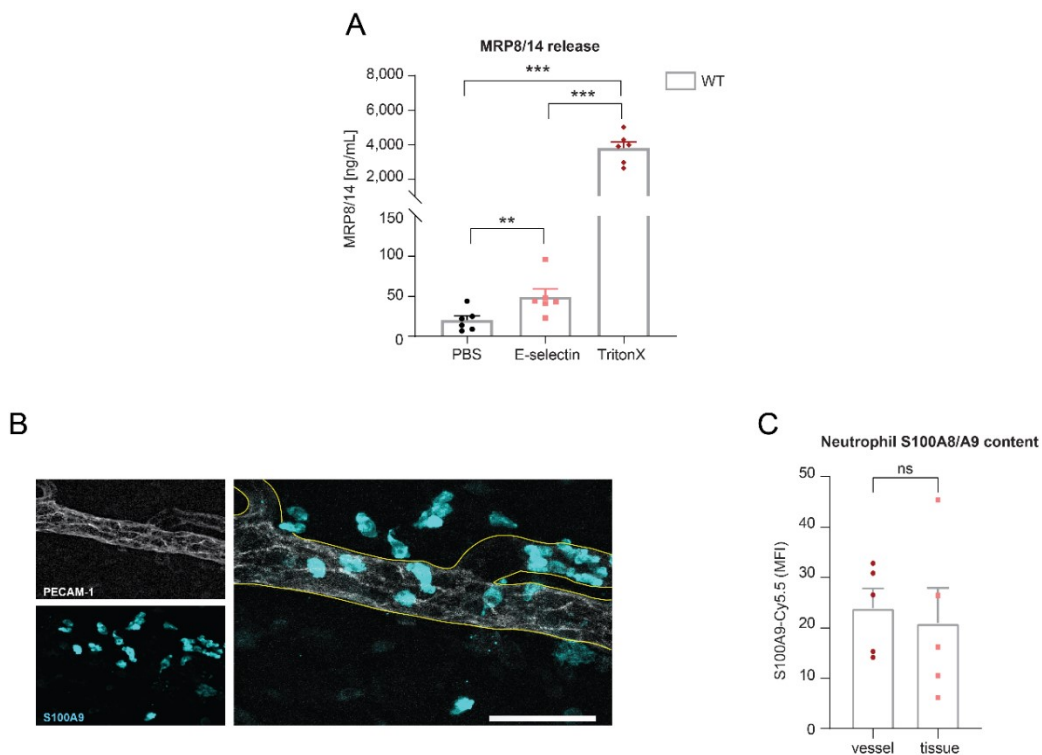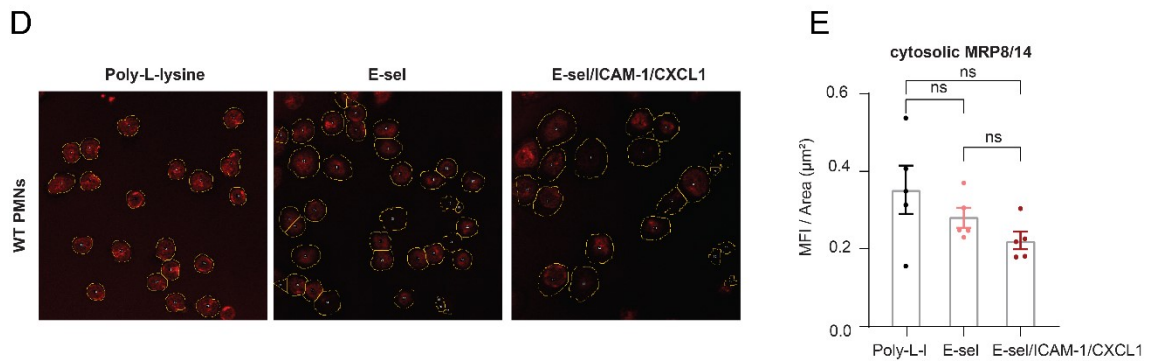
Figure 4.1: Intracellular MRP8/14 levels remain high under inflammatory conditions *in vitro* **and** *in vivo*. (**A**) WT neutrophils were stimulated for 10min with E-selectin, PBS control or lysed with TritonX, supernatants were then collected and MRP8/14 levels were analyzed by ELISA (mean±SEM, n=6 mice per group, RM one-way ANOVA, Holm-Sidak's multiple comparison). (**B**) TNF-α stimulated WT cremaster muscles were stained for PECAM1 (grey) and MRP14 (cyan) and (**C**) amount of intracellular MRP14 between intravascular and extravascular neutrophils was quantified using immunofluorescence. [mean±SEM, n=5 mice per group, 602 (intravascular) and 326 (extravasated) neutrophils, unpaired Student's t-test]. (**D**) WT neutrophils were stimulated for 10min with E-selectin, Poly-L-lysine control or a combination of E-selectin, ICAM-1 and CXCL1 and (**E**) intracellular MRP8/14 levels were quantified and normalized to the cell area (mean±SEM, n=5 mice per group, RM one-way ANOVA, Tukey's multiple comparison). ns, not significant; *P≤0.05, **P≤0.01, ***P≤0.001.

4.1.2   MRP8/14 does not affect E-selectin-mediated slow rolling *in vivo*, *ex vivo* and *in vitro*

E-selectin mediated neutrophil rolling is a prerequisite for β_2 integrin mediated slow rolling and firm adhesion [157]. Therefore, the TNF-α –induced inflammation model of the mouse cremaster muscle was adopted in order to study leukocyte rolling in an acute and mostly neutrophil-driven inflammatory scenario*, in vivo*. First, to assess E-selectin upregulation upon TNF-α stimulation, WT mice were injected i.s. with TNF-α or NaCl control 2h prior to microsurgical catheterization of the carotid artery and cremaster muscle exteriorization for Intravital microscopy (IVM). Then, leukocyte rolling velocities were quantified before and after intra-arterial injection of E-selectin blocking Ab. WT leukocytes treated with NaCl showed P-sel dependent rolling velocities (~20µm/s) while WT leukocytes treated with TNF-α showed E-selectin dependent rolling velocities (~10µm/s). As expected, E-selectin Ab injection led to an increase in rolling velocities only in the TNF-α treated group (Fig.4.2-A). To investigate the role of cytosolic MRP8/14 on neutrophil E-selectin dependent rolling, WT and *Mrp14−/−* mice were injected i.s. with TNF-α. Two hours later, the cremaster muscle was exteriorized and IVM conducted. No difference was observed in rolling flux fraction (Fig.4.2-B) or rolling velocities (Fig.4.2-C, -D) between WT and *Mrp14−/−* leukocytes. To investigate *Mrp14−/−* leukocyte rolling without the endothelial counterpart, *ex vivo* and *in vitro* experiments were conducted coating microflow chambers with rmE-selectin, rmICAM-1, and rmCXCL1 to mimic the inflamed endothelium. Then, blood from WT and *Mrp14−/−* was either directly perfused into the chambers through a carotid artery catheter (*ex vivo*) or perfused with a high-precision pump (*in vitro*) at physiological shear stress (2dyne cm⁻²) conditions. Consistently, number of rolling cells did not differ between WT and *Mrp14−/−* leukocytes in neither *ex vivo*

(Fig.4.2-E) or *in vitro* (Fig.4.2-F) settings. Taken together, these data indicate that MRP8/14 is dispensable for leukocyte rolling under inflammatory conditions.

4.1.3 Loss of MRP8/14 impairs neutrophil adhesion *in vivo, ex vivo* and *in vitro*

β_2 integrin mediated slow rolling is a prerequisite for leukocyte firm adhesion [157]. First, to study MRP8/14 contribution on leukocyte adhesion, *in vivo* experiments were performed through TNF-α induced inflammation of the mouse cremaster muscle as explained in 4.1.2. Contrarily to rolling, *Mrp14-/-* mice showed decreased leukocyte adhesion compared to WT mice (Fig.4.3-A). Importantly, no differences in overall white blood cell counts (WBC) could be found between WT and *Mrp14-/-* animals (Tab.4.1). Again, to dissect the complexity of the *in vivo* scenario, *ex vivo* and *in vitro* experiments were performed as described in 4.1.2. Shortly,microflow chambers were coated with rmE-selectin, rmICAM-1, and rmCXCL1 and directly (carotid catheter) or indirectly (high-precision pump) perfused with WT and *Mrp14-/-* blood. In line with the in vivo results, *Mrp14-/-* leukocytes showed lower adhesion efficiency in both *ex vivo* (Fig.4.3-B) and *in vitro* (Fig.4.3-C) settings, compared to WT leukocytes. Yet, WBCs and number of cells per field of view (FOV) were comparable between groups (Tab.4.2). These results indicate that MRP8/14 is dispensable for leukocyte rolling, but indispensable for leukocyte adhesion in an inflamed environment.
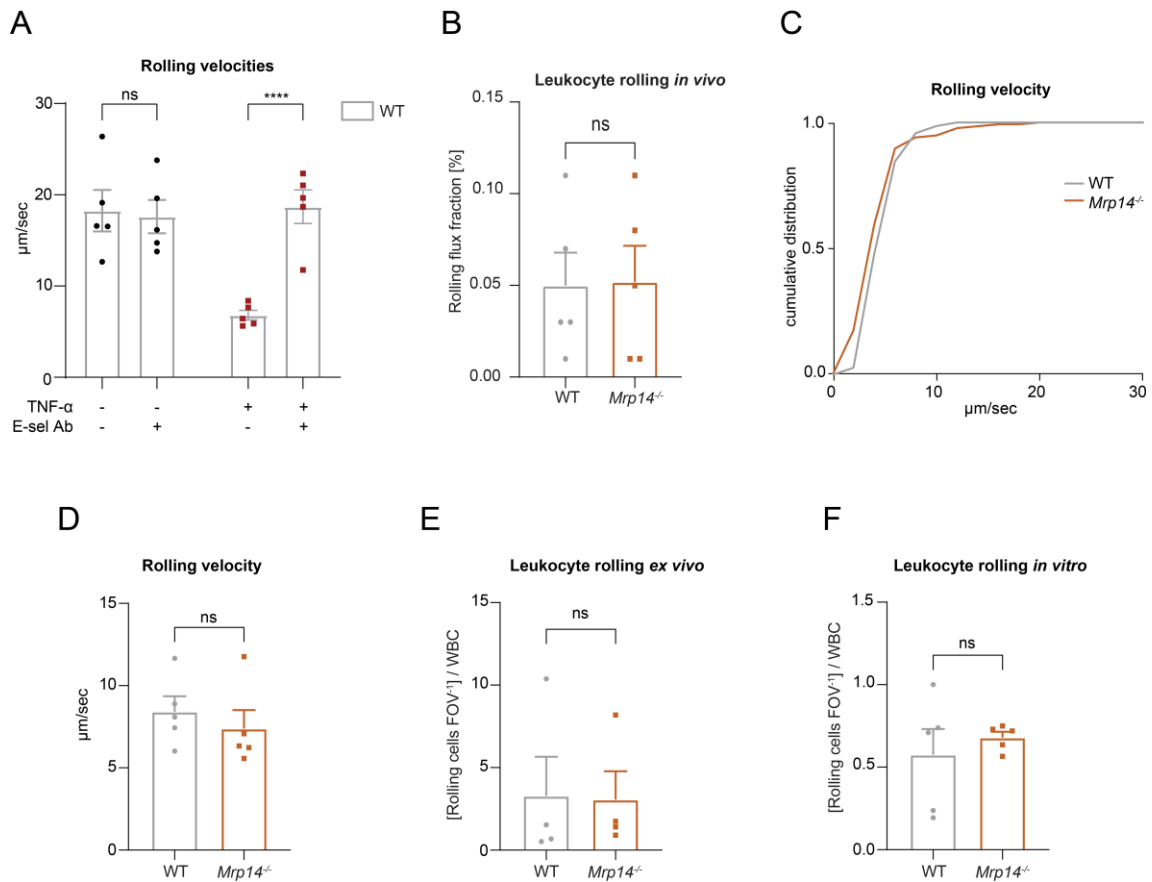
Figure 4.2: MRP8/14 does not affect E-selectin-mediated slow rolling *in vivo*, *ex vivo* and *in vitro*. (**A**) Intrascrotal (i.s.) injection of TNF-α (TNF-α +) or NaCl control (TNF-α -) was performed in WT mice, cremaster muscle exteriorized and leukocyte rolling velocities quantified before and after intra-arterial injection of E-selectin blocking antibody (mean±SEM, *n*=70 cells of 5 mice per group, 2way ANOVA, Sidak's multiple comparison). (**B**) Number of rolling leukocytes per vessel surface in TNF-α treated WT and *Mrp14-/-* cremaster muscles were analyzed [mean±SEM, *n*=5 mice per group, 25 (WT) and 30 (*Mrp14-/-*) vessels, unpaired Student's *t*-test]. (**C**) Cumulative distribution and (**D**) quantification of WT and *Mrp14-/-* leukocyte rolling velocity in TNF-α stimulated cremaster muscles (mean±SEM, n=5 mice per group, paired Student's t-test). Microflow chambers were coated with E-selectin, ICAM-1, and CXCL1 and blood from WT and *Mrp14-/-* mice (**E**) directly perfused via the carotid catheter *ex vivo* or (**F**) harvested and perfused via a high-precision pump *in vitro* into the chambers and number of rolling cells quantified and normalized to the WBC (mean±SEM, n≥4 mice per group, paired Student's t-test). ns, not significant; *P≤0.05, **P≤0.01, ***P≤0.001.

A Leukocyte adhesion *in vivo*
B Leukocyte adhesion *ex vivo*
C Leukocyte adhesion *in vitro*
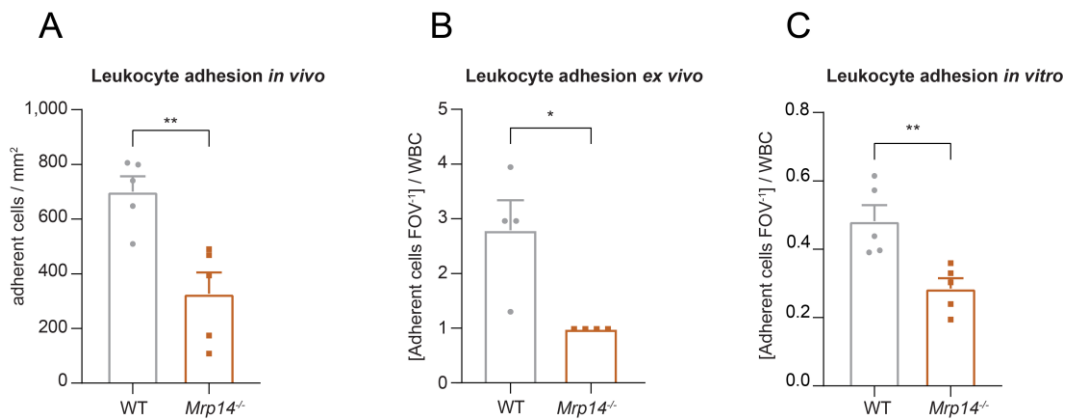
Figure 4.3: Loss of MRP8/14 impairs neutrophil adhesion *in vivo*, *ex vivo* and *in vitro*. (**A**) number of adherent leukocytes per vessel surface in TNF-α treated WT and *Mrp14-/-* cremaster muscles were analyzed [mean±SEM, *n*=5 mice per group, 25 (WT) and 30 (*Mrp14-/-*) vessels, unpaired Student's *t*-test]. (**B**) Microflow chambers were coated with E-selectin, ICAM-1, and CXCL1 and blood from WT and *Mrp14-/-* mice (**E**) directly perfused via the carotid catheter *ex vivo* or (**F**) harvested and perfused via a high-precision pump *in vitro* into the chambers and number of adherent cells were quantified and normalized to the WBC (mean±SEM, n≥4 mice per group, paired Student's t-test). ns, not significant; *P≤0.05, **P≤0.01, ***P≤0.001.

	Mice (n)	Flow chambers (n)	Cells FOV^{-1}	WBC [µl^{-1}]
WT	4	8	39+5	8630+1200
Mrp14-/-	4	10	37+5	8600+1200
			ns.	ns.
			(p=0.7332)	(p=0.9772)

Table 4.1: Flow chamber experiments using WT and *Mrp14-/-* neutrophils *ex vivo*. Field of view (FOV), white blood cell count (WBC). n.s.: not significant (Mean+SEM, unpaired student's t-test).

4.1.4   Extracellular MRP8/14 cannot rescue the adhesion defect caused by the lack of cytosolic MRP8/14, *in vivo* and *in vitro*

Pruenster et al recently described a novel role for extracellular MRP8/14 as β_2 integrin activator of neutrophils, as outlined on p.25. To clarify whether the adhesion defect observed in MRP8/14 deficient leukocytes was caused by intracellular or extracellular MRP8/14, additional *in vivo* and *in vitro* rescue experiments were performed. First, TNF-α stimulated cremaster muscles of WT and *Mrp14*^{-/-} mice were conducted, as described in 4.1.2. MutantMRP8/14 (N70A/E79A AA change) [mutMRP8/14] was injected intra-arterial and number of adherent leukocytes quantified. While WT leukocytes showed induction of adhesion, no difference was observed in *Mrp14*^{-/-} leukocytes upon mutMRP8/14 application (Fig.4.4-A). However, we could not exclude that the effect on WT neutrophils was due to the E-selectin–mediated release of intracellular MRP8/14, which does not occur in *Mrp14*^{-/-} neutrophils. To exclude this, we then investigated WT and *Mrp14*^{-/-} neutrophil adhesion upon mutMRP8/14 application in the trauma –induced inflammation model. Indeed, while TNF-α induces transcriptional E-selectin upregulation, sterile inflammation results in P-selectin mediated rolling [140] and does not induce MRP8/14 release [12]. Since we observed induction of adhesion in WT neutrophils, we confirmed that it was caused by mutMRP8/14 injection (Fig.4.4-B). Surprisingly, the defective adhesion could not be rescue by extracellular MRP8/14 in *Mrp14*^{-/-} neutrophils (Fig.4.4-B). In addition, *in vitro* experiments were conducted through microflow chambers coated with rmE-selectin, rmICAM-1, and rmCXCL1 as described in 4.1.2 and additionally with or without rmMRP8/14. As shown *in vivo*, *in vitro* additional coating with rmMRP8/14 induced adhesion of WT leukocytes but not of *Mrp14*^{-/-} leukocytes (Fig.4.4-C). Of note, no difference in WBCs or cells per FOV could be observed in the different experimental groups (Tab.4.3). Overall, the adhesion defect observed in MRP8/14 deficient leukocytes is intrinsic, caused by the lack of cytosolic MRP8/14, and cannot be rescued by addition of extracellular MRP8/14.
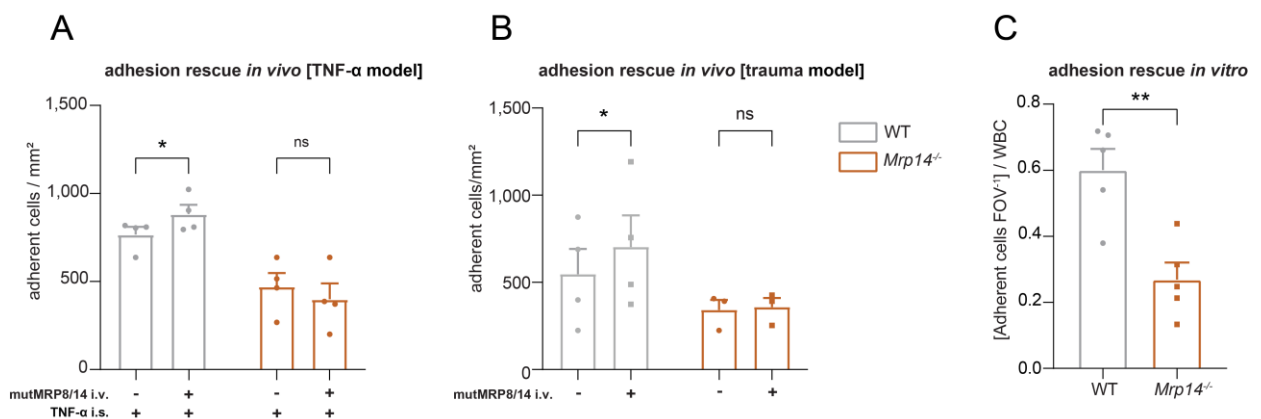
Figure 4.4: Extracellular MRP8/14 cannot rescue the adhesion defect caused by the lack of cytosolic MRP8/14, *in vivo* and *in vitro*. Number of adherent leukocyte per vessel surface were quantified in the same vessel of (**A**) TNF-α or (**B**) trauma induced inflammation of WT and *Mrp14*^{-/-} cremaster muscles before and after intra-arterial injection of mutantMRP8/14 (aa exchange N70A and E79A) [mean±SEM, n≥3 mice per group, 4 and 3 (WT) and 4 and 3 (*Mrp14*^{-/-}) vessels respectively, 2way ANOVA, Sidak's multiple comparison]. Microflow chambers were coated with E-selectin, ICAM-1, CXCL1,and rmMRP8/14 and blood from WT and *Mrp14*^{-/-} mice was harvested and (**C**) perfused via a high-precision pump *in vitro* into the chambers and number of adherent

cells were quantified and normalized to the WBC (mean±SEM, n=4 mice per group, paired Student's t-test). ns, not significant; *P≤0.05, **P≤0.01, ***P≤0.001.

4.1.5 Loss of MRP8/14 reduces neutrophil extravasation into inflamed cremaster muscle tissue

Leukocyte firm adhesion is a prerequisite for postarrest modifications–dependent extravasation into the inflamed tissue [138]. In order to investigate the impact of MRP8/14 on leukocyte extravasation, TNF-α stimulated WT and *Mrp14*$^{-/-}$ cremaster muscles were removed at the end of the experiment. Subsequently, the tissues were fixed, permeabilized and stained with giemsa for later detection of the number of extravasated neutrophils. In line with our previous data, in the absence of MRP8/14: reduced numbers of extravasated neutrophils were found in the inflamed perivascular cremaster tissue (Fig.4.5-A, -B). No difference in extravasation was observed in other leukocyte subsets in the absence of MRP8/14 (Fig.4.5-B).

In summary, MRP8/14 remains abundantly expressed in the neutrophil cytosolic compartment after cell activation. Lack of MRP8/14 decreases leukocyte adhesion without affecting leukocyte slow rolling *in vivo* in TNF-α stimulated inflammation and *in vitro* and *ex vivo* in flow chamber assays. Importantly, administration of soluble rmMRP8/14 could not rescue the adhesion defect neither *in vivo* nor *in vitro* in the absence of intrinsic MRP8/14. In addition, MRP8/14 turned out to be indispensable for neutrophil, but not other leukocyte, extravasation into inflamed tissue.
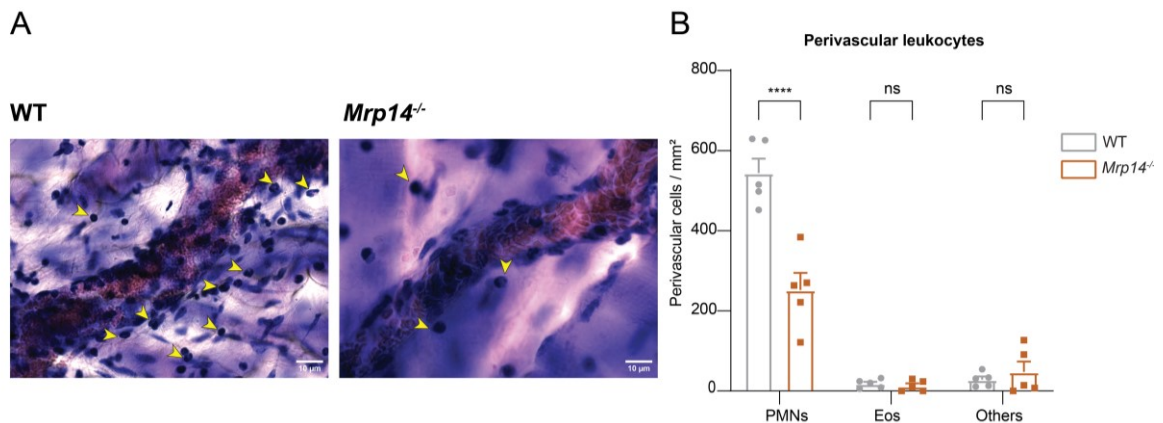
Figure 4.5: Loss of MRP8/14 reduces neutrophil extravasation into inflamed cremaster muscle tissue. (**A**) Giemsa staining of TNF-α stimulated WT and *Mrp14*$^{-/-}$ cremaster muscles was performed (representative micrographs, scale bar =30 μm, arrows: transmigrated neutrophils) and (**B**) number of perivascular neutrophils, eosinophils and other leukocytes was quantified [mean±SEM, *n*=5 mice per group, 56 (WT) and 55 (*Mrp14*$^{-/-}$) vessels, unpaired Student's *t*-test]. ns, not significant; *P≤0.05, **P≤0.01, ***P≤0.001.

	Mice (n)	Venules (n)	Diameter [µm]	Centerline velocity [µm s^{-1}]	Wall shear rate [s^{-1}]	WBC [µl^{-1}]
WT+ TNF-α	5	21	32.5+0.5	1130+50	920+50	3580+450
Mrp14$^{-/-}$+ TNF-α	5	20	34.0+1.5	1320+50	1010+50	3520+200
			ns. (p=0.606)	ns. (p=0.1534)	ns. (p=0.6091)	ns. (p=0.9723)
WT + mutS100A8/A9	4	4	30.0+5.0	2030+300	1800+420	5720+800
Mrp14$^{-/-}$+ mutS100A8/A9	3	3	30.0+2.5	1540+350	1300+350	5460+650
			ns. (p=0.835)	ns. (p=0.3416)	ns. (p=0.3898)	ns. (p=0.7979)
WT + TNF-α + mutS100A8/A9	4	18	31.0+3.0	1330+330	1450+400	4100+1000
Mrp14$^{-/-}$+ TNF-α + mutS100A8/A9	5	24	30.0+3.0	1700+130	1500+300	3900+500
			ns. (p=0.647)	ns. (p=0.8341)	ns. (p=0.3947)	ns. (p=0.6677)

Table 4.2: Geometric and haemodynamic parameters of TNF-α treated WT and *Mrp14$^{-/-}$* mice. White blood cell count (WBC). n.s.: not significant (Mean+SEM, unpaired student's t-test).

4.2 MRP8/14 is dispensable for β$_2$ integrin activation but essential for β$_2$ integrin outside-in signaling–dependent postarrest modifications

4.2.1 Neutrophil surface adhesion markers are not altered in the absence of MRP8/14

To find out what lies behind the adhesion defect caused by the lack of MRP8/14, neutrophil adhesion molecule expression was investigated. Neutrophil adhesion is dependent on surface adhesion molecules, which are upregulated upon stimulation [242]. In order to assess neutrophil adhesion molecule expression, blood neutrophils from WT and *Mrp14$^{-/-}$* mice were challenged with CXCL1 or PBS (control) and flow cytometry analysis was performed. No differences were detected in CD11a, CD11b, CD18, CD62L, CD44, PSGL1 and CXCR2 surface expression under homeostatic conditions and upon cell stimulation between WT and *Mrp14$^{-/-}$* neutrophils (Fig.4.6).
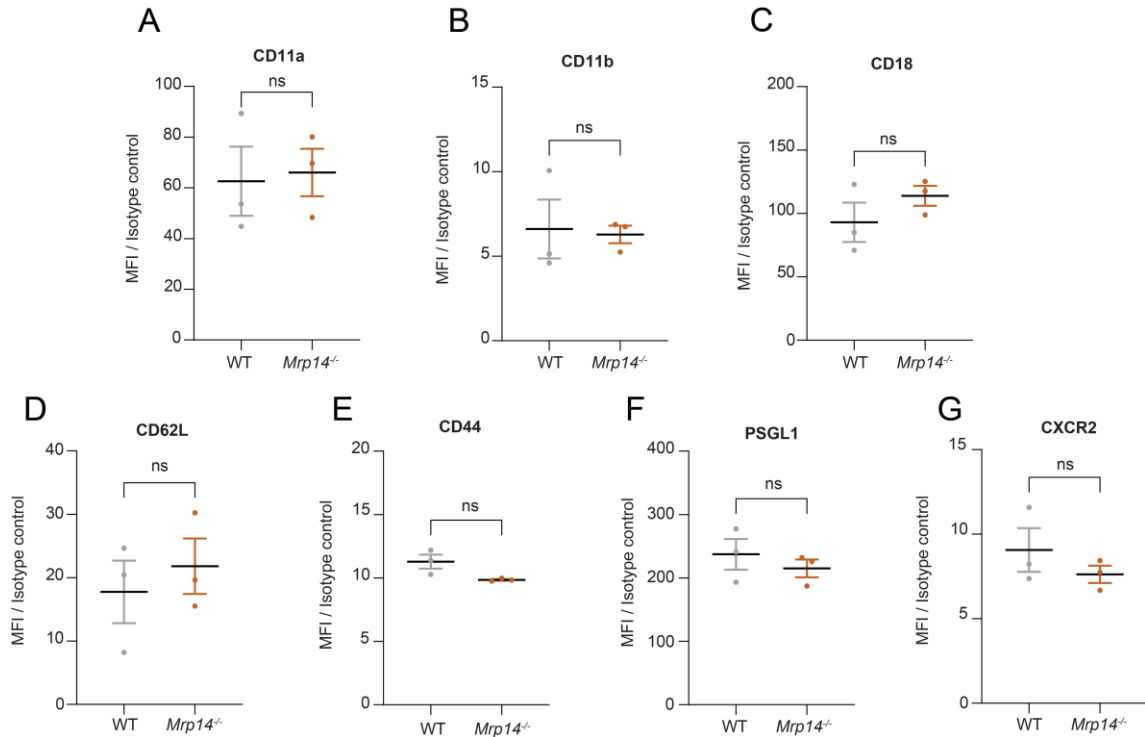
Figure 4.6: Neutrophil surface adhesion markers are not altered in the absence of MRP8/14. (**A**) CD11a, (**B**) CD11b, (**C**) CD18 [lymphocyte function-associated antigen 1 (LFA-1) and Macrophage antigen 1 (Mac-1)], (D) L-selectin, E-selectin ligands [(**E**) CD44 and (**F**) PSGL1], (**G**) chemokine receptor CXCR2, surface levels were analyzed by flow cytometry in WT and *Mrp14*-/- whole blood neutrophils (data are given as mean±SEM, *n*=3 mice per group, unpaired Student's *t*-test). ns, not significant; *$P \leq 0.05$, **$P \leq 0.01$, ***$P \leq 0.001$.

4.2.2 Neutrophil β_2 integrin activation (inside-out signaling) is not dependent on MRP8/14

In order to better understand the role of MRP8/14 on neutrophil adhesion, β_2 integrin activation (inside-out signaling) was studied. To do that, WT and *Mrp14*-/- bone marrow-derived neutrophils were stimulated with CXCL1 or PBS (control) and incubated with soluble fluorescently labelled ICAM-1 for β_2 integrin activation. Surprisingly, no difference was detected in ICAM-1 binding between WT and *Mrp14*-/- neutrophils upon CXCL1 stimulation (Fig.4.7-A). To further confirm these results, WT and *Mrp14*-/- bone marrow-derived neutrophils were stimulated with CXCL1 or PBS (control), plated over rmICAM-1 coated dishes and a static adhesion assay was performed. In line with the results on soluble ICAM-1 binding, no difference in static adhesion was observed between WT and *Mrp14*-/- neutrophils upon CXCL1 stimulation (Fig.4.7-B).
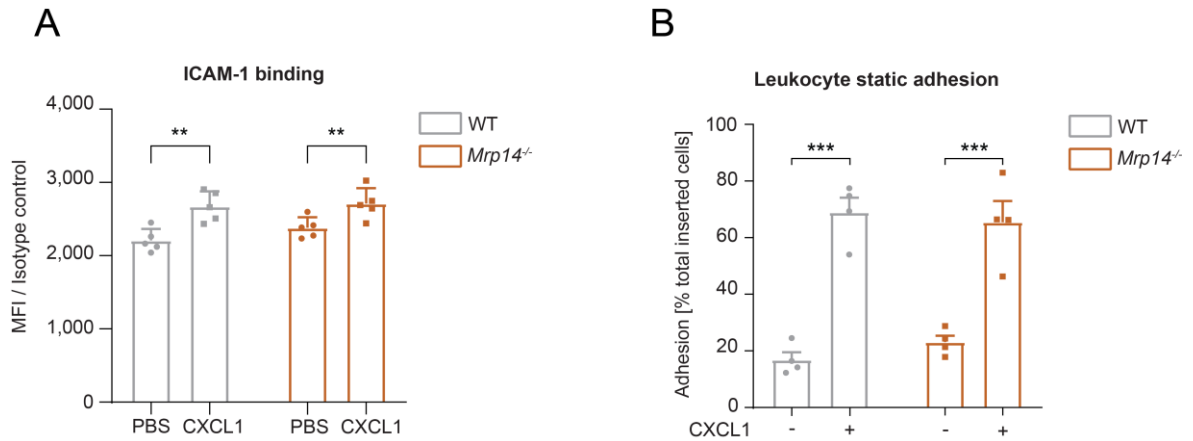
Figure 4.7: Neutrophil β₂ integrin activation (inside-out signaling) is not dependent on MRP8/14. (**A**) β₂ Integrin full activation state was measured by ICAM-1 binding to WT and *Mrp14⁻/⁻* neutrophils upon CXCL1 stimulation (10nM), compared to PBS control, by flow cytometry (MFI=median fluorescence intensity, mean±SEM, *n*=5 mice per group, 2way ANOVA, Sidak's multiple comparison). (**B**)) WT and *Mrp14⁻/⁻* isolated neutrophils were stimulated with CXCL1 (10nM) or PBS control for 10min, seeded on ICAM-1 coated plates for 45min and the percentage of adherent cells was analyzed through fluorescence intensity by spectroscopy (mean±SEM, *n*=4 mice per group, 2way ANOVA, Sidak's multiple comparison). ns, not significant; *P≤0.05, **P≤0.01, ***P≤0.001.

4.2.3 MRP8/14 sustains neutrophil spreading and polarization

Since β₂ integrin outside-in signaling and hydrodynamic shear forces have been demonstrated to be crucial for neutrophil recruitment and migration [227], we examined shear dependent neutrophil spreading and polarization. Flow chambers were coated with rmE-selectin, rmICAM-1 and rmCXCL1 and bone marrow–derived neutrophils from WT and *Mrp14⁻/⁻* mice were introduced and allowed to settle down for 2min. Thereafter, low shear stress was applied and time-lapse movies recorded. In order to study neutrophil spreading and polarization capacity, cell shape parameters were quantified (Fig.4.8-A). WT neutrophils displayed increased area (Fig.4.8-B) and perimeter (Fig.4.8-C), whilst they showed reduced circularity (Fig.4.8-D) and solidity (Fig.4.8-E) compared to *Mrp14⁻/⁻* neutrophils. Summarizing, MRP8/14 is dispensable for β₂ integrin activation under static conditions but indispensable for β₂ integrin outside-in signaling dependent neutrophil spreading and polarization under flow.
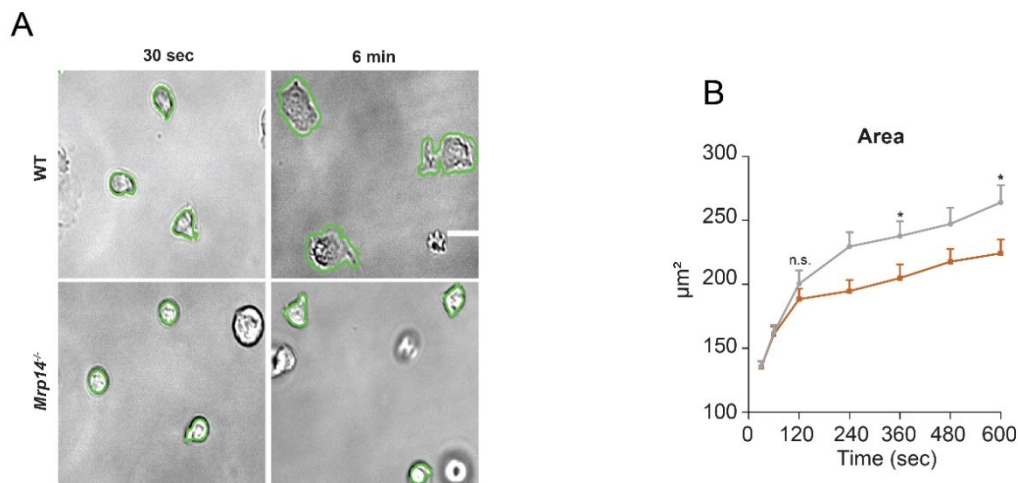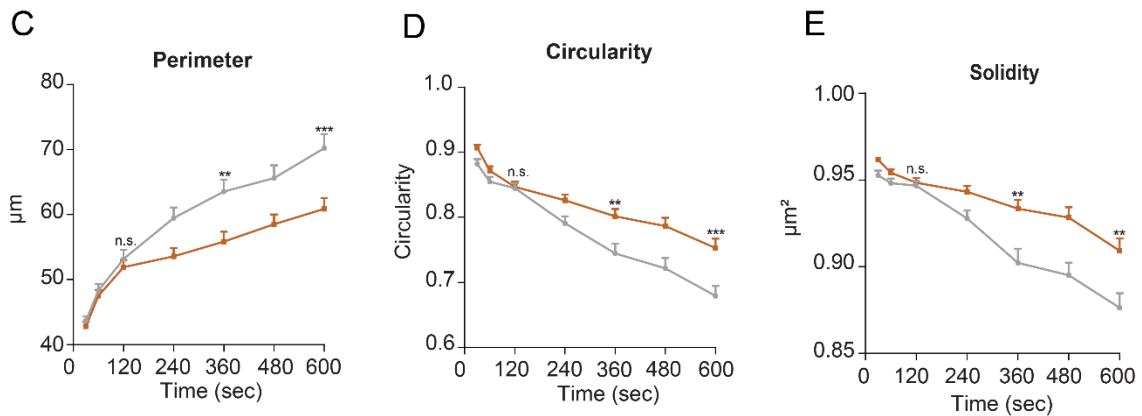
Figure 4.8: MRP8/14 sustains neutrophil spreading and polarization. (**A**) Representative bright-field images from 10min movies of WT and *Mrp14^{-/-}* isolated neutrophils spreading over E-selectin, ICAM-1, and CXCL1 coated plates (scale bar=10μm). Cell shape parameters like (**B**) area, (**C**) perimeter, (**D**) circularity [4π * (Area/Perimeter)] and (**E**) solidity [Area/Convex area] were analyzed over time [mean±SEM, *n*=103 (WT) and 96 (*Mrp14^{-/-}*) neutrophils of 4 mice per group, unpaired Student's *t*-test].

4.2.4   Loss of MRP8/14 negatively affects neutrophil crawling

It has been shown that post-arrest modifications, such as spreading and polarization, are crucial for intraluminal crawling of neutrophils, which allows them to finally find the right place to transmigrate into the inflamed tissue [223, 226]. Therefore, we studied the contribution of MRP8/14 to neutrophil crawling. In order to properly dissect the crawling behavior of neutrophils, *in vitro* experiments were conducted. As in the spreading experiments, flow chambers coated with rmE-selectin, rmICAM-1 and rmCXCL1 were used. However, after allowing WT and *Mrp14^{-/-}* bone marrow-derived neutrophils to settle down for 2 minutes, a higher but physiological shear rate (2dyn cm^{-1}) was used for the observation of crawling. In neutrophils lacking MRP8/14 a crawling pattern more inclined to direction of flow was observed, in contrast to WT neutrophils, which showed random behavior and also crawled in the opposite direction and perpendicular to the flow (Fig.4.9-A). In line with those findings, *Mrp14^{-/-}* neutrophils showed higher crawling travel distance in comparison to WT neutrophils (Fig.4.9-B). In addition, in the absence of MRP8/14, neutrophils displayed faster crawling velocities (Fig.4.9-C). Overall, MRP8/14 is indispensable for regular neutrophil crawling, which is another functional outcome dependent on outside-in integrin β$_2$ signaling.

B Accumulated Distance

C Leukocyte velocity

D Directionality
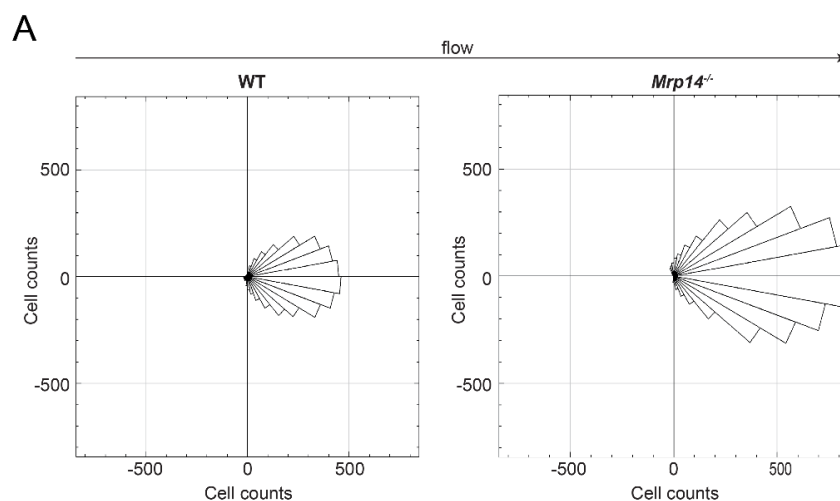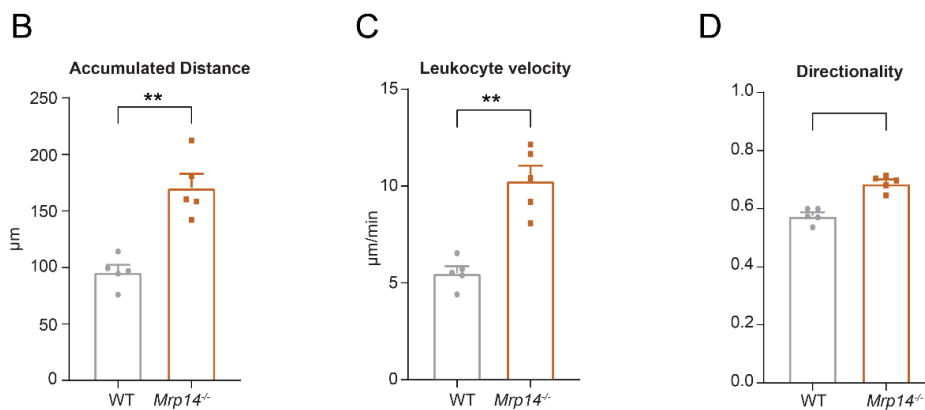
Figure 4.9: Loss of MRP8/14 negatively affects neutrophil crawling. (**A**) Representative rose plot diagrams indicating migratory trajectories of bone marrow-derived and matured WT and *Mrp14*^{-/-} neutrophils seeded in flow chambers, previously coated with E-selectin, ICAM-1, and CXCL1, under physiological shear stress (2dyne cm^{-2}). In addition, (**B**) crawling distance and (**C**) crawling velocity were calculated [mean±SEM, *n*=5 mice per group , 113 (WT) and 109 (*Mrp14*^{-/-}) neutrophils, paired Student's *t*-test]. ns, not significant; *$P \leq 0.05$, **$P \leq 0.01$, ***$P \leq 0.001$.

4.2.5 CXCL1 induced cytoskeletal rearrangements are decreased in the absence of MRP8/14

During integrin activation different cytoskeletal adapter proteins are recruited to the integrin tail to form adhesion complexes that link integrins to the actin cytoskeleton and create signaling hubs [243] sustaining neutrophil crawling and transmigration [242]. Therefore, Pyk2 and paxillin phosphorylation was investigated. WT and *Mrp14*^{-/-} bone marrow-derived neutrophils were seeded on ICAM-1 coated plates before being stimulated with CXCL1 or PBS control for 5min at 37°C. Cells were then lysed and western blotting performed. Phosphorylation of both Pyk2 (Fig.4.10-A) and paxillin (Fig.4.10-B) was reduced in *Mrp14*^{-/-} as compared to WT neutrophils, related to the total amount of protein.
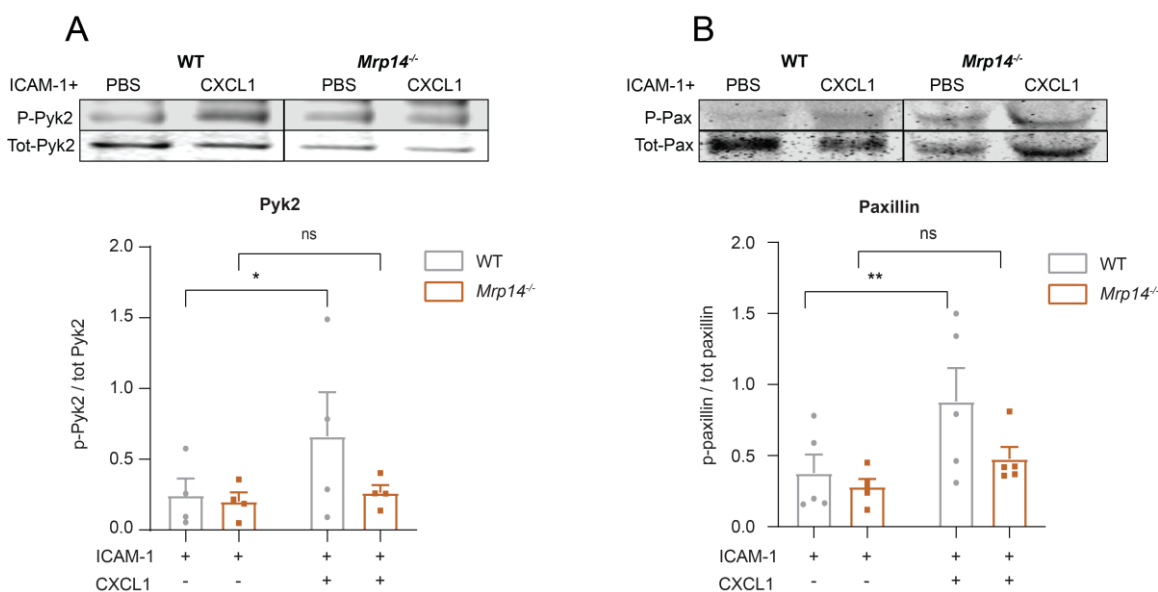
Figure 4.10: CXCL1 induced cytoskeletal rearrangements are decreased in the absence of MRP8/14. Representative western blot images and quantification of (**A**) Pyk2 and (**B**) Paxillin phosphorylation in WT and *Mrp14*^{-/-} neutrophils induced by CXCL1 stimulation (10nM) and ICAM-

1 binding compared to PBS control. (mean±SEM, representative western blot of *n*≥4 mice per group, 2way ANOVA, Sidak's multiple comparison). ns, not significant; *P≤0.05, **P≤0.01, ***P≤0.001.

4.2.6 MRP8/14 increases shear resistance *in vivo* and *in vitro*, supporting postarrest modifications

Neutrophils have been described to resist high shear stress during recruitment under inflammatory conditions [244] and this has been demonstrated to be dependent on β_2 integrin outside-in signaling [230]. Due to the previous results on defective outside-in signaling in the absence of MRP8/14, shear stress resistance was tested *in vivo* and *in vitro*. First, murine cremaster experiments in TNF-α treated WT and *Mrp14*$^{-/-}$ mice were conducted as described earlier (4.1.1). Vessels with high, however physiological, shear rates were considered and correlated to the number of adherent leukocytes quantified in those vessels. While no correlation was detected in WT vessels, in *Mrp14*$^{-/-}$ vessels a negative correlation between increasing vessel shear rates and the number of adherent cells was found (Fig.4.11-A). To further confirm those results, *in vitro* experiments were conducted adopting rmE-selectin, rmICAM-1, and rmCXCL1 coated flow chambers in which WT and *Mrp14*$^{-/-}$ neutrophils were inserted and increasing shear rates applied. In line with the *in vivo* findings, *Mrp14*$^{-/-}$ neutrophils were more susceptible to high shear forces and detached easier as compared to WT neutrophils (Fig.4.11-B). To recapitulate, the absence of MRP8/14 does not alter neutrophil surface marker expression and is not critical for β_2 integrin activation (inside-out signaling) under static conditions. However, MRP8/14 is indispensable for outside-in signaling dependent neutrophil postarrest modifications, crawling and cytoskeletal rearrangements together with shear resistance.
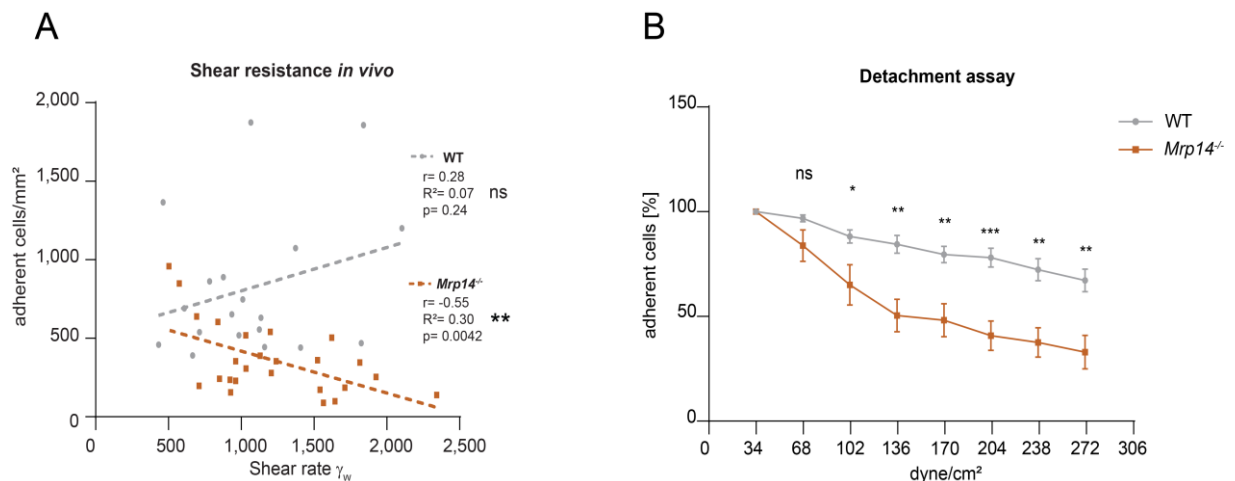
Figure 4.11: MRP8/14 increases shear resistance *in vivo* and *in vitro*, supporting postarrest modifications. (**A**) Correlation between increasing physiological shear stress and number of adherent leukocytes per vessel surface was determined in TNF-α treated WT and *Mrp14*$^{-/-}$ cremaster muscles [*n*=25 (WT) and 30 (*Mrp14*$^{-/-}$) vessels of 5 mice per group, Pearson correlation]. (**B**) Number of adherent WT and *Mrp14*$^{-/-}$ neutrophils as % of initially adherent cells was quantified in E-selectin, ICAM-1, and CXCL1 coated flow chambers after increasing shear stress was applied through a high-precision pump (30sec intervals) [mean±SEM, *n*=3 (WT) and 3 (*Mrp14*$^{-/-}$) flow chambers of 3 mice per group, unpaired Student's *t*-test]. ns, not significant; *P≤0.05, **P≤0.01, ***P≤0.001.

4.2.7 MRP8/14 prolongs extracellular Ca^{2+} entry without affecting ER store release

Next, the influence of MRP8/14 on neutrophil Ca^{2+} signaling was analyzed. Neutrophil Ca^{2+} flux increases in a shear dependent manner, and serves to mediate β_2 integrin adhesiveness and cytoskeletal rearrangements driven –postarrest modifications [227]. Hence, WT and *Mrp14*-/- bone marrow-derived neutrophils were fluorescently labelled with INDO-1, a ratiometric dye, and Ca^{2+} influx measured by flow cytometry (Fig.4.12-A). No difference could be detected in basal Ca^{2+} levels (Fig.4.12-B) or in calcium release-activated calcium channels (CRAC)–mediated early store-operated calcium entry (SOCE) (Fig.4.12-C) upon CXCL1 stimulation, in the presence or absence of MRP8/14 during the early phase of rapid Ca^{2+} entry. However, during late SOCE, a faster (Fig.4.12-D) and steeper (Fig.4.12-E) Ca^{2+} decay was observed in *Mrp14*-/- neutrophils compared to WT neutrophils. In order to see whether intracellular endoplasmic reticulum (ER) store release was also affected by MRP8/14, Ca^{2+} flux assays were repeated in the absence of extracellular Ca^{2+} (Fig.4.12-F). Again, no difference could be observed in basal Ca^{2+} levels prior to CXCL1 application (Fig.4.12-G). Interestingly, there was no difference in intracellular Ca^{2+} store release after cell stimulation between WT and *Mrp14*-/- neutrophils (Fig.4.12-H), suggesting that MRP8/14 affects mostly SOCE, which is dependent on extracellular free Ca^{2+}. Taken together, MRP8/14 does not affect neutrophil basal Ca^{2+} levels, ER store release or early SOCE phase. However, MRP8/14 prolongs late SOCE phases in murine neutrophils, which depends on extracellular Ca^{2+}.
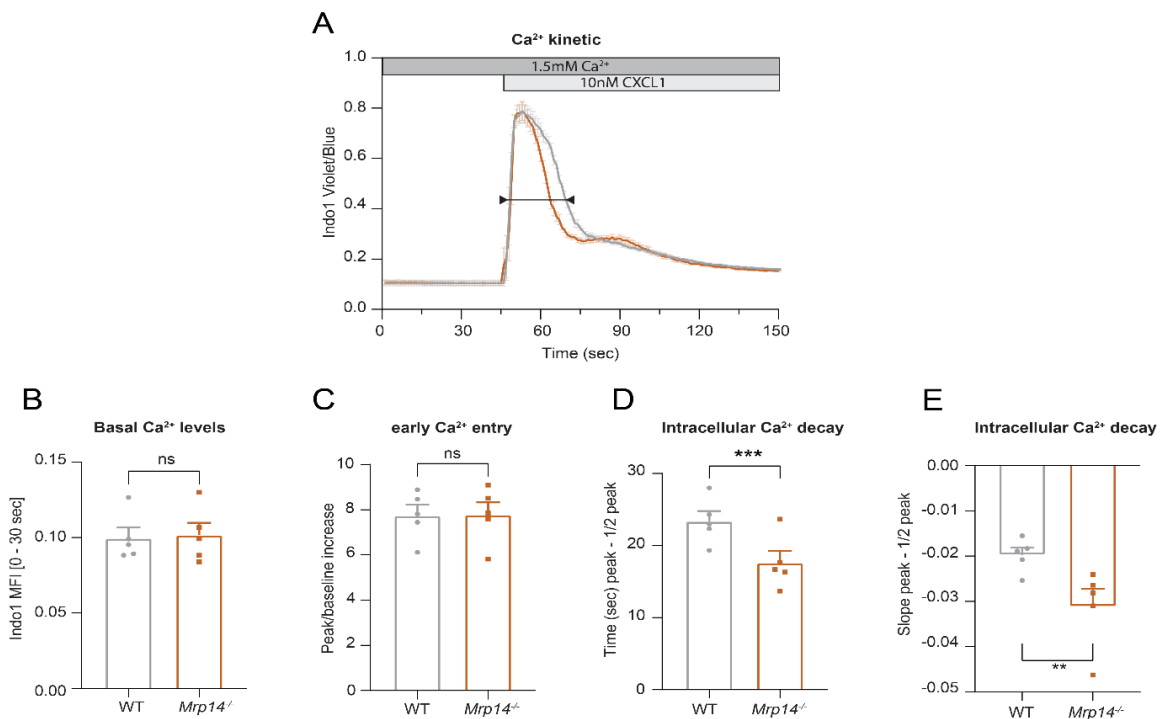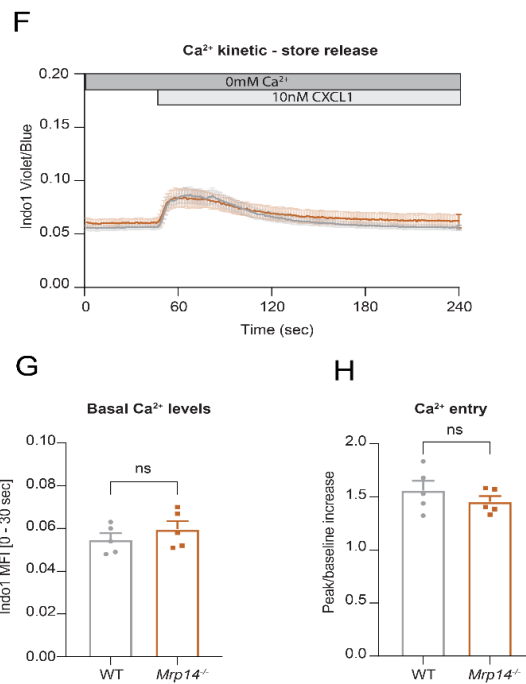
Figure 4.12: MRP8/14 prolongs extracellular Ca^{2+} entry without affecting ER store release.
(**A**) Average kinetic graphs of Ca^{2+} influx in the presence of extracellular Ca^{2+}(HBSS medium, 1.5mM Ca^{2+}) in WT and *Mrp14$^{-/-}$* neutrophils upon CXCL1 stimulation by flow cytometry (traces are shown as mean±SEM, *n*=5 mice per group, double-headed arrow represents the time points of quantification). (**B**) Quantification of Ca^{2+} levels before stimulation (MFI $_{0-30s}$) [mean±SEM, *n*=5 mice per group, paired Student's *t*-test]. (**C**) Quantification of endoplasmic reticulum (ER) store Ca^{2+} release and calcium released activated calcium channel (CRAC) store-operated Ca^{2+} entry (MFI $_{peak}$/ MFI $_{0-30s}$) [mean±SEM, *n*=5 mice per group, paired Student's *t*-test]. (**D**) Quantification of the Ca^{2+} influx time delay after CXCL1 stimulation (Time $_{peak - ½ peak}$) [mean±SEM, *n*=5 mice per group, paired Student's *t*-test]. (**E**) Quantification of the Ca^{2+} influx decay rate after CXCL1 stimulation (Slope $_{peak - ½ peak}$) [mean±SEM, *n*=5 mice per group, paired Student's *t*-test]. (**F**) Average kinetic graphs of Ca^{2+} store release in the absence of extracellular Ca^{2+} (Ca^{2+} free medium) in WT and *Mrp14$^{-/-}$* neutrophils upon CXCL1 stimulation by flow cytometry (traces are shown as mean±SEM, *n*=5 mice per group). (**G**) Quantification of Ca^{2+} levels before stimulation (MFI $_{0-30s}$) [mean±SEM, *n*=5 mice per group, paired Student's *t*-test]. (**H**) Quantification of rapid endoplasmic reticulum (ER) store Ca^{2+} release (MFI $_{peak}$/ MFI $_{0-30s}$) [mean±SEM, *n*=5 mice per group, paired Student's *t*-test]. ns, not significant; *P≤0.05, **P≤0.01, ***P≤0.001.

4.2.8 Loss of MRP8/14 does not alter intracellular basal Ca^{2+} levels but reduces Ca^{2+} levels upon neutrophil stimulation

To tackle the late SOCE effect caused by the lack of MRP8/14 in different experimental settings, confocal microscopy and fluorescence-lifetime imaging microscopy (FLIM) were adopted. For basal Ca^{2+} levels, bone marrow-derived Ca^{2+} reporter neutrophils from *Lyz2 GCaMP5* and *Mrp14$^{-/-}$ Lyz2 GCaMP5* mice were seeded on poly-L-lysine coated slides under static conditions. Single cell analysis and semi-automatic segmentation through the *Lyz2* channel were used. No difference in basal Ca^{2+} levels could be observed between *Lyz2 GCaMP5* and *Mrp14$^{-/-}$ Lyz2 GCaMP5* neutrophils (Fig.4.13-A). Then, rmE-selectin, rmICAM-1, and rmCXCL1 coated flow chambers were used to analyze Ca^{2+} levels in stimulated WT and *Mrp14$^{-/-}$* neutrophils under flow. Initially, confocal microscopy was adopted, *Lyz2 GCaMP5* and *Mrp14$^{-/-}$ Lyz2 GCaMP5* neutrophils were semi-automatically segmented through the *Lyz2* channel and cytosolic Ca^{2+} levels measured (Fig.4.13-B). *Mrp14$^{-/-}$ Lyz2 GCaMP5* neutrophils showed lower Ca^{2+} levels over

time, compared to *Lyz2 GCaMP5* neutrophils (Fig.4.13-C). Importantly, equal Calmodulin (CaM) levels were measured by western blotting in *Lyz2 GCaMP5* and *Mrp14$^{-/-}$ Lyz2 GCaMP5* neutrophil lysates (Fig. 4.13-D). In addition, FLIM was adopted in the same experimental settings. WT and *Mrp14$^{-/-}$* neutrophils were fluorescently labelled with oregon green bapta-1 and fluorescence lifetime measured. In line, *Mrp14$^{-/-}$* neutrophils showed decreased lifetime over time, compared to WT neutrophils (Fig.4.13-E, -F). Altogether, these results indicate that while MRP8/14 is dispensable for Ca^{2+} homeostasis under baseline conditions, it is critical for high Ca^{2+} fluxes during neutrophil activation.
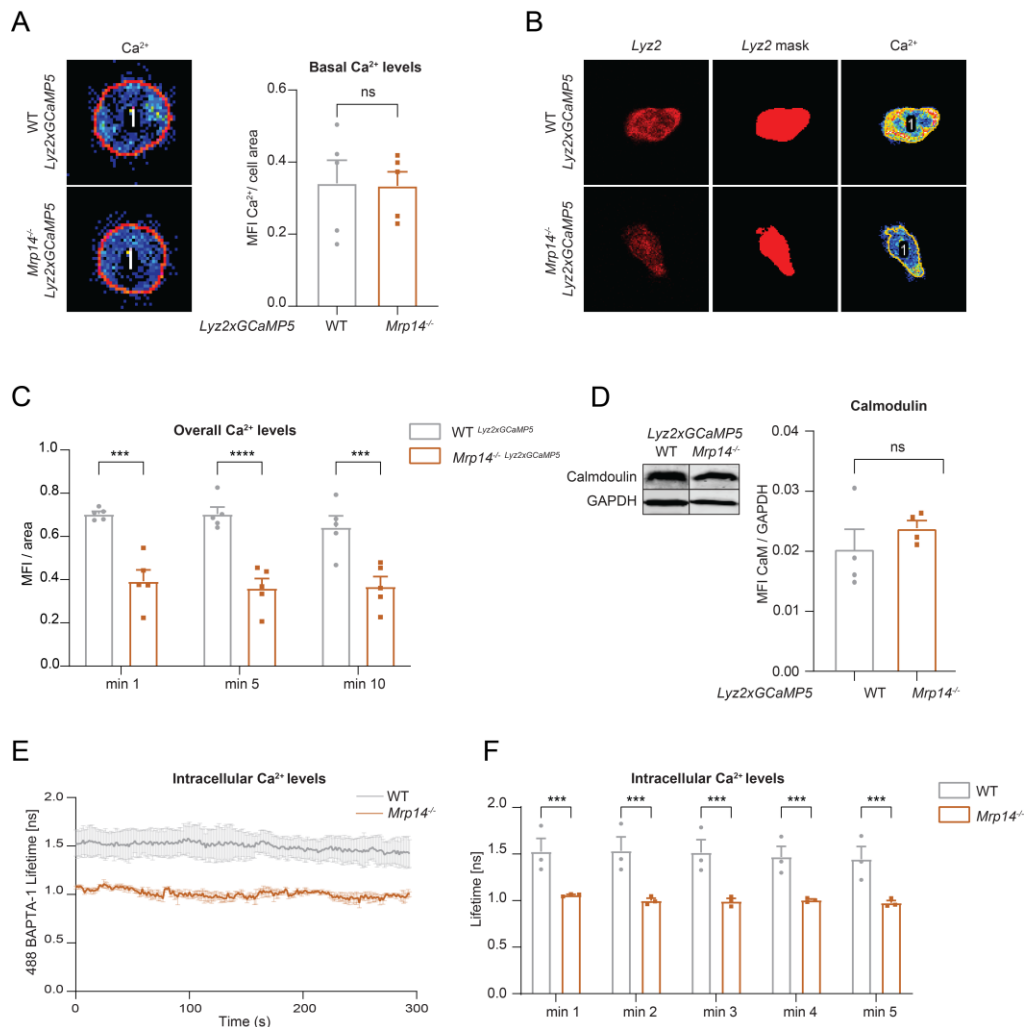
Figure 4.13: Loss of MRP8/14 does not alter intracellular basal Ca^{2+} but reduces Ca^{2+} levels upon neutrophil stimulation. (**A**) Representative confocal images and quantification of basal Ca^{2+} levels are shown in *Lyz2xGCaMP5* and *Mrp14$^{-/-}$ Lyz2xGCaMP5* neutrophils seeded over Poly-L-lysine coated slides and normalized to the cell area [mean±SEM, *n*=234 (WT) and 192 (*Mrp14$^{-/-}$*) neutrophils of 5 mice per group, paired Student's *t*-test]. (**B**) Segmentation strategy for overall Ca^{2+} measurement is displayed in *Lyz2xGCaMP5* and *Mrp14$^{-/-}$ Lyz2xGCaMP5* neutrophils crawling over E-selectin, ICAM-1, and CXCL1 coated flow chambers under physiological shear stress (2 dyn cm^{-1}). (**C**) Quantification of min0-1, min5-6 and min9-10 out of 10min time-lapse movie [mean±SEM, *n*=74 (WT) and 66 (*Mrp14$^{-/-}$*) neutrophils of 5 mice per group, 2way ANOVA, Sidak's multiple comparison]. (**D**) Representative western blot images and quantification of total calmodulin levels normalized to GAPDH signal, of *Lyz2xGCaMP5* and *Mrp14$^{-/-}$ Lyz2xGCaMP5* neutrophils (mean±SEM, *n*=4 mice per group, unpaired Student's *t*-test). (**E**) Average kinetic graph of Oregon green BAPTA-1 lifetime in WT and *Mrp14$^{-/-}$* neutrophils crawling over E-selectin, ICAM-1, and CXCL1 coated flow chambers under physiological shear stress (2 dyn cm^{-1}). (**F**)

Quantification of each of the 5min of time-lapse movie [mean±SEM, *n*=111 (WT) and 95 (*Mrp14⁻/⁻*) neutrophils of 3 mice per group, 2way ANOVA, Sidak's multiple comparison]. ns, not significant; *P≤0.05, **P≤0.01, ***P≤0.001.

4.2.9 Loss of MRP8/14 decreases Ca²⁺ availability at the LFA-1 cluster areas affecting LFA-1 cluster formation

The loss of MRP8/14 impaired β_2 integrin outside-in signaling dependent postarrest modifications. Outside-in signaling relies on Ca²⁺ availability at those adhesion complexes. To understand whether the differences in cytosolic Ca²⁺ levels were confined to the adhesion complexes or also observed in other parts of the cell, Ca²⁺ levels in the LFA-1 cluster sites were measured. *Lyz2 GCaMP5* and *Mrp14⁻/⁻ Lyz2 GCaMP5* neutrophils were fluorescently labelled for LFA-1 and inserted in rmE-selectin, rmICAM-1, and rmCXCL1 coated flow chambers. Then, the LFA-1 channel was semi-automatically segmented, size thresholded and region of interest (ROIs) of at least $0.15\mu m^2$ defined as LFA-1 nanoclusters (Fig.4.14-A). Interestingly, the number of LFA-1 nanoclusters was reduced in *Mrp14⁻/⁻ Lyz2 GCaMP5* compared to *Lyz2 GCaMP5* neutrophils (Fig.4.14-B). In addition, the segmented LFA-1 channel was back applied to the Ca²⁺ channel and Ca²⁺ levels in the LFA-1 nanocluster sites were measured (Fig.4.14-C). Strikingly, lower Ca²⁺ intensities in the LFA-1 nanocluster sites of *Mrp14⁻/⁻ Lyz2 GCaMP5* compared to *Lyz2 GCaMP5* neutrophils were detected over time (Fig.4.14-D). Importantly, Ca²⁺ intensities were normalized to the LFA-1 nanocluster areas. Afterwards, analysis of Ca²⁺ levels in the cytoplasmic area outside the LFA-1 nanocluster sites was carried out. *Lyz2 GCaMP5* and *Mrp14⁻/⁻ Lyz2 GCaMP5* neutrophils were first semi-automatically segmented through the *Lyz2* channel, then the LFA-1 mask (LFA-1 semi-automatically segmented channel) was subtracted from the *Lyz2* channel and LFA-1 negative areas obtained (fig.4.14-E). Surprisingly, no difference of Ca²⁺ levels in the LFA-1 negative areas between *Lyz2 GCaMP5* and *Mrp14⁻/⁻ Lyz2 GCaMP5* neutrophils were measured over time (Fig.4.14-F), suggesting that the differences observed in the whole cytosolic compartment (see Fig.4.13-B, -C, -E, -F) were entirely caused by differences in Ca²⁺ intensities in the LFA-1 nanoclusters. In summary, MRP8/14 is critical for Ca²⁺ supply at the LFA-1 nanocluster sites and maintains high Ca²⁺ levels only in those areas, sustaining LFA-1 nanocluster formation and turnover.
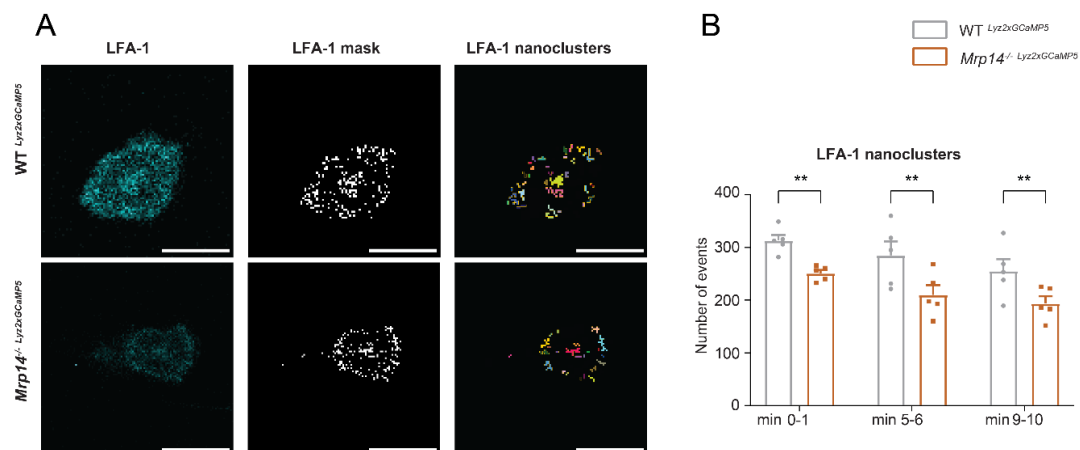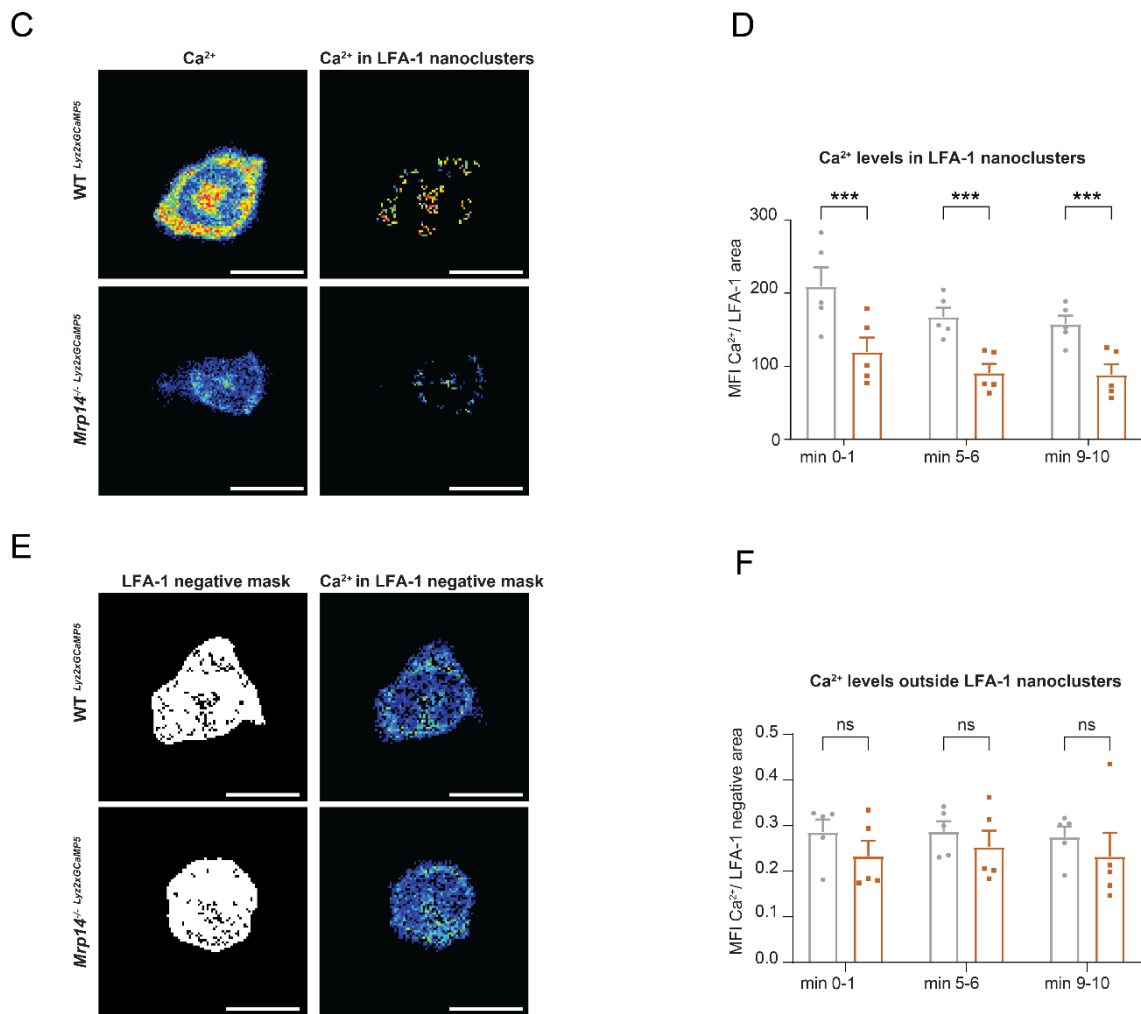
Figure 4.14: Loss of MRP8/14 decreases Ca²⁺ supply to LFA-1 cluster areas and affects LFA-1 cluster formation. (**A**) Semi-automatically segmented LFA-1 channel was size thresholded and LFA-1 nanoclusters (minimum 0.15μm²) were defined in *Lyz2xGCaMP5* and *Mrp14⁻/⁻ Lyz2xGCaMP5* neutrophils crawling over E-selectin, ICAM-1, and CXCL1 coated flow chambers under physiological shear stress (2 dyn cm⁻¹). (**B**) Quantification of the number of LFA-1 nanoclusters in min0-1, min5-6 and min9-10 out of 10min time-lapse movie [mean±SEM, *n*=56 (WT) and 54 (*Mrp14⁻/⁻*) neutrophils of 5 mice per group, 2way ANOVA, Sidak's multiple comparison]. (**C**) Size-excluded LFA-1 nanocluster mask was applied to the Ca²⁺ channel and (**D**) Ca²⁺ levels in the LFA-1 nanoclusters analyzed in *Lyz2xGCaMP5* and *Mrp14⁻/⁻ Lyz2xGCaMP5* neutrophils and normalized to the LFA-1 nanocluster areas with the previous time point strategy [mean±SEM, *n*=5 mice per group, 56 (WT) and 54 (*Mrp14⁻/⁻*) neutrophils, 2way ANOVA, Sidak's multiple comparison]. (**E**) LFA-1 negative cluster areas were obtained through automatic thresholding and segmentation of the *Lyz2* channel to which the LFA-1 size-excluded channel (LFA-1 nanocluster mask) was subtracted and applied to the Ca²⁺ channel. (**F**) Quantification of the cytosolic Ca²⁺ in the LFA-1 negative cluster areas was conducted in *Lyz2xGCaMP5* and *Mrp14⁻/⁻ Lyz2xGCaMP5* neutrophils and normalized to the negative cluster areas with the previous time point strategy [mean±SEM, *n*=5 mice per group, 56 (WT) and 54 (*Mrp14⁻/⁻*) neutrophils, 2way ANOVA, Sidak's multiple comparison]. ns, not significant; *$P \leq 0.05$, **$P \leq 0.01$, ***$P \leq 0.001$.

4.2.10 MRP8/14 increases F-actin polymerization, without affecting total actin levels

Sustained Ca^{2+} influx at the LFA-1 focal adhesion spots has been shown to enhance LFA-1 cluster formation and actin cytoskeleton remodeling, inducing postarrest modifications in neutrophils [245]. Therefore, F-actin polymerization was investigated. *Lyz2 GCaMP5* and *Mrp14^{-/-} Lyz2 GCaMP5* neutrophils were fluorescently labelled for F-actin and inserted in rmE-selectin, rmICAM-1, and rmCXCL1 coated flow chambers. Cells were semi-automatically segmented through the *Lyz2* channel and F-actin levels measured (Fig.4.15-A). *Mrp14^{-/-} Lyz2 GCaMP5* neutrophils showed lower F-actin levels over time, compared to *Lyz2 GCaMP5* neutrophils (Fig.4.15-B). Importantly, total actin levels, measured in cell lysates by wester blotting, were equal between *Lyz2 GCaMP5* and *Mrp14^{-/-} Lyz2 GCaMP5* neutrophils (Fig.4.15-C). To conclude, MRP8/14 prolongs late SOCE in neutrophils supplying Ca^2 specifically at the LFA-1 nanocluster areas, without affecting basal Ca^2 levels or Ca^2 levels outside the clusters. Through this specific Ca^{2+} modulation, MRP8/14 sustains neutrophil adhesion and postarrest modifications, mediating LFA-1 cluster formation and F-actin polymerization.
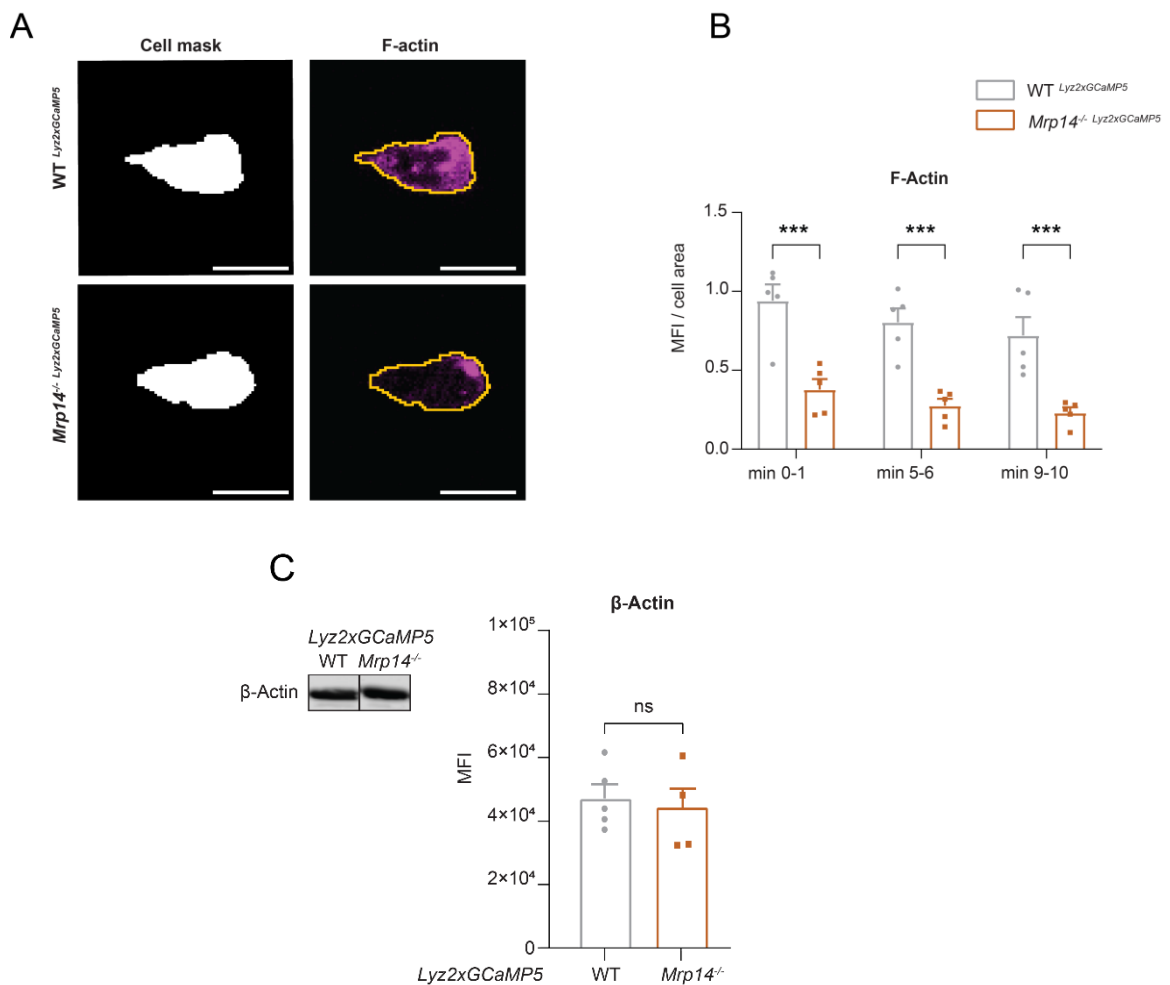
Figure 4.15: MRP8/14 increases F-actin polymerization without affecting total actin levels. (**A**) Segmentation strategy for overall F-actin measurement in *Lyz2xGCaMP5* and *Mrp14^{-/-} Lyz2xGCaMP5* neutrophils crawling over E-selectin, ICAM-1, and CXCL1 coated flow chambers under physiological shear stress (2 dyn cm^{-1}) and (**B**) F-actin quantification of min0-1, min5-6 and

min9-10 out of 10min time-lapse movie [mean±SEM, *n*=74 (WT) and 66 (*Mrp14⁻/⁻*) neutrophils of 5 mice per group, 2way ANOVA, Sidak's multiple comparison]. (**C**) Representative western blot images and quantification of total actin levels (β-Actin) of *Lyz2xGCaMP5* and *Mrp14⁻/⁻ Lyz2xGCaMP5* neutrophils (mean±SEM, *n*≥4 mice per group, unpaired Student's *t*-test). ns, not significant; *P≤0.05, **P≤0.01, ***P≤0.001.

4.3   MRP8/14 is critical for neutrophil inflammatory responses and effector functions

4.3.1   Decreased CREB1 and p38 phosphorylation in the absence of cytosolic MRP8/14, regardless of extracellular MRP8/14

In neutrophils, Ca^{2+} together with calmodulin (CaM) are the only activators of the CaM kinase I D (CaMKID), which in human neutrophils has been demonstrated to regulate proliferative responses, respiratory burst and cytokine transcription, principally through CAMP responsive element binding protein 1 (CREB1) and p38 phosphorylation [246, 247]. To investigate CREB1 and p38 phosphorylation, WT and *Mrp14⁻/⁻* bone marrow-derived neutrophils were plated over ICAM-1 coated slides and stimulated with PBS control, CXCL1 or Phorbol-12-Myristate-13-Acetate (PMA), as positive control, 5min and 20min at 37°C. Then, cells were lysed and western blotting performed. CREB1 phosphorylation, normalized to total CREB1 levels, was increased in WT but not in *Mrp14⁻/⁻* neutrophils upon CXCL1 stimulation (Fig.4.16-A and -B). Alike, p38 phosphorylation, normalized to total p38 levels, was induced after 5min of CXCL1 stimulation in WT neutrophils (Fig.4.16-C) but not in *Mrp14⁻/⁻* neutrophils (Fig.4.16-D). Next, we tested whether CREB1 and p38 phosphorylation depends on extracellular MRP8/14. To do so, WT and *Mrp14⁻/⁻* neutrophils were pre-treated with Paquinimod to block extracellular MRP8/14 interaction with TLR-4 (in WT cells) and CREB1 and p38 phosphorylation was again investigated after 5min of CXCL1 stimulation. Treatment of WT neutrophils with Paquinimod did not change CREB1 and P38 phosphorylation rate upon CXCL1 stimulation (Fig.4.16-E and -F) suggesting that cytosolic but not extracellular MRP8/14 mediates CREB1 and p38 phosphorylation.
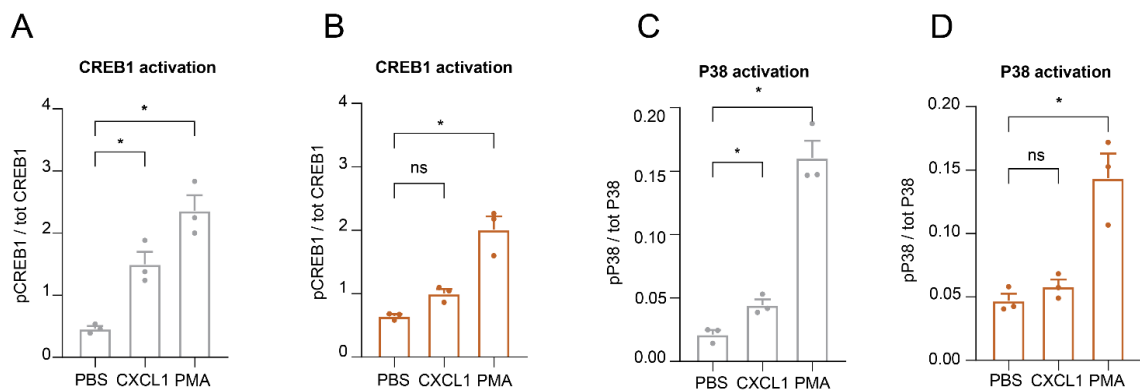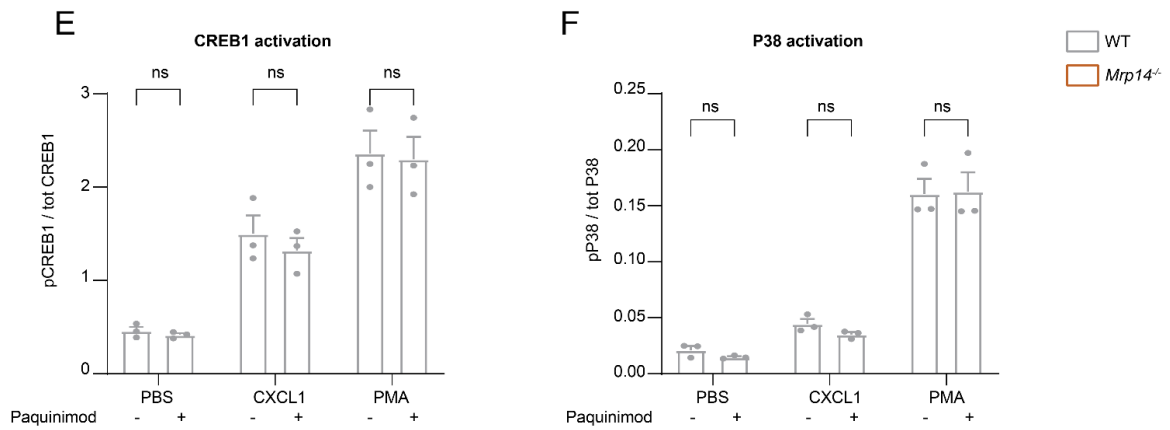
Figure 4.16: Decreased CREB1 and p38 phosphorylation in the absence of cytosolic MRP8/14, regardless of extracellular MRP8/14. (**A**) WT and (**B**) *Mrp14*-/- neutrophils were plated over ICAM-1 coated dishes, stimulated with CXCL1, PMA or PBS control and CREB1 phosphorylation was analyzed by western blotting (mean±SEM, n=3 mice per group, RM one-way ANOVA, Tukey's multiple comparison). (**C**) WT and (**D**) *Mrp14*-/- neutrophils were plated over ICAM-1 coated dishes, stimulated with CXCL1, PMA or PBS control and P38 phosphorylation was analyzed by western blotting (mean±SEM, n=3 mice per group, RM one-way ANOVA, Tukey's multiple comparison). (**E**) WT neutrophils were plated over ICAM-1 coated dishes, stimulated with CXCL1, PMA or PBS control after Paquinimod or NaCl treatment. CREB1 phosphorylation was analyzed by western blotting (mean±SEM, n=3 mice per group,2way ANOVA, Sidak's multiple comparison). (**F**) WT neutrophils were plated over ICAM-1 coated dishes, stimulated with CXCL1, PMA or PBS control after Paquinimod or NaCl treatment. P38 phosphorylation was analyzed by western blotting (mean±SEM, n=3 mice per group,2way ANOVA, Sidak's multiple comparison). ns, not significant; *$P \leq 0.05$, **$P \leq 0.01$, ***$P \leq 0.001$.

4.3.2 Loss of MRP8/14 results in lower neutrophil phagocytic activity

Cytosolic Ca^{2+} oscillations also control uptake and embedding of foreign particles [248] during neutrophil phagocytosis. To study the role of MRP8/14 in neutrophil phagocytosis, whole blood from WT and *Mrp14*-/- mice was harvested, incubated with *E.coli* fluorescently labelled particles for 30min at 37°C or 4°C and flow cytometry used for analysis. As expected, almost no phagocytic activity was observed in WT or *Mrp14*-/- neutrophils at 4°C. At 37°C, *Mrp14*-/- neutrophils showed decreased phagocytic capacity compared to WT neutrophils (Fig.4.17-A). Representative images, taken by confocal microscopy, confirmed those results showing lower intracellular bacterial burden in *Mrp14*-/- compared to WT neutrophils (Fig.4.17-B). In conclusion, MRP8/14 and its Ca^{2+} regulation are fundamental for neutrophil intracellular signaling pathways during phagocytosis.
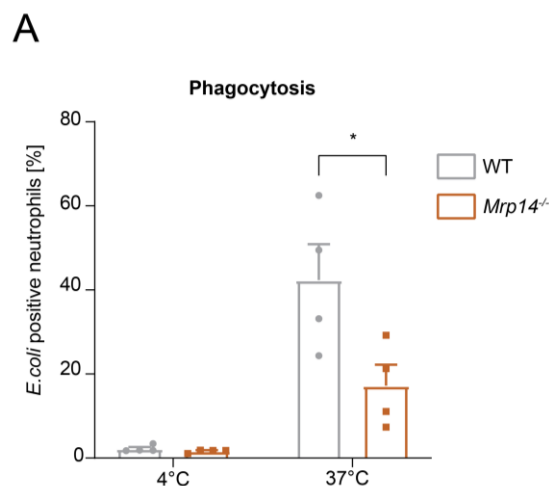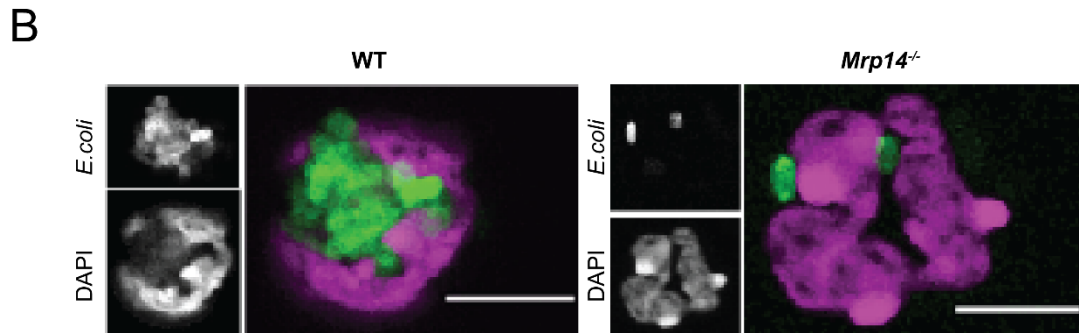
Figure 4.17: Loss of MRP8/14 results in lower neutrophil phagocytic activity. Blood from WT and *Mrp14^{-/-}* mice was incubated with *E.coli* fluorescently labelled particles at 4°C or 37°C for 30min and rate of neutrophil phagocytosis was determined (**A**) by flow cytometry (mean±SEM, n=4 mice per group,2way ANOVA, Sidak's multiple comparison). (**B**) Representative confocal images of *E.coli* phagocyted particles by WT and *Mrp14^{-/-}* neutrophils. ns, not significant; *$P \le 0.05$, **$P \le 0.01$, ***$P \le 0.001$.

5.   Discussion

The fine-tuning of the different steps during neutrophil recruitment is fundamental to carry out an appropriate immune response and avoid tissue damage [136]. During rolling, rather roundish neutrophils start to scan the surroundings to look for environmental cues that lead them to firmly adhere to the endothelial surface and crawl to find appropriate spots to extravasate. Upon adhesion and concomitantly high Ca^{2+} influx, neutrophils polarize and change their shape to flatten over the endothelial surface. Ca^{2+} is a fundamental second messenger, which in neutrophils, like in other immune cells, only rises during cell activation to support a wide range of processes [207]. In addition, Ca^{2+} levels in neutrophils must be tightly controlled to avoid hyperactivation and cell death. MRP8/14 is a Ca^{2+} binding protein expressed predominantly by myeloid cells, particularly neutrophils, where it represents nearly half of the cytosolic protein content. Once secreted, it was shown to act as a DAMP activating neutrophil β_2 integrins through an autocrine TLR-4 dependent positive feedback loop [12]. Its presence in patients serum correlates with a series of different acute and chronic inflammatory diseases [4]. However, the abundance of cytosolic MRP8/14 hints at an intracellular function of the protein, which remained elusive for many years. This work examined potential roles of intracellular MRP8/14 during neutrophil recruitment, especially during Ca^{2+} -dependent steps like adhesion, crawling and postarrest modifications. Our data demonstrated that intracellular MRP8/14 acts as a local Ca^{2+} supplier at LFA-1 focal adhesion spots during β_2 integrin outside-in signaling–dependent neutrophil functions. Local Ca^{2+} supply provided by intracellular MRP8/14 supported LFA-1 nanocluster formation and aggregation together with F-actin polymerization supporting cell polarization, crawling and finally transendothelial migration.

5.1   Intracellular MRP8/14 affects neutrophil recruitment, independent of extracellular MRP8/14

5.1.1   Intracellular MRP8/14 remains abundant in neutrophil cytoplasm upon inflammation

During neutrophil recruitment, MRP8/14 has been shown to be released from neutrophil cytoplasm [12] through a newly described NLRP3 - Caspase 1 – N-terminal GSDMD pathway, which causes the release of small molecules such as alarmins in a timely restricted manner during intravascular neutrophil recruitment [64]. Interestingly, ELISA assays demonstrated that as much as E-selectin triggers MRP8/14 release in neutrophils, only as little as ~1% of the total protein content in neutrophils is released during intravascular recruitment. In line, MRP14 immunofluorescence staining of TNF-α –treated cremaster muscles of WT mice showed no difference in MRP8/14 levels between intravascular and extravasated neutrophils. In addition, WT neutrophils seeded on Poly-L-lysine, E-selectin or E-selectin, ICAM-1 and CXCL1 coated slides and immunofluorescently labelled for MRP14 did not show any significant difference in MRP14

levels. These results show that even though MRP8/14 release enhances and strengthen neutrophil recruitment during inflammation, the major part of the protein still remains in the neutrophil cytosolic compartment.

5.1.2 Neutrophil show functional rolling but impaired adhesion in the absence of intracellular MRP8/14

The first step of the neutrophil recruitment cascade is characterized by the inducible expression of selectins on the endothelial surface caused by sterile injury or inflammatory stimuli like TNF-α. [138]. While P-selectin initiates neutrophil rolling, it is E-selectin that mediates neutrophil slow rolling due to a slower bond dissociation rate and higher density expression, with rolling velocities 5-10 times slower than P-selectin rolling velocities [147]. Indeed, in untreated WT mice, we recorded rolling velocities of ~20µm/s, expected for P-selectin dependent rolling [148, 249], and upon E-selectin blocking antibody injection no difference could be observed. However, when we treated mice with TNF-α, neutrophil rolling velocities significantly dropped to ~5-8µm/s, as previously reported for E-selectin-dependent rolling [147, 242]. Then, when we injected E-selectin blocking antibody we could functionally restore P-selectin–dependent rolling, with rolling velocities of ~20µm/s. When we treated $Mrp14^{-/-}$ mice with TNF-α, we observed no difference in number of rolling neutrophils compared to WT mice. In addition, during acute inflammation, intracellular MRP8/14 is dispensable for E-selectin–mediated rolling behavior of neutrophils, since WT and $Mrp14^{-/-}$ neutrophils showed comparable rolling velocities. Contrarily, Pruenster et al. showed that extracellular MRP8/14 reduces neutrophil rolling velocity in vivo, acting through TLR4 [12]. In line with our *in vivo* findings, when we coated glass capillaries with E-selectin, ICAM-1 and CXCL1 and assembled them into microflow chambers, we did not detect any difference in number of rolling cells both *in vitro* and *ex vivo* between WT and $Mrp14^{-/-}$ neutrophils. When we analyzed number of adherent cells we observed significant lower number of adherent $Mrp14^{-/-}$ neutrophils compared to WT ones, both *in vivo*, *ex vivo* and *in vitro*. However, previous publications already showed that extracellular MRP8/14 enhances neutrophil recruitment through increasing Mac-1 binding affinity on the neutrophil surface [250] or inducing a thrombogenic response in microvascular endothelial cells (ECs) [84], indicating that the absence of MRP8/14 causes the adhesion defect in $Mrp14^{-/-}$ neutrophils. As shown below and discussed in the next paragraphs, intracellular MRP8/14 is critical for sustained firm adhesion and the following postarrest modifications whereas extracellular MRP8/14 is mostly involved in activating neutrophils and leading them to firm adhesion.

5.1.3 Genetic loss of MRP8/14 cannot be rescued by extracellular MRP8/14

As already mentioned earlier, extracellular MRP8/14 induces the switch of β$_2$ integrins from low to intermediate and high-affinity conformation through a TLR4 autocrine activation loop in neutrophils [12], inducing the transition from slow rolling to adhesion in a parallel fashion

compared to the classical GPCR signaling pathway [136]. In addition, MRP8/14 was also shown to induce upregulation of CD11b surface expression on monocytes, triggering adhesion to fibrinogen and consequently increasing number of adherent cells at sites of inflammation [251]. Therefore, we investigated WT and $Mrp14^{-/-}$ neutrophil adhesion in a TNF-α–induced acute inflammation model upon mutMRP8/14 application. It was already known that mutMRP8/14 is not able to form tetramers in the presence of Ca^{2+} and that this allows the heterodimer to still bind TLR4 and induce signaling even in a high Ca^{2+} milieu such as in blood plasma [65]. While mutMRP8/14 induced adhesion in WT neutrophils, no difference could be detected after mutMRP8/14 application in $Mrp14^{-/-}$ neutrophils. In addition, same results were obtained after mutMRP8/14 application in trauma-induced inflammation leading to P-selectin but not E-selectin expression [148], and therefore no MRP8/14 release from WT neutrophils [12]. In line with those results, when we adopted microflow chamber devices coated with E-selectin, ICAM-1, CXCL1 and additionally mutMRP8/14 we could not rescue the lower adhesion observed in $Mrp14^{-/-}$ neutrophils. Therefore, mutMRP8/14 triggered adhesion in WT neutrophils but had no effect in $Mrp14^{-/-}$ neutrophils. Russo et al. already described the antagonizing effects of mutMRP8/14 and wildtype MRP8/14 complexes [252]. While mutMRP8/14 promoted inflammation through TLR4 binding, wildtype MRP8/14 rapidly formed tetramers at high Ca^{2+} concentration [65] and lowered STAT3 phosporylation restoring adhesion and migration properties in $Mrp14^{-/-}$ monocytes, signaling through CD69 [252]. Therefore, our findings imply a distinct role for intracellular MRP8/14 during neutrophil recruitment, whose deficiency cannot be substituted by adding extracellular MRP8/14 to restore the TLR4 autocrine activation loop.

5.1.4 Intracellular MRP8/14 is essential for efficient neutrophil extravasation during inflammation

During the last steps of the recruitment cascade a series of interactions between different endothelial cell adhesion molecules, mainly ICAM-1 and VCAM-1, and neutrophil integrins, mainly LFA-1 and Mac-1, occurs to help neutrophils to transmigrate into the perivascular tissue via the paracellular or transcellular route [114]. In line with defective neutrophil adhesion, Giemsa staining of TNF-α stimulated cremaster muscle tissue revealed lower leukocyte extravasation in the absence of intracellular MRP8/14. Similar results were obtained with the Rap1 binding–deficient Talin1 knock-in mice, which had comparable rolling velocities but defective adhesion and impaired extravasation compared to WT animals [253]. Kurz et al. uncovered that Mst1 deficiency lead to decreased transmigration into inflamed tissue, with neutrophil accumulation at the abluminal site of the posticapillary venules failing to penetrate the basement membrane [239]. Similarly, Rohwedder et al. discovered that Src family kinases are required for Rab27a-dependent mobilization of NE, VLA3 and VLA6 vesicles leading to basement membrane penetration and extravasation [254]. The evaluation of different leukocyte subsets in the perivascular area showed that the extravasation defect only occurred in $Mrp14^{-/-}$ neutrophils but not in other leukocyte subtypes, indicating again that it is an intrinsic cellular defect rather than a generalized one.

5.2 Intracellular MRP8/14 is dispensable for inside-out signaling but critical for outside-in signaling of β_2 integrins

5.2.1 Static activation of β_2 integrins is not dependent on intracellular MRP8/14

Among the family of adhesion molecules that have been identified on both the endothelial and neutrophil surface we find the integrin family, the selectin family, the Ig superfamily such as ICAMs, as well as chemokine receptors and some other transmembrane proteins [255]. When we checked expression of surface adhesion markers in blood neutrophils, like LFA-1 and Mac-1, L-selectin, PSGL-1, CD44 and CXCR2, we could not detect any difference between WT and *Mrp14*$^{-/-}$ cells. In addition, other colleagues showed that members of the Src kinase family like Hck and Fgr altered neutrophil outside-in dependent sustained adhesion without affecting rapid inside-out integrin activation under static conditions [256]. Similarly, when we checked inside-out β_2 integrin activation under static conditions with a soluble ICAM-1 binding assay upon CXCL1 stimulation we measured equal amount of ICAM-1 bound to WT and *Mrp14*$^{-/-}$ neutrophils, indicating the same degree of β_2 integrin activation. Although neutrophil firm adhesion to the inflamed endothelium has been demonstrated to be dependent on both LFA-1 and Mac-1 β_2 integrins [171], blocking LFA-1 nearly completely abolished any chemokine-triggered adhesion indicating that LFA-1 is the main β_2 integrin mediating initial firm adhesion in neutrophils under shear conditions [257].

5.2.2 Outside-in signaling-dependent postarrest modifications, cytoskeletal rearrangements, crawling and shear resistance rely on intracellular MRP8/14

To elucidate the mechanisms of MRP8/14-dependent neutrophil adhesion and extravasation, we investigated outside-in signaling initiated by high-affinity β_2 integrins and ligand binding, necessary to stabilize β_2 integrin mediated adhesion and postarrest modifications [258]. *Hck*$^{-/-}$ and *Fgr*$^{-/-}$ neutrophils showed functional β_2 integrin activation under static conditions but reduced capability to spread over β_2 integrin ligands. In the same way, MRP8/14 influenced outside-in dependent neutrophil spreading inducing an increment of cell surface area and perimeter, decreasing cell circularity and solidity. Intraluminal crawling is the subsequent step following firm adhesion, polarization and cell spreading. Philipson et al. described that in inflamed microvessels there was equivalent adhesion in wildtype or Mac-1 deficient neutrophils but lower adhesion in LFA-1 deficient neutrophils while Mac-1, but not LFA-1, deficiency let to impaired neutrophil crawling [259]. In T cells, it was demonstrated that crawling is mainly dependent on LFA-1 [260] as only a subset of CD8$^+$ T cells expresses Mac-1 [261]. In addition, LFA-1-mediated crawling distances are higher than Mac-1 mediated crawling distances in monocytes [262, 263]. When we

studied neutrophil crawling, we used *in vitro* flow chamber devices that would support LFA-1 mediated crawling and we observed that in the absence of MRP8/14, neutrophils crawled in an intermittent fashion, like the one recently described by Vadillo and colleagues [264]. Indeed, *Mrp14⁻/⁻* neutrophils crawled for longer distances, with more directional behavior and higher velocity. During crawling, ligand-bound integrins are connected to the cortical actin via multiple adapters and mediators such as talin, kindlin3 [265], paxillin and others [266], allowing cytoskeleton remodeling and cell shape modification. Among those, paxillin has been shown to be an essential player in linking talin with the integrin co-activator kindling-2 [267]. In addition, in stimulated primary human PMNs, paxillin has been demonstrated to associate with Pyk2, another adapter protein of the FAK family that localizes to focal adhesions and podosomes [268]. In adherent neutrophils spread over ICAM-1 coated wells and stimulated with CXCL1, MRP8/14 was essential to guarantee appropriate Pyk2 and paxillin phosphorylation. It was shown that during early activation stages, physiological shear forces dampened neutrophil activation through internalization of the formyl peptide receptor (FPR), reducing L-selectin shedding and Mac-1 activation [269]. However, shear stress acting on already adherent PMNs was demonstrated to be crucial to mechanically transmit tensile forces to LFA-1/ICAM-1 adhesive bonds providing PMNs with migration guidance and spatial cues in response to vascular inflammation [227]. In addition, different spatial localization of β_2 integrins results in a different force regime and resistance in shear flow: Mac-1 is distributed equally over the cell body and serves primarily in cell migration, while LFA-1 locates mainly at the microvilli, accumulates at the uropod and is the integrin mediating shear resistant neutrophil arrest [230]. Further, shear-induced signaling through LFA-1 has demonstrated to be essential since T cells fail to perform TEM under shear-free conditions, even in the presence of chemokines [270]. In line with our findings on spreading and crawling, when we re-analyzed intravital videos looking at the correlation between adherent cells and increasing physiological shear rates we found no correlation in WT neutrophils but a negative correlation in *Mrp14⁻/⁻* neutrophils. Furthermore, number of adherent *Mrp14⁻/⁻* neutrophils decreased significantly compared to WT neutrophils in vitro, when increasing shear rates were applied in E-selectin, ICAM-1 and CXCL1 coated flow chambers.

5.3 Intracellular MRP8/14 controls and supplies Ca^{2+} in neutrophils

5.3.1 Altered overall Ca^{2+} kinetics in the absence of MRP8/14

Already in the early 2000s, McNeill showed that MRP8/14 was critical to maintain Ca^{2+} influx in neutrophils upon application of different stimuli, including CXCL1 [74]. In addition, Hobbs and colleagues showed that the Ca^{2+} response of *Mrp14⁻/⁻* neutrophils to the chemokine MIP-2 was diminished by ~40% but that Ca^{2+} release from intracellular stores and Ca^{2+} entry through the plasma membrane were perfectly functioning [8]. To decipher the contribution of MRP8/14 to neutrophil Ca^{2+} signaling, we investigated ER store release induced by CXCL1 stimulation in the

absence of extracellular Ca^{2+} and observed similar kinetics between WT and $Mrp14^{-/-}$ neutrophils by flow cytometry. Indeed, basal Ca^{2+} levels prior to CXCL1 stimulation were equal and Ca^{2+} store release was not impaired in MRP14-deficient neutrophils, similarly to what was shown for ORAI1 and ORAI2-decifient neutrophils [240]. However, when we analyzed SOCE induced by CXCL1 in the presence of extracellular Ca^{2+} we observed a different signal kinetic in the absence of MRP8/14. While basal Ca^{2+} levels and CRAC channel functionality were unaffected by the lack of MRP8/14, as previously shown by McNeill et al. [74], late SOCE had shorter duration with a faster and steeper decay in MRP14-deficient neutrophils. McNeill et al. also observed reduced calcium response to CXCL1, but only at lower chemokine concentrations [74]. We further confirmed those flow cytometry data by confocal microscopy, where Ca^{2+} reporter neutrophils lacking MRP8/14 showed comparable Ca^{2+} intensities before any stimulus was applied under static conditions. In addition, when we seeded those Ca^{2+} reporter neutrophils into E-selectin, ICAM-1 and CXCL1 coated flow chambers under physiological shear conditions, we also observed lower intracellular Ca^{2+} flickers intensity in $Mrp14^{-/-}$ compared to WT neutrophils. We also used *Lyz2xGCaMP5* and *Mrp14$^{-/-}$ Lyz2xGCaMP5* mice, which are Ca^{2+} reporter mice and rely on the CaM binding motif [271]. No differences in CaM levels were detected by western blotting between *Lyz2xGCaMP5* and *Mrp14$^{-/-}$ Lyz2xGCaMP5* neutrophils. In order to strengthen our findings on impaired Ca^{2+} signaling in the absence of MRP8/14, we implemented FLIM, which gives access to the fluorescence decay time and is independent of variations in dye concentration, allowing a more reliable quantification [272]. Adopting the same flow chamber settings as before, we measured lower Ca^{2+} lifetime in neutrophils, in the absence of MRP8/14, confirming our previous results. Altogether, these results show altered Ca^{2+} signaling kinetics in $Mrp14^{-/-}$ neutrophils during the late SOCE phases with lower intracellular Ca^{2+} levels and faster signal decay, while basal Ca^{2+} levels and Ca^{2+} release from intracellular stores are not affected.

5.3.2 MRP8/14 supports LFA-1 clustering and F-actin polymerization through subcellular Ca^{2+} supply at the adhesion spots

Recent work showed that ORAI1 mediated Ca^{2+} influx reflects a signal transduction mechanism that via mechanical force translates the tension on high-affinity LFA-1 into a Ca^{2+} signal, stabilizing the high-affinity LFA-1 bond clusters during neutrophil firm arrest [223]. In addition, LFA-1 clustering has been shown to be tightly dependent on intracellular Ca^{2+} as Ca^{2+} depletion resulted in impaired LFA-1 clustering in PMNs [229]. Indeed, because of the disturbed Ca^{2+} signaling in $Mrp14^{-/-}$ neutrophils, these cells formed less LFA-1 nanoclusters compared to WT neutrophils in flow chamber experiments when shear stress was applied. Using the LFA-1 nanocluster mask, we investigated Ca^{2+} events in the LFA-1 nanocluster areas and detected lower Ca^{2+} flicker intensities in $Mrp14^{-/-}$ neutrophils compared to WT neutrophils. However, using a LFA-1 negative mask, obtained by subtracting the LFA-1 mask from the neutrophil cell mask, we could not observe any difference in Ca^{2+} flicker intensities outside the LFA-1 nanocluster areas between WT and $Mrp14^{-/-}$ neutrophils. These results indicate that the disturbed Ca^{2+} events observed in $Mrp14^{-/-}$ neutrophils are rather subcellular than broad-cytosolic defective Ca^{2+} signals. In

neutrophils, Ca^{2+} influx relies on the amount and conformation of LFA-1/ORAI1 clusters, which in turn correlates with F-actin polymerization [229]. It occurs primarily through ORAI1, which colocalizes at the LFA-1 focal adhesion sites, promoting LFA-1 clustering and F-actin polymerization at the leading and trailing edge of polarized PMNs [227, 273]. In line with that, we found lower F-actin levels during crawling and postarrest modifications in $Mrp14^{-/-}$ neutrophils compared to WT neutrophils despite equal total actin levels measured by western blotting. These findings indicate that the faulty Ca^{2+} signaling in the absence of MRP8/14 is not a generalized defect but rather a subcellular one with impaired Ca^{2+} supply only at the LFA-1 nanocluster sites and consequent less LFA-1 nanocluster formation, F-actin polymerization and diminished neutrophil adhesion and transmigration.
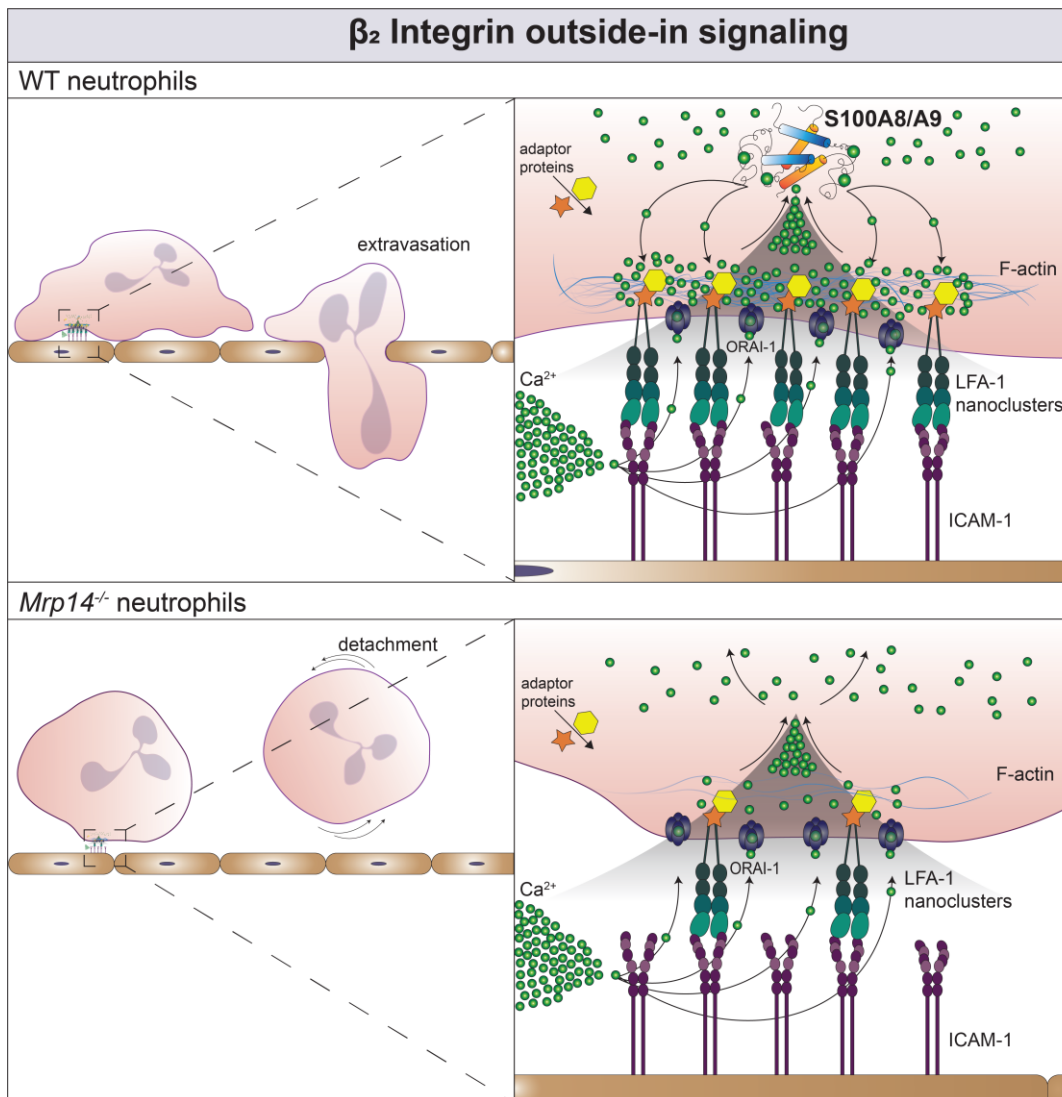
Figure 5.1: MRP8/14 delivers and supplies Ca^{2+} at the LFA-1 and F-actin clusters sustaining neutrophil postarrest modifications and transmigration. MRP8/14 acts as a subcellular Ca^{2+} supplier, delivering Ca^{2+} at the LFA-1 and F-actin clusters during neutrophil outside-in signaling dependent postarrest modifications. High Ca^{2+} at the focal cluster sites enhances adhesion finally leading to neutrophil transendothelial migration during inflammation.

5.4 Intracellular MRP8/14 switches neutrophil inflammatory potential

It has been shown that neutrophils can regulate the expression of pro-apoptotic or pro-survival genes during recruitment from the bone marrow to the sites of inflammation, in order to preserve their function [274]. In addition, it has been demonstrated that neutrophils are capable of protein synthesis and that they are transcriptionally active cells [183, 275]. Cytokine production in neutrophil varies depending on different agonists [276] and immunomodulatory cytokines produced by other immune cell subsets [277], which trigger different pathways involving a wide range of protein kinases, small molecules and transcription factors. CAMKID is one among other kinases, which is activated only by Ca^{2+} and CaM, triggering cytokine production in neutrophils through phosphorylation and activation of CREB-1 and p38 [278]. In fact, WT neutrophils showed an increase in both CREB-1 and p38 phosphorylation upon CXCL1 stimulation, while only little phosphorylation was observed in $Mrp14^{-/-}$ neutrophils. Recent work showed that CREB-1 is activated by TNF-α and CXCL12 on human and murine neutrophils, causing CXCR4 expression leading to skin inflammation [279]. Others have demonstrated that in human neutrophils CREB-1 induces inflammatory cytokine production, such as CXCL8, CCL3, CCL4 and TNF-α, downstream of the p38 MAPK signaling axis [280]. In addition, pharmacological inhibition of p38 MAPK showed impaired CXCL1-dependent neutrophil recruitment in the murine inflamed cremaster muscle [281]. Subsequently, we excluded that both CREB-1 and p38 phosphorylation were dependent on TLR4 signaling triggered by released extracellular MRP8/14. We observed the same extent of phosphorylation in WT neutrophils pre-incubated with Paquinimod, an S100A9 (MRP14)-TLR4 binding site inhibitor, demonstrating that it is the intracellular MRP8/14, which regulates CREB-1 and p38 phosphorylation. Finally, Ca^{2+} oscillations are essential for the dissolution of the periphagosomal actin rings and for the fusion of granules with phagosomes [282]. In line with our previous Ca^{2+} data, $Mrp14^{-/-}$ neutrophils showed roughly 50% less ability to phagocytose $E.coli$ particles compared to WT neutrophils.

5.5 Conclusion

This PhD work demonstrates that intracellular MRP8/14 bears distinct functions during neutrophil recruitment under acute inflammation compared to extracellular MRP8/14. First, we found that intracellular MRP8/14 is a strong modulator of neutrophil adhesion under shear stress conditions *in vivo*, without affecting neutrophil rolling capacity. In addition, we did not detect any differences neither in surface adhesion marker expression nor in $β_2$ integrin activation under static conditions in the presence or absence of MRP8/14. On the contrary, lack of MRP8/14 caused defective spreading, impaired crawling behavior and altered cytoskeletal rearragements under physiological shear conditions in neutrophils. Furthermore, we observed that in the absence of MRP8/14, neutrophils showed an increased susceptibility to increasing shear rates both *in vivo* and *in vitro*. Since MRP8/14 is well known for its Ca^{2+} binding ability and being Ca^{2+} essential for

the outside-in signaling events that guide neutrophil postarrest modifications we investigated Ca^{2+} signaling in neutrophils lacking MRP8/14. Initially, we detected normal basal Ca^{2+} levels and normal ER store release but faster and steeper SOCE exhaustion in neutrophil lacking MRP8/14. We could then demonstrate that this was caused by lower and irregular Ca^{2+} supply at the LFA-1 cluster sites. In turn, this also caused lower F-actin polymerization in MRP8/14 deficient neutrophils. Finally, we could demonstrate that other than impairing neutrophil recruitment, the lack of MRP8/14 also dampens neutrophil phagocytosis to a certain extent. These findings reveal a new and so far underappreciated role of intracellular MRP8/14. Further studies need to be performed to test whether those results could be translated into clinical applications targeting intracellular MRP8/14 to control acute and chronic inflammatory diseases as well as autoimmune diseases.

6. References

1.   Pruenster, M., et al., *S100A8/A9: From basic science to clinical application.* Pharmacology & Therapeutics, 2016. **167**: p. 120-131.

2.   Leukert, N., C. Sorg, and J. Roth, *Molecular basis of the complex formation between the two calcium-binding proteins S100A8 (MRP8) and S100A9 (MRP14).* 2005. **386**(5): p. 429-434.

3.   Vogl, T., A.L. Gharibyan, and L.A. Morozova-Roche, *Pro-Inflammatory S100A8 and S100A9 Proteins: Self-Assembly into Multifunctional Native and Amyloid Complexes.* International Journal of Molecular Sciences, 2012. **13**(3): p. 2893-2917.

4.   Wang, S., et al., *S100A8/A9 in Inflammation.* Front Immunol, 2018. **9**: p. 1298.

5.   Lagasse, E. and I.L. Weissman, *Mouse MRP8 and MRP14, Two Intracellular Calcium-Binding Proteins Associated With the Development of the Myeloid Lineage.* Blood, 1992. **79**(8): p. 1907-1915.

6.   Passey, R.J., et al., *A Null Mutation in the Inflammation-Associated S100 Protein S100A8 Causes Early Resorption of the Mouse Embryo1.* The Journal of Immunology, 1999. **163**(4): p. 2209-2216.

7.   Passey, R.J., et al., *S100A8: emerging functions and regulation.* J Leukoc Biol, 1999. **66**(4): p. 549-56.

8.   Hobbs, J.A., et al., *Myeloid cell function in MRP-14 (S100A9) null mice.* Mol Cell Biol, 2003. **23**(7): p. 2564-76.

9.   Manitz, M.P., et al., *Loss of S100A9 (MRP14) results in reduced interleukin-8-induced CD11b surface expression, a polarized microfilament system, and diminished responsiveness to chemoattractants in vitro.* Mol Cell Biol, 2003. **23**(3): p. 1034-43.

10.   Edgeworth, J., et al., *Identification of p8,14 as a highly abundant heterodimeric calcium binding protein complex of myeloid cells.* J Biol Chem, 1991. **266**(12): p. 7706-13.

11.   Odink, K., et al., *Two calcium-binding proteins in infiltrate macrophages of rheumatoid arthritis.* Nature, 1987. **330**(6143): p. 80-82.

12.   Pruenster, M., et al., *Extracellular MRP8/14 is a regulator of β2 integrin-dependent neutrophil slow rolling and adhesion.* Nature Communications, 2015. **6**(1): p. 6915.

13.   ANDERSSON, K.B., et al., *The Leucocyte L1 Protein: Identity with the Cystic Fibrosis Antigen and the Calcium-Binding MRP-8 and MRP-14 Macrophage Components.* Scandinavian Journal of Immunology, 1988. **28**(2): p. 241-245.

14.   Cohen, J.C. and J.E. Larson, *Pathophysiologic consequences following inhibition of a CFTR-dependent developmental cascade in the lung.* BMC Developmental Biology, 2005. **5**(1): p. 2.

15.   Dorin, J.R., et al., *A clue to the basic defect in cystic fibrosis from cloning the CF antigen gene.* Nature, 1987. **326**(6113): p. 614-617.

16.   Wilkinson, M.M., et al., *Expression pattern of two related cystic fibrosis-associated calcium-binding proteins in normal and abnormal tissues.* Journal of Cell Science, 1988. **91**(2): p. 221-230.

17.   Fagerhol, M.K., *Nomenclature for proteins: is calprotectin a proper name for the elusive myelomonocytic protein?* Clin Mol Pathol, 1996. **49**(2): p. M74-9.

18.   Moore, B.W., *A soluble protein characteristic of the nervous system.* Biochem Biophys Res Commun, 1965. **19**(6): p. 739-44.

19.   Marenholz, I., C.W. Heizmann, and G. Fritz, *S100 proteins in mouse and man: from evolution to function and pathology (including an update of the nomenclature).* Biochem Biophys Res Commun, 2004. **322**(4): p. 1111-22.

20. Zimmer, D.B., et al., *The S100 protein family: history, function, and expression.* Brain Res Bull, 1995. **37**(4): p. 417-29.

21. Ravasi, T., et al., *Probing the S100 protein family through genomic and functional analysis.* Genomics, 2004. **84**(1): p. 10-22.

22. Donato, R., *S100: a multigenic family of calcium-modulated proteins of the EF-hand type with intracellular and extracellular functional roles.* Int J Biochem Cell Biol, 2001. **33**(7): p. 637-68.

23. Heizmann, C.W. and G. Fritz, *Chapter 124 - The Family of S100 Cell Signaling Proteins*, in *Handbook of Cell Signaling (Second Edition)*, R.A. Bradshaw and E.A. Dennis, Editors. 2010, Academic Press: San Diego. p. 983-993.

24. Heizmann, C.W., *The multifunctional S100 protein family.* Methods Mol Biol, 2002. **172**: p. 69-80.

25. Camby, I., et al., *Supratentorial pilocytic astrocytomas, astrocytomas, anaplastic astrocytomas and glioblastomas are characterized by a differential expression of S100 proteins.* Brain Pathol, 1999. **9**(1): p. 1-19.

26. Yonemura, Y., et al., *Inverse expression of S100A4 and E-cadherin is associated with metastatic potential in gastric cancer.* Clin Cancer Res, 2000. **6**(11): p. 4234-42.

27. Mouta Carreira, C., et al., *S100A13 is involved in the regulation of fibroblast growth factor-1 and p40 synaptotagmin-1 release in vitro.* J Biol Chem, 1998. **273**(35): p. 22224-31.

28. van de Graaf, S.F., et al., *Functional expression of the epithelial Ca(2+) channels (TRPV5 and TRPV6) requires association of the S100A10-annexin 2 complex.* Embo j, 2003. **22**(7): p. 1478-87.

29. Sturchler, E., et al., *S100A16, a novel calcium-binding protein of the EF-hand superfamily.* J Biol Chem, 2006. **281**(50): p. 38905-17.

30. Sakaguchi, M., et al., *Relationship between contact inhibition and intranuclear S100C of normal human fibroblasts.* J Cell Biol, 2000. **149**(6): p. 1193-206.

31. Hagens, G., et al., *Calcium-binding protein S100A7 and epidermal-type fatty acid-binding protein are associated in the cytosol of human keratinocytes.* Biochem J, 1999. **339 (Pt 2)**(Pt 2): p. 419-27.

32. Semprini, S., et al., *Genomic structure, promoter characterisation and mutational analysis of the S100A7 gene: exclusion of a candidate for familial psoriasis susceptibility.* Hum Genet, 1999. **104**(2): p. 130-4.

33. Heizmann, C.W., *Ca(2+)-Binding Proteins of the EF-Hand Superfamily: Diagnostic and Prognostic Biomarkers and Novel Therapeutic Targets.* Methods Mol Biol, 2019. **1929**: p. 157-186.

34. Heizmann, C.W. and J.A. Cox, *New perspectives on S100 proteins: a multi-functional Ca(2+)-, Zn(2+)- and Cu(2+)-binding protein family.* Biometals, 1998. **11**(4): p. 383-97.

35. Boeshans, K.M., et al., *Purification, crystallization and preliminary X-ray diffraction of human S100A15.* Acta Crystallogr Sect F Struct Biol Cryst Commun, 2006. **62**(Pt 5): p. 467-70.

36. Foell, D., et al., *S100 proteins expressed in phagocytes: a novel group of damage-associated molecular pattern molecules.* J Leukoc Biol, 2007. **81**(1): p. 28-37.

37. Edgeworth, J., P. Freemont, and N. Hogg, *Ionomycin-regulated phosphorylation of the myeloid calcium-binding protein p14.* Nature, 1989. **342**(6246): p. 189-92.

38. van den Bos, C., et al., *Phosphorylation of MRP14, an S100 protein expressed during monocytic differentiation, modulates Ca(2+)-dependent translocation from cytoplasm to membranes and cytoskeleton.* J Immunol, 1996. **156**(3): p. 1247-54.

39. Vogl, T., et al., *MRP8 and MRP14 control microtubule reorganization during transendothelial migration of phagocytes.* Blood, 2004. **104**(13): p. 4260-8.

40. Ishikawa, K., et al., *The structure of human MRP8, a member of the S100 calcium-binding protein family, by MAD phasing at 1.9 Å resolution.* Acta Crystallographica Section D, 2000. **56**(5): p. 559-566.

41. Itou, H., et al., *The crystal structure of human MRP14 (S100A9), a Ca2+-dependent regulator protein in inflammatory process Edited by R. Huber.* Journal of Molecular Biology, 2002. **316**(2): p. 265-276.

42. Harrison, C.A., et al., *Oxidation Regulates the Inflammatory Properties of the Murine S100 Protein S100A8*.* Journal of Biological Chemistry, 1999. **274**(13): p. 8561-8569.

43. Geczy, C., *Regulation and proinflammatory properties of the chemotactic protein, CP-10.* Biochim Biophys Acta, 1996. **1313**(3): p. 246-52.

44. Vogl, T., et al., *Mrp8 and Mrp14 are endogenous activators of Toll-like receptor 4, promoting lethal, endotoxin-induced shock.* Nature Medicine, 2007. **13**(9): p. 1042-1049.

45. Pröpper, C., et al., *Analysis of the MRP8-MRP14 protein-protein interaction by the two-hybrid system suggests a prominent role of the C-terminal domain of S100 proteins in dimer formation.* J Biol Chem, 1999. **274**(1): p. 183-8.

46. Hunter, M.J. and W.J. Chazin, *High level expression and dimer characterization of the S100 EF-hand proteins, migration inhibitory factor-related proteins 8 and 14.* J Biol Chem, 1998. **273**(20): p. 12427-35.

47. Vogl, T., et al., *Biophysical characterization of S100A8 and S100A9 in the absence and presence of bivalent cations.* Biochimica et Biophysica Acta (BBA) - Molecular Cell Research, 2006. **1763**(11): p. 1298-1306.

48. Donato, R., *Functional roles of S100 proteins, calcium-binding proteins of the EF-hand type.* Biochimica et Biophysica Acta (BBA) - Molecular Cell Research, 1999. **1450**(3): p. 191-231.

49. Vogl, T., et al., *Calcium-induced noncovalently linked tetramers of MRP8 and MRP14 detected by ultraviolet matrix-assisted laser desorption/ionization mass spectrometry.* J Am Soc Mass Spectrom, 1999. **10**(11): p. 1124-30.

50. Strupat, K., et al., *Calcium-induced noncovalently linked tetramers of MRP8 and MRP14 are confirmed by electrospray ionization-mass analysis.* J Am Soc Mass Spectrom, 2000. **11**(9): p. 780-8.

51. Korndörfer, I.P., F. Brueckner, and A. Skerra, *The crystal structure of the human (S100A8/S100A9)2 heterotetramer, calprotectin, illustrates how conformational changes of interacting alpha-helices can determine specific association of two EF-hand proteins.* J Mol Biol, 2007. **370**(5): p. 887-98.

52. Damo, S.M., et al., *Molecular basis for manganese sequestration by calprotectin and roles in the innate immune response to invading bacterial pathogens.* Proc Natl Acad Sci U S A, 2013. **110**(10): p. 3841-6.

53. Leukert, N., et al., *Calcium-dependent tetramer formation of S100A8 and S100A9 is essential for biological activity.* J Mol Biol, 2006. **359**(4): p. 961-72.

54. Zwadlo, G., et al., *Two calcium-binding proteins associated with specific stages of myeloid cell differentiation are expressed by subsets of macrophages in inflammatory tissues.* Clin Exp Immunol, 1988. **72**(3): p. 510-5.

55. Nacken, W., et al., *Biochemical characterization of the murine S100A9 (MRP14) protein suggests that it is functionally equivalent to its human counterpart despite its low degree of sequence homology.* European Journal of Biochemistry, 2000. **267**(2): p. 560-565.

56. Roth, J., et al., *MRP8 and MRP14, S-100-Like Proteins Associated With Myeloid Differentiation, Are Translocated to Plasma Membrane and Intermediate Filaments in a Calcium-Dependent Manner.* Blood, 1993. **82**(6): p. 1875-1883.

57. Lagasse, E. and R.G. Clerc, *Cloning and expression of two human genes encoding calcium-binding proteins that are regulated during myeloid differentiation.* Mol Cell Biol, 1988. **8**(6): p. 2402-10.

58. Foell, D., et al., *Phagocyte-specific S100 proteins are released from affected mucosa and promote immune responses during inflammatory bowel disease.* J Pathol, 2008. **216**(2): p. 183-92.

59. Brandtzaeg, P., I. Dale, and M.K. Fagerhol, *Distribution of a formalin-resistant myelomonocytic antigen (L1) in human tissues. II. Normal and aberrant occurrence in various epithelia.* Am J Clin Pathol, 1987. **87**(6): p. 700-7.

60. Longbottom, D., J.-M. Sallenave, and V. van Heyningen, *Subunit structure of calgranulins A and B obtained from sputum, plasma, granulocytes and cultured epithelial cells.* Biochimica et Biophysica Acta (BBA) - Protein Structure and Molecular Enzymology, 1992. **1120**(2): p. 215-222.

61. Zenz, R., et al., *Psoriasis-like skin disease and arthritis caused by inducible epidermal deletion of Jun proteins.* Nature, 2005. **437**(7057): p. 369-75.

62. Muesch, A., et al., *A novel pathway for secretory proteins?* Trends Biochem Sci, 1990. **15**(3): p. 86-8.

63. Frosch, M., et al., *Myeloid-related proteins 8 and 14 are specifically secreted during interaction of phagocytes and activated endothelium and are useful markers for monitoring disease activity in pauciarticular-onset juvenile rheumatoid arthritis.* Arthritis & Rheumatism, 2000. **43**(3): p. 628-637.

64. Pruenster, M., et al., *E-selectin-mediated rapid NLRP3 inflammasome activation regulates S100A8/S100A9 release from neutrophils via transient gasdermin D pore formation.* Nature Immunology, 2023.

65. Vogl, T., et al., *Autoinhibitory regulation of S100A8/S100A9 alarmin activity locally restricts sterile inflammation.* J Clin Invest, 2018. **128**(5): p. 1852-1866.

66. McNamara, M.P., et al., *Neutrophil death as a defence mechanism against Candida albicans infections.* Lancet, 1988. **2**(8621): p. 1163-5.

67. Steinbakk, M., et al., *Antimicrobial actions of calcium binding leucocyte L1 protein, calprotectin.* Lancet, 1990. **336**(8718): p. 763-5.

68. Sohnle, P.G., et al., *Zinc-reversible antimicrobial activity of recombinant calprotectin (migration inhibitory factor-related proteins 8 and 14).* J Infect Dis, 2000. **182**(4): p. 1272-5.

69. Corbin, B.D., et al., *Metal Chelation and Inhibition of Bacterial Growth in Tissue Abscesses.* Science, 2008. **319**(5865): p. 962-965.

70. Gaddy, J.A., et al., *The host protein calprotectin modulates the Helicobacter pylori cag type IV secretion system via zinc sequestration.* PLoS Pathog, 2014. **10**(10): p. e1004450.

71. Urban, C.F., et al., *Neutrophil extracellular traps contain calprotectin, a cytosolic protein complex involved in host defense against Candida albicans.* PLoS Pathog, 2009. **5**(10): p. e1000639.

72. Hood, M.I., et al., *Identification of an Acinetobacter baumannii zinc acquisition system that facilitates resistance to calprotectin-mediated zinc sequestration.* PLoS Pathog, 2012. **8**(12): p. e1003068.

73. Achouiti, A., et al., *Myeloid-related protein-14 contributes to protective immunity in gram-negative pneumonia derived sepsis.* PLoS Pathog, 2012. **8**(10): p. e1002987.

74. McNeill, E., et al., *Defective chemoattractant-induced calcium signalling in S100A9 null neutrophils.* Cell Calcium, 2007. **41**(2): p. 107-21.

75. Lominadze, G., et al., *Myeloid-Related Protein-14 Is a p38 MAPK Substrate in Human Neutrophils1.* The Journal of Immunology, 2005. **174**(11): p. 7257-7267.

76. Goebeler, M., et al., *Increase of calcium levels in epithelial cells induces translocation of calcium-binding proteins migration inhibitory factor-related protein 8 (MRP8) and MRP14 to keratin intermediate filaments.* Biochemical Journal, 1995. **309**(2): p. 419-424.

77.   Murao, S., F.R. Collart, and E. Huberman, *A protein containing the cystic fibrosis antigen is an inhibitor of protein kinases.* J Biol Chem, 1989. **264**(14): p. 8356-60.

78.   Siegenthaler, G., et al., *A heterocomplex formed by the calcium-binding proteins MRP8 (S100A8) and MRP14 (S100A9) binds unsaturated fatty acids with high affinity.* J Biol Chem, 1997. **272**(14): p. 9371-7.

79.   Doussiere, J., F. Bouzidi, and P.V. Vignais, *The S100A8/A9 protein as a partner for the cytosolic factors of NADPH oxidase activation in neutrophils.* Eur J Biochem, 2002. **269**(13): p. 3246-55.

80.   Schonthaler, H.B., et al., *S100A8-S100A9 protein complex mediates psoriasis by regulating the expression of complement factor C3.* Immunity, 2013. **39**(6): p. 1171-81.

81.   Foell, D. and J. Roth, *Proinflammatory S100 proteins in arthritis and autoimmune disease.* Arthritis Rheum, 2004. **50**(12): p. 3762-71.

82.   Choi, I.Y., et al., *MRP8/14 serum levels as a strong predictor of response to biological treatments in patients with rheumatoid arthritis.* Ann Rheum Dis, 2015. **74**(3): p. 499-505.

83.   Tibble, J.A. and I. Bjarnason, *Non-invasive investigation of inflammatory bowel disease.* World J Gastroenterol, 2001. **7**(4): p. 460-5.

84.   Viemann, D., et al., *Myeloid-related proteins 8 and 14 induce a specific inflammatory response in human microvascular endothelial cells.* Blood, 2005. **105**(7): p. 2955-62.

85.   Benoit, S., et al., *Elevated serum levels of calcium-binding S100 proteins A8 and A9 reflect disease activity and abnormal differentiation of keratinocytes in psoriasis.* British Journal of Dermatology, 2006. **155**(1): p. 62-66.

86.   Pechkovsky, D.V., et al., *Calprotectin (MRP8/14 protein complex) release during mycobacterial infection in vitro and in vivo.* FEMS Immunol Med Microbiol, 2000. **29**(1): p. 27-33.

87.   Soyfoo, M.S., et al., *Phagocyte-specific S100A8/A9 protein levels during disease exacerbations and infections in systemic lupus erythematosus.* J Rheumatol, 2009. **36**(10): p. 2190-4.

88.   Nistala, K., et al., *Myeloid related protein induces muscle derived inflammatory mediators in juvenile dermatomyositis.* Arthritis Res Ther, 2013. **15**(5): p. R131.

89.   Xu, X., et al., *Increased expression of S100A8 and S100A9 in patients with diffuse cutaneous systemic sclerosis. A correlation with organ involvement and immunological abnormalities.* Clin Rheumatol, 2013. **32**(10): p. 1501-10.

90.   Rekers, N.V., et al., *Beneficial Immune Effects of Myeloid-Related Proteins in Kidney Transplant Rejection.* American Journal of Transplantation, 2016. **16**(5): p. 1441-1455.

91.   van Zoelen, M.A., et al., *Expression and role of myeloid-related protein-14 in clinical and experimental sepsis.* Am J Respir Crit Care Med, 2009. **180**(11): p. 1098-106.

92.   Austermann, J., et al., *Alarmins MRP8 and MRP14 induce stress tolerance in phagocytes under sterile inflammatory conditions.* Cell Rep, 2014. **9**(6): p. 2112-23.

93.   Altwegg, L.A., et al., *Myeloid-related protein 8/14 complex is released by monocytes and granulocytes at the site of coronary occlusion: a novel, early, and sensitive marker of acute coronary syndromes.* European Heart Journal, 2007. **28**(8): p. 941-948.

94.   Healy, A.M., et al., *Platelet expression profiling and clinical validation of myeloid-related protein-14 as a novel determinant of cardiovascular events.* Circulation, 2006. **113**(19): p. 2278-84.

95.   Moncrieffe, H., et al., *A subgroup of juvenile idiopathic arthritis patients who respond well to methotrexate are identified by the serum biomarker MRP8/14 protein.* Rheumatology, 2013. **52**(8): p. 1467-1476.

96.   Nordal, H.H., et al., *Calprotectin (S100A8/A9) should preferably be measured in EDTA-plasma; results from a longitudinal study of patients with rheumatoid arthritis.* Scand J Clin Lab Invest, 2018. **78**(1-2): p. 102-108.

97. Keskitalo, P.L., et al., *Myeloid-related protein 8/14 in plasma and serum in patients with new-onset juvenile idiopathic arthritis in real-world setting in a single center.* Pediatric Rheumatology, 2022. **20**(1): p. 42.

98. Heller, F., et al., *Urinary calprotectin and the distinction between prerenal and intrinsic acute kidney injury.* Clin J Am Soc Nephrol, 2011. **6**(10): p. 2347-55.

99. Eikmans, M., et al., *Expression of Surfactant Protein-C, S100A8, S100A9, and B Cell Markers in Renal Allografts: Investigation of the Prognostic Value.* Journal of the American Society of Nephrology, 2005. **16**(12): p. 3771-3786.

100. Hirono, K., et al., *Expression of Myeloid-Related Protein-8 and -14 in Patients With Acute Kawasaki Disease.* Journal of the American College of Cardiology, 2006. **48**(6): p. 1257-1264.

101. Smith, L.A. and D.R. Gaya, *Utility of faecal calprotectin analysis in adult inflammatory bowel disease.* World J Gastroenterol, 2012. **18**(46): p. 6782-9.

102. Markowitz, J. and W.E. Carson, 3rd, *Review of S100A9 biology and its role in cancer.* Biochim Biophys Acta, 2013. **1835**(1): p. 100-9.

103. Kwon, C.H., et al., *S100A8 and S100A9 promotes invasion and migration through p38 mitogen-activated protein kinase-dependent NF-κB activation in gastric cancer cells.* Mol Cells, 2013. **35**(3): p. 226-34.

104. Ghavami, S., et al., *S100A8/A9 at low concentration promotes tumor cell growth via RAGE ligation and MAP kinase-dependent pathway.* J Leukoc Biol, 2008. **83**(6): p. 1484-92.

105. Ichikawa, M., et al., *S100A8/A9 activate key genes and pathways in colon tumor progression.* Mol Cancer Res, 2011. **9**(2): p. 133-48.

106. Hiratsuka, S., et al., *Tumour-mediated upregulation of chemoattractants and recruitment of myeloid cells predetermines lung metastasis.* Nat Cell Biol, 2006. **8**(12): p. 1369-75.

107. Sinha, P., et al., *Proinflammatory S100 proteins regulate the accumulation of myeloid-derived suppressor cells.* J Immunol, 2008. **181**(7): p. 4666-75.

108. Wang, C., et al., *CD300ld on neutrophils is required for tumour-driven immune suppression.* Nature, 2023. **621**(7980): p. 830-839.

109. Zhang, X., et al., *Inflammation-induced S100A8 activates Id3 and promotes colorectal tumorigenesis.* Int J Cancer, 2015. **137**(12): p. 2803-14.

110. Lv, Z., W. Li, and X. Wei, *S100A9 promotes prostate cancer cell invasion by activating TLR4/NF-κB/integrin β1/FAK signaling.* Onco Targets Ther, 2020. **13**: p. 6443-6452.

111. Pili, R., et al., *Phase II Randomized, Double-Blind, Placebo-Controlled Study of Tasquinimod in Men With Minimally Symptomatic Metastatic Castrate-Resistant Prostate Cancer.* Journal of Clinical Oncology, 2011. **29**(30): p. 4022-4028.

112. Pelletier, M., et al., *Quinoline-3-carboxamides such as tasquinimod are not specific inhibitors of S100A9.* Blood Adv, 2018. **2**(10): p. 1170-1171.

113. Dale, D.C., L. Boxer, and W.C. Liles, *The phagocytes: neutrophils and monocytes.* Blood, 2008. **112**(4): p. 935-945.

114. Mayadas, T.N., X. Cullere, and C.A. Lowell, *The Multifaceted Functions of Neutrophils.* Annual Review of Pathology: Mechanisms of Disease, 2014. **9**(1): p. 181-218.

115. O'Connell, K.E., et al., *Practical murine hematopathology: a comparative review and implications for research.* Comp Med, 2015. **65**(2): p. 96-113.

116. Immler, R., et al., *The voltage-gated potassium channel KV1.3 regulates neutrophil recruitment during inflammation.* Cardiovascular Research, 2021. **118**(5): p. 1289-1302.

117. Masgrau-Alsina, S., et al., *MST1 controls murine neutrophil homeostasis via the G-CSFR/STAT3 axis.* Front Immunol, 2022. **13**: p. 1038936.

118. Németh, T., M. Sperandio, and A. Mócsai, *Neutrophils as emerging therapeutic targets.* Nature Reviews Drug Discovery, 2020. **19**(4): p. 253-275.

119. Burn, G.L., et al., *The Neutrophil.* Immunity, 2021. **54**(7): p. 1377-1391.

120. CARTWRIGHT, G.E., J.W. ATHENS, and M.M. WINTROBE, *Analytical Review: The Kinetics of Granulopoiesis in Normal Man.* Blood, 1964. **24**(6): p. 780-803.

121. *The development and structure of mature neutrophils*, in *Biochemistry and Physiology of the Neutrophil*, S.W. Edwards, Editor. 1994, Cambridge University Press: Cambridge. p. 33-76.

122. Ley, K., et al., *Neutrophils: New insights and open questions.* Science Immunology, 2018. **3**(30): p. eaat4579.

123. Pillay, J., et al., *In vivo labeling with 2H2O reveals a human neutrophil lifespan of 5.4 days.* Blood, 2010. **116**(4): p. 625-627.

124. Stark, M.A., et al., *Phagocytosis of apoptotic neutrophils regulates granulopoiesis via IL-23 and IL-17.* Immunity, 2005. **22**(3): p. 285-94.

125. Bendall, L.J. and K.F. Bradstock, *G-CSF: From granulopoietic stimulant to bone marrow stem cell mobilizing agent.* Cytokine Growth Factor Rev, 2014. **25**(4): p. 355-67.

126. Cain, D.W., et al., *Inflammation triggers emergency granulopoiesis through a density-dependent feedback mechanism.* PLoS One, 2011. **6**(5): p. e19957.

127. Bugl, S., et al., *Steady-state neutrophil homeostasis is dependent on TLR4/TRIF signaling.* Blood, 2013. **121**(5): p. 723-33.

128. Eash, K.J., et al., *CXCR2 and CXCR4 antagonistically regulate neutrophil trafficking from murine bone marrow.* J Clin Invest, 2010. **120**(7): p. 2423-31.

129. Suratt, B.T., et al., *Neutrophil maturation and activation determine anatomic site of clearance from circulation.* Am J Physiol Lung Cell Mol Physiol, 2001. **281**(4): p. L913-21.

130. Furze, R.C. and S.M. Rankin, *Neutrophil mobilization and clearance in the bone marrow.* Immunology, 2008. **125**(3): p. 281-288.

131. Furze, R.C. and S.M. Rankin, *The role of the bone marrow in neutrophil clearance under homeostatic conditions in the mouse.* Faseb j, 2008. **22**(9): p. 3111-9.

132. Lum, J.J., et al., *Elimination of senescent neutrophils by TNF-related apoptosis-inducing [corrected] ligand.* J Immunol, 2005. **175**(2): p. 1232-8.

133. Bevilacqua, M.P., et al., *Interleukin 1 acts on cultured human vascular endothelium to increase the adhesion of polymorphonuclear leukocytes, monocytes, and related leukocyte cell lines.* J Clin Invest, 1985. **76**(5): p. 2003-11.

134. Butcher, E.C., *Leukocyte-endothelial cell recognition: three (or more) steps to specificity and diversity.* Cell, 1991. **67**(6): p. 1033-6.

135. Menger, M.D., D. Steiner, and K. Messmer, *Microvascular ischemia-reperfusion injury in striated muscle: significance of "no reflow".* American Journal of Physiology-Heart and Circulatory Physiology, 1992. **263**(6): p. H1892-H1900.

136. Ley, K., et al., *Getting to the site of inflammation: the leukocyte adhesion cascade updated.* Nature Reviews Immunology, 2007. **7**(9): p. 678-689.

137. Ley, K., *The role of selectins in inflammation and disease.* Trends Mol Med, 2003. **9**(6): p. 263-8.

138. Schmidt, S., M. Moser, and M. Sperandio, *The molecular basis of leukocyte recruitment and its deficiencies.* Mol Immunol, 2013. **55**(1): p. 49-58.

139. Kansas, G.S., *Selectins and their ligands: current concepts and controversies.* Blood, 1996. **88**(9): p. 3259-87.

140. Sperandio, M., C.A. Gleissner, and K. Ley, *Glycosylation in immune cell trafficking.* Immunological Reviews, 2009. **230**(1): p. 97-113.

141. Hafezi-Moghadam, A., et al., *L-selectin shedding regulates leukocyte recruitment.* J Exp Med, 2001. **193**(7): p. 863-72.

142. Hickey, M.J., et al., *L-selectin facilitates emigration and extravascular locomotion of leukocytes during acute inflammatory responses in vivo.* J Immunol, 2000. **165**(12): p. 7164-70.

143. Grailer, J.J., M. Kodera, and D.A. Steeber, *L-selectin: role in regulating homeostasis and cutaneous inflammation.* J Dermatol Sci, 2009. **56**(3): p. 141-7.

144. McEver, R.P., *Selectins: initiators of leucocyte adhesion and signalling at the vascular wall.* Cardiovascular Research, 2015. **107**(3): p. 331-339.

145. Sperandio, M., et al., *Analysis of leukocyte rolling in vivo and in vitro.* Methods Enzymol, 2006. **416**: p. 346-71.

146. Kraiss, L.W., et al., *Fluid flow regulates e-selectin protein levels in human endothelial cells by inhibiting translation.* Journal of Vascular Surgery, 2003. **37**(1): p. 161-168.

147. Kunkel, E.J. and K. Ley, *Distinct Phenotype of E-Selectin–Deficient Mice.* Circulation Research, 1996. **79**(6): p. 1196-1204.

148. Ley, K., et al., *Sequential contribution of L- and P-selectin to leukocyte rolling in vivo.* J Exp Med, 1995. **181**(2): p. 669-75.

149. Hocdé, S.A., O. Hyrien, and R.E. Waugh, *Cell adhesion molecule distribution relative to neutrophil surface topography assessed by TIRFM.* Biophys J, 2009. **97**(1): p. 379-87.

150. Xia, L., et al., *P-selectin glycoprotein ligand-1-deficient mice have impaired leukocyte tethering to E-selectin under flow.* J Clin Invest, 2002. **109**(7): p. 939-50.

151. Eriksson, E.E., et al., *Importance of primary capture and L-selectin-dependent secondary capture in leukocyte accumulation in inflammation and atherosclerosis in vivo.* J Exp Med, 2001. **194**(2): p. 205-18.

152. Sperandio, M., *Selectins and glycosyltransferases in leukocyte rolling in vivo.* The FEBS Journal, 2006. **273**(19): p. 4377-4389.

153. Yang, J., et al., *Targeted gene disruption demonstrates that P-selectin glycoprotein ligand 1 (PSGL-1) is required for P-selectin-mediated but not E-selectin-mediated neutrophil rolling and migration.* J Exp Med, 1999. **190**(12): p. 1769-82.

154. Hidalgo, A., et al., *Complete identification of E-selectin ligands on neutrophils reveals distinct functions of PSGL-1, ESL-1, and CD44.* Immunity, 2007. **26**(4): p. 477-489.

155. Sundd, P., et al., *'Slings' enable neutrophil rolling at high shear.* Nature, 2012. **488**(7411): p. 399-403.

156. Finger, E.B., et al., *Adhesion through L-selectin requires a threshold hydrodynamic shear.* Nature, 1996. **379**(6562): p. 266-269.

157. McEver, R.P. and C. Zhu, *Rolling cell adhesion.* Annu Rev Cell Dev Biol, 2010. **26**: p. 363-96.

158. Lawrence, M.B., et al., *Threshold levels of fluid shear promote leukocyte adhesion through selectins (CD62L,P,E).* J Cell Biol, 1997. **136**(3): p. 717-27.

159. Walzog, B. and P. Gaehtgens, *Adhesion Molecules: The Path to a New Understanding of Acute Inflammation.* News Physiol Sci, 2000. **15**: p. 107-113.

160. Mócsai, A., B. Walzog, and C.A. Lowell, *Intracellular signalling during neutrophil recruitment.* Cardiovasc Res, 2015. **107**(3): p. 373-85.

161. Ginsberg, M.H., A. Partridge, and S.J. Shattil, *Integrin regulation.* Curr Opin Cell Biol, 2005. **17**(5): p. 509-16.

162. Lefort, C.T., et al., *Distinct roles for talin-1 and kindlin-3 in LFA-1 extension and affinity regulation.* Blood, 2012. **119**(18): p. 4275-82.

163. Paulis, L.E.M., et al., *Targeting of ICAM-1 on vascular endothelium under static and shear stress conditions using a liposomal Gd-based MRI contrast agent.* Journal of Nanobiotechnology, 2012. **10**(1): p. 25.

164. Halai, K., et al., *ICAM-2 facilitates luminal interactions between neutrophils and endothelial cells in vivo.* J Cell Sci, 2014. **127**(Pt 3): p. 620-9.

165. Frommhold, D., et al., *RAGE and ICAM-1 cooperate in mediating leukocyte recruitment during acute inflammation in vivo.* Blood, 2010. **116**(5): p. 841-9.

166. Fan, Z., et al., *High-Affinity Bent β(2)-Integrin Molecules in Arresting Neutrophils Face Each Other through Binding to ICAMs In cis.* Cell Rep, 2019. **26**(1): p. 119-130.e5.

167. Morikis, V.A., et al., *Selectin catch-bonds mechanotransduce integrin activation and neutrophil arrest on inflamed endothelium under shear flow.* Blood, 2017. **130**(19): p. 2101-2110.

168. Futosi, K. and A. Mócsai, *Tyrosine kinase signaling pathways in neutrophils.* Immunological Reviews, 2016. **273**(1): p. 121-139.

169. Schymeinsky, J., M. Sperandio, and B. Walzog, *The mammalian actin-binding protein 1 (mAbp1): a novel molecular player in leukocyte biology.* Trends Cell Biol, 2011. **21**(4): p. 247-55.

170. Carman, C.V. and T.A. Springer, *Integrin avidity regulation: are changes in affinity and conformation underemphasized?* Current Opinion in Cell Biology, 2003. **15**(5): p. 547-556.

171. Rohwedder, I., et al., *Src family kinase-mediated vesicle trafficking is critical for neutrophil basement membrane penetration.* Haematologica, 2020. **105**(7): p. 1845-1856.

172. Klapproth, S., et al., *A kindlin-3-leupaxin-paxillin signaling pathway regulates podosome stability.* J Cell Biol, 2019. **218**(10): p. 3436-3454.

173. Harburger, D.S. and D.A. Calderwood, *Integrin signalling at a glance.* Journal of Cell Science, 2009. **122**(2): p. 159-163.

174. Mitra, S.K., D.A. Hanson, and D.D. Schlaepfer, *Focal adhesion kinase: in command and control of cell motility.* Nat Rev Mol Cell Biol, 2005. **6**(1): p. 56-68.

175. Nourshargh, S. and R. Alon, *Leukocyte migration into inflamed tissues.* Immunity, 2014. **41**(5): p. 694-707.

176. Barreiro, O., et al., *Endothelial adhesion receptors are recruited to adherent leukocytes by inclusion in preformed tetraspanin nanoplatforms.* J Cell Biol, 2008. **183**(3): p. 527-42.

177. Barreiro , O., et al., *Dynamic interaction of VCAM-1 and ICAM-1 with moesin and ezrin in a novel endothelial docking structure for adherent leukocytes.* Journal of Cell Biology, 2002. **157**(7): p. 1233-1245.

178. Vestweber, D., *How leukocytes cross the vascular endothelium.* Nature reviews. Immunology, 2015. **15**(11): p. 692-704.

179. Rowe, R.G. and S.J. Weiss, *Breaching the basement membrane: who, when and how?* Trends Cell Biol, 2008. **18**(11): p. 560-74.

180. Wang, S., et al., *Venular basement membranes contain specific matrix protein low expression regions that act as exit points for emigrating neutrophils.* J Exp Med, 2006. **203**(6): p. 1519-32.

181. Lämmermann, T., et al., *Rapid leukocyte migration by integrin-independent flowing and squeezing.* Nature, 2008. **453**(7191): p. 51-55.

182. de Oliveira, S., E.E. Rosowski, and A. Huttenlocher, *Neutrophil migration in infection and wound repair: going forward in reverse.* Nat Rev Immunol, 2016. **16**(6): p. 378-91.

183. Witko-Sarsat, V., et al., *Neutrophils: Molecules, Functions and Pathophysiological Aspects.* Laboratory Investigation, 2000. **80**(5): p. 617-653.

184. Crowley, M.T., et al., *A critical role for Syk in signal transduction and phagocytosis mediated by Fcgamma receptors on macrophages.* J Exp Med, 1997. **186**(7): p. 1027-39.

185. Caron, E. and A. Hall, *Identification of two distinct mechanisms of phagocytosis controlled by different Rho GTPases.* Science, 1998. **282**(5394): p. 1717-21.

186. Greenberg, S., et al., *Clustered syk tyrosine kinase domains trigger phagocytosis.* Proc Natl Acad Sci U S A, 1996. **93**(3): p. 1103-7.

187. Massol, P., et al., *Fc receptor-mediated phagocytosis requires CDC42 and Rac1.* The EMBO Journal, 1998. **17**(21): p. 6219-6229.

188. Fällman, M., et al., *Receptor-mediated phagocytosis in human neutrophils is associated with increased formation of inositol phosphates and diacylglycerol. Elevation in cytosolic free calcium and formation of inositol phosphates can be dissociated from accumulation of diacylglycerol.* J Clin Invest, 1989. **84**(3): p. 886-91.

189. Wright, S.D. and S.C. Silverstein, *Receptors for C3b and C3bi promote phagocytosis but not the release of toxic oxygen from human phagocytes.* J Exp Med, 1983. **158**(6): p. 2016-23.

190. Dana, N., et al., *Deficiency of a surface membrane glycoprotein (Mo1) in man.* J Clin Invest, 1984. **73**(1): p. 153-9.

191. Lacy, P., *Mechanisms of degranulation in neutrophils.* Allergy Asthma Clin Immunol, 2006. **2**(3): p. 98-108.

192. Fouret, P., et al., *Expression of the neutrophil elastase gene during human bone marrow cell differentiation.* J Exp Med, 1989. **169**(3): p. 833-45.

193. Borregaard, N. and J.B. Cowland, *Granules of the human neutrophilic polymorphonuclear leukocyte.* Blood, 1997. **89**(10): p. 3503-21.

194. Othman, A., M. Sekheri, and J.G. Filep, *Roles of neutrophil granule proteins in orchestrating inflammation and immunity.* Febs j, 2022. **289**(14): p. 3932-3953.

195. Sengeløv, H., L. Kjeldsen, and N. Borregaard, *Control of exocytosis in early neutrophil activation.* J Immunol, 1993. **150**(4): p. 1535-43.

196. Burgoyne, R.D. and A. Morgan, *Secretory granule exocytosis.* Physiol Rev, 2003. **83**(2): p. 581-632.

197. Parker, H. and C.C. Winterbourn, *Reactive oxidants and myeloperoxidase and their involvement in neutrophil extracellular traps.* Front Immunol, 2012. **3**: p. 424.

198. Davies, M.J., *Myeloperoxidase-derived oxidation: mechanisms of biological damage and its prevention.* J Clin Biochem Nutr, 2011. **48**(1): p. 8-19.

199. Reber, L.L., et al., *Neutrophil myeloperoxidase diminishes the toxic effects and mortality induced by lipopolysaccharide.* J Exp Med, 2017. **214**(5): p. 1249-1258.

200. Pérez-Figueroa, E., et al., *Neutrophils: Many Ways to Die.* Front Immunol, 2021. **12**: p. 631821.

201. Shiloh, M.U., et al., *Phenotype of Mice and Macrophages Deficient in Both Phagocyte Oxidase and Inducible Nitric Oxide Synthase.* Immunity, 1999. **10**(1): p. 29-38.

202. Dubey, M., et al., *Nitric oxide-mediated apoptosis of neutrophils through caspase-8 and caspase-3-dependent mechanism.* Cell Death & Disease, 2016. **7**(9): p. e2348-e2348.

203. Cahilog, Z., et al., *The Role of Neutrophil NETosis in Organ Injury: Novel Inflammatory Cell Death Mechanisms.* Inflammation, 2020. **43**(6): p. 2021-2032.

204. Saffarzadeh, M., et al., *Neutrophil extracellular traps directly induce epithelial and endothelial cell death: a predominant role of histones.* PLoS One, 2012. **7**(2): p. e32366.

205. Ermert, D., et al., *Mouse neutrophil extracellular traps in microbial infections.* J Innate Immun, 2009. **1**(3): p. 181-93.

206. Kaplan, M.J. and M. Radic, *Neutrophil extracellular traps: double-edged swords of innate immunity.* J Immunol, 2012. **189**(6): p. 2689-95.

207. Clapham, D.E., *Calcium signaling.* Cell, 2007. **131**(6): p. 1047-58.

208. Clemens, R.A. and C.A. Lowell, *Store-operated calcium signaling in neutrophils.* Journal of Leukocyte Biology, 2015. **98**(4): p. 497-502.

209. Pozzan, T., et al., *Is cytosolic ionized calcium regulating neutrophil activation?* Science, 1983. **221**(4618): p. 1413-5.

210. Immler, R., S.I. Simon, and M. Sperandio, *Calcium signalling and related ion channels in neutrophil recruitment and function.* Eur J Clin Invest, 2018. **48 Suppl 2**(Suppl 2): p. e12964.

211. Feske, S., H. Wulff, and E.Y. Skolnik, *Ion Channels in Innate and Adaptive Immunity.* Annual Review of Immunology, 2015. **33**(1): p. 291-353.

212. Schaff, U.Y., et al., *Calcium flux in neutrophils synchronizes beta2 integrin adhesive and signaling events that guide inflammatory recruitment.* Ann Biomed Eng, 2008. **36**(4): p. 632-46.

213. Jakus, Z., et al., *Critical role of phospholipase Cγ2 in integrin and Fc receptor-mediated neutrophil functions and the effector phase of autoimmune arthritis.* Journal of Experimental Medicine, 2009. **206**(3): p. 577-593.

214. Itagaki, K., et al., *Store-operated calcium entry in human neutrophils reflects multiple contributions from independently regulated pathways.* J Immunol, 2002. **168**(8): p. 4063-9.

215. Lewis, R.S., *Store-operated calcium channels: new perspectives on mechanism and function.* Cold Spring Harb Perspect Biol, 2011. **3**(12).

216. Shaw, P.J. and S. Feske, *Regulation of lymphocyte function by ORAI and STIM proteins in infection and autoimmunity.* J Physiol, 2012. **590**(17): p. 4157-67.

217. Srikanth, S., et al., *A novel EF-hand protein, CRACR2A, is a cytosolic Ca2+ sensor that stabilizes CRAC channels in T cells.* Nat Cell Biol, 2010. **12**(5): p. 436-46.

218. Clemens, R.A. and C.A. Lowell, *CRAC channel regulation of innate immune cells in health and disease.* Cell Calcium, 2019. **78**: p. 56-65.

219. Lindemann, O., et al., *TRPC1 regulates fMLP-stimulated migration and chemotaxis of neutrophil granulocytes.* Biochim Biophys Acta, 2015. **1853**(9): p. 2122-30.

220. Henríquez, C., et al., *The calcium-activated potassium channel KCa3.1 plays a central role in the chemotactic response of mammalian neutrophils.* Acta Physiol (Oxf), 2016. **216**(1): p. 132-45.

221. Di Virgilio, F., et al., *The P2X7 Receptor in Infection and Inflammation.* Immunity, 2017. **47**(1): p. 15-31.

222. Mehari, F.T., et al., *Intravital calcium imaging in myeloid leukocytes identifies calcium frequency spectra as indicators of functional states.* Sci Signal, 2022. **15**(744): p. eabe6909.

223. Dixit, N. and S.I. Simon, *Chemokines, selectins and intracellular calcium flux: temporal and spatial cues for leukocyte arrest.* Front Immunol, 2012. **3**: p. 188.

224. Bréchard, S. and E.J. Tschirhart, *Regulation of superoxide production in neutrophils: role of calcium influx.* Journal of Leukocyte Biology, 2008. **84**(5): p. 1223-1237.

225. Morikis, V.A., E. Masadeh, and S.I. Simon, *Tensile force transmitted through LFA-1 bonds mechanoregulate neutrophil inflammatory response.* Journal of Leukocyte Biology, 2020. **108**(6): p. 1815-1828.

226. Green, C.E., et al., *Dynamic shifts in LFA-1 affinity regulate neutrophil rolling, arrest, and transmigration on inflamed endothelium.* Blood, 2006. **107**(5): p. 2101-11.

227. Dixit, N., et al., *Migrational Guidance of Neutrophils Is Mechanotransduced via High-Affinity LFA-1 and Calcium Flux.* The Journal of Immunology, 2011. **187**(1): p. 472-481.

228. Bootman, M.D., et al., *2-aminoethoxydiphenyl borate (2-APB) is a reliable blocker of store-operated Ca2+ entry but an inconsistent inhibitor of InsP3-induced Ca2+ release.* Faseb j, 2002. **16**(10): p. 1145-50.

229. Dixit, N., et al., *Leukocyte function antigen-1, kindlin-3, and calcium flux orchestrate neutrophil recruitment during inflammation.* J Immunol, 2012. **189**(12): p. 5954-64.

230. Morikis, V.A. and S.I. Simon, *Neutrophil Mechanosignaling Promotes Integrin Engagement With Endothelial Cells and Motility Within Inflamed Vessels.* Front Immunol, 2018. **9**: p. 2774.

231. Vogl, T., et al., *Alarmin S100A8/S100A9 as a biomarker for molecular imaging of local inflammatory activity.* Nature Communications, 2014. **5**(1): p. 4593.

232. Ley, K. and P. Gaehtgens, *Endothelial, not hemodynamic, differences are responsible for preferential leukocyte rolling in rat mesenteric venules.* Circ Res, 1991. **69**(4): p. 1034-41.

233. Schindelin, J., et al., *Fiji: an open-source platform for biological-image analysis.* Nat Methods, 2012. **9**(7): p. 676-82.

234. Jung, U. and K. Ley, *Regulation of E-selectin, P-selectin, and intercellular adhesion molecule 1 expression in mouse cremaster muscle vasculature.* Microcirculation, 1997. **4**(2): p. 311-9.

235. Sperandio, M. and K. Ley, *The physiology and pathophysiology of P-selectin.* Mod.Asp.Immunobiol., 2005. **15**: p. 24-26.

236. Smith, M.L., et al., *Autoperfused mouse flow chamber reveals synergistic neutrophil accumulation through P-selectin and E-selectin.* J Leukoc Biol, 2004. **76**(5): p. 985-93.

237. Zehrer, A., et al., *A Fundamental Role of Myh9 for Neutrophil Migration in Innate Immunity.* The Journal of Immunology, 2018. **201**(6): p. 1748.

238. Schymeinsky, J., et al., *A fundamental role of mAbp1 in neutrophils: impact on β2 integrin–mediated phagocytosis and adhesion in vivo.* Blood, 2009. **114**(19): p. 4209-4220.

239. Kurz, A.R., et al., *MST1-dependent vesicle trafficking regulates neutrophil transmigration through the vascular basement membrane.* J Clin Invest, 2016. **126**(11): p. 4125-4139.

240. Grimes, D., et al., *ORAI1 and ORAI2 modulate murine neutrophil calcium signaling, cellular activation, and host defense.* Proceedings of the National Academy of Sciences of the United States of America, 2020. **117**(39): p. 24403-24414.

241. Fan, Z., et al., *Neutrophil recruitment limited by high-affinity bent β2 integrin binding ligand in cis.* Nat Commun, 2016. **7**: p. 12658.

242. Zarbock, A. and K. Ley, *Neutrophil adhesion and activation under flow.* Microcirculation, 2009. **16**(1): p. 31-42.

243. Bouti, P., et al., *β2 Integrin Signaling Cascade in Neutrophils: More Than a Single Function.* Front Immunol, 2020. **11**: p. 619925.

244. Begandt, D., et al., *How neutrophils resist shear stress at blood vessel walls: molecular mechanisms, subcellular structures, and cell–cell interactions.* Journal of Leukocyte Biology, 2017. **102**(3): p. 699-709.

245. Immler, R., S.I. Simon, and M. Sperandio, *Calcium signalling and related ion channels in neutrophil recruitment and function.* European journal of clinical investigation, 2018. **48 Suppl 2**(Suppl 2): p. e12964-e12964.

246.   Verploegen, S., et al., *Characterization of the role of CaMKI-like kinase (CKLiK) in human granulocyte function.* Blood, 2005. **106**(3): p. 1076-83.

247.   Gaines, P., et al., *A cascade of Ca(2+)/calmodulin-dependent protein kinases regulates the differentiation and functional activation of murine neutrophils.* Exp Hematol, 2008. **36**(7): p. 832-44.

248.   Nunes-Hasler, P., M. Kaba, and N. Demaurex, *Molecular Mechanisms of Calcium Signaling During Phagocytosis.* Adv Exp Med Biol, 2020. **1246**: p. 103-128.

249.   Jung, U., et al., *Velocity differences between L- and P-selectin-dependent neutrophil rolling in venules of mouse cremaster muscle in vivo.* Am J Physiol, 1996. **271**(6 Pt 2): p. H2740-7.

250.   Newton, R.A. and N. Hogg, *The Human S100 Protein MRP-14 Is a Novel Activator of the β2 Integrin Mac-1 on Neutrophils1.* The Journal of Immunology, 1998. **160**(3): p. 1427-1435.

251.   Bouma, G., et al., *Increased serum levels of MRP-8/14 in type 1 diabetes induce an increased expression of CD11b and an enhanced adhesion of circulating monocytes to fibronectin.* Diabetes, 2004. **53**(8): p. 1979-86.

252.   Russo, A., et al., *Alarming and Calming: Opposing Roles of S100A8/S100A9 Dimers and Tetramers on Monocytes.* Advanced Science, 2022. **9**(36): p. 2201505.

253.   Bromberger, T., et al., *Direct Rap1/Talin1 interaction regulates platelet and neutrophil integrin activity in mice.* Blood, 2018. **132**(26): p. 2754-2762.

254.   Ina, R., et al., *Src family kinase-mediated vesicle trafficking is critical for neutrophil basement membrane penetration.* Haematologica, 2020. **105**(7): p. 1845-1856.

255.   Etzioni, A., *Adhesion Molecules-Their Role in Health and Disease.* Pediatric Research, 1996. **39**(2): p. 191-198.

256.   Giagulli, C., et al., *The Src family kinases Hck and Fgr are dispensable for inside-out, chemoattractant-induced signaling regulating beta 2 integrin affinity and valency in neutrophils, but are required for beta 2 integrin-mediated outside-in signaling involved in sustained adhesion.* J Immunol, 2006. **177**(1): p. 604-11.

257.   Lum, A.F.H., et al., *Dynamic Regulation of LFA-1 Activation and Neutrophil Arrest on Intercellular Adhesion Molecule 1 (ICAM-1) in Shear Flow*.* Journal of Biological Chemistry, 2002. **277**(23): p. 20660-20670.

258.   Piccardoni, P., et al., *SRC-dependent outside-in signalling is a key step in the process of autoregulation of beta2 integrins in polymorphonuclear cells.* Biochem J, 2004. **380**(Pt 1): p. 57-65.

259.   Phillipson , M., et al., *Intraluminal crawling of neutrophils to emigration sites: a molecularly distinct process from adhesion in the recruitment cascade.* Journal of Experimental Medicine, 2006. **203**(12): p. 2569-2575.

260.   Park, E.J., et al., *Distinct roles for LFA-1 affinity regulation during T-cell adhesion, diapedesis, and interstitial migration in lymph nodes.* Blood, 2010. **115**(8): p. 1572-1581.

261.   Christensen, J.E., et al., *CD11b expression as a marker to distinguish between recently activated effector CD8+ T cells and memory cells.* International Immunology, 2001. **13**(4): p. 593-600.

262.   Sumagin, R., et al., *LFA-1 and Mac-1 define characteristically different intralumenal crawling and emigration patterns for monocytes and neutrophils in situ.* J Immunol, 2010. **185**(11): p. 7057-66.

263.   Hornung, A., et al., *A Bistable Mechanism Mediated by Integrins Controls Mechanotaxis of Leukocytes.* Biophys J, 2020. **118**(3): p. 565-577.

264.   Vadillo, E., et al., *Intermittent rolling is a defect of the extravasation cascade caused by Myosin1e-deficiency in neutrophils.* Proc Natl Acad Sci U S A, 2019. **116**(52): p. 26752-26758.

265. Moser, M., et al., *Kindlin-3 is required for beta2 integrin-mediated leukocyte adhesion to endothelial cells.* Nat Med, 2009. **15**(3): p. 300-5.

266. Friedl, P., S. Borgmann, and E.-B. Bröcker, *Amoeboid leukocyte crawling through extracellular matrix: lessons from the Dictyostelium paradigm of cell movement.* Journal of Leukocyte Biology, 2001. **70**(4): p. 491-509.

267. Lu, F., et al., *Mechanism of integrin activation by talin and its cooperation with kindlin.* Nature Communications, 2022. **13**(1): p. 2362.

268. Fuortes, M., et al., *Role of the tyrosine kinase pyk2 in the integrin-dependent activation of human neutrophils by TNF.* J Clin Invest, 1999. **104**(3): p. 327-35.

269. Mitchell, M.J. and M.R. King, *Shear-induced resistance to neutrophil activation via the formyl peptide receptor.* Biophys J, 2012. **102**(8): p. 1804-14.

270. Schreiber, T.H., et al., *Shear flow-dependent integration of apical and subendothelial chemokines in T-cell transmigration: implications for locomotion and the multistep paradigm.* Blood, 2007. **109**(4): p. 1381-6.

271. Yang, Y., et al., *Improved calcium sensor GCaMP-X overcomes the calcium channel perturbations induced by the calmodulin in GCaMP.* Nature Communications, 2018. **9**(1): p. 1504.

272. Sagolla, K., H.-G. Löhmannsröben, and C. Hille, *Time-resolved fluorescence microscopy for quantitative Ca2+ imaging in living cells.* Analytical and Bioanalytical Chemistry, 2013. **405**(26): p. 8525-8537.

273. Schaff, U.Y., et al., *Orai1 regulates intracellular calcium, arrest, and shape polarization during neutrophil recruitment in shear flow.* Blood, 2010. **115**(3): p. 657-666.

274. Lakschevitz, F.S., et al., *Neutrophil transcriptional profile changes during transit from bone marrow to sites of inflammation.* Cellular & Molecular Immunology, 2015. **12**(1): p. 53-65.

275. Cassatella, M.A., *Neutrophil-Derived Proteins: Selling Cytokines by the Pound*, in *Advances in Immunology*, F.J. Dixon, Editor. 1999, Academic Press. p. 369-509.

276. Cassatella, M.A., et al., *Interleukin-12 production by human polymorphonuclear leukocytes.* European Journal of Immunology, 1995. **25**(1): p. 1-5.

277. Romagnani, S., *Lymphokine Production by Human T Cells in Disease States.* Annual Review of Immunology, 1994. **12**(1): p. 227-257.

278. Ma, H., et al., *γCaMKII Shuttles Ca2+/CaM to the Nucleus to Trigger CREB Phosphorylation and Gene Expression.* Cell, 2014. **159**(2): p. 281-294.

279. Chen, J., et al., *CREB1-driven CXCR4hi neutrophils promote skin inflammation in mouse models and human patients.* Nature Communications, 2023. **14**(1): p. 5894.

280. Mayer, T.Z., et al., *The p38-MSK1 signaling cascade influences cytokine production through CREB and C/EBP factors in human neutrophils.* J Immunol, 2013. **191**(8): p. 4299-307.

281. Xu, N., M. Hossain, and L. Liu, *Pharmacological Inhibition of p38 Mitogen-Activated Protein Kinases Affects KC/CXCL1-Induced Intraluminal Crawling, Transendothelial Migration, and Chemotaxis of Neutrophils <i>In Vivo</i>.* Mediators of Inflammation, 2013. **2013**: p. 290565.

282. Nunes, P. and N. Demaurex, *The role of calcium signaling in phagocytosis.* J Leukoc Biol, 2010. **88**(1): p. 57-68.

7. Appendix

7.1 Results from collaboration partners

7.1.1 Intracellular MRP8/14 induce LFA-1 spatial aggregation in crawling neutrophils

To test whether intracellular MRP8/14 influences also LFA-1 nanocluster spatial disposition and arrangement, other than affecting LFA-1 nanocluster number, semi-automatic analysis with a custom-made pipeline was conducted on previously generated movies of *Lyz2 GCaMP5* and *Mrp14$^{-/-}$ Lyz2 GCaMP5* crawling neutrophils. To do that, Ripley's K statistics was calculated to assess random, dispersed or clustered distribution of LFA-1 nanoclusters in crawling cells (Fig. A.1-A). *Lyz2 GCaMP5* neutrophils showed higher LFA-1 cluster spatial aggregation as compared to *Mrp14$^{-/-}$ Lyz2 GCaMP5* neutrophils (Fig. A.1-B and A.1-C).
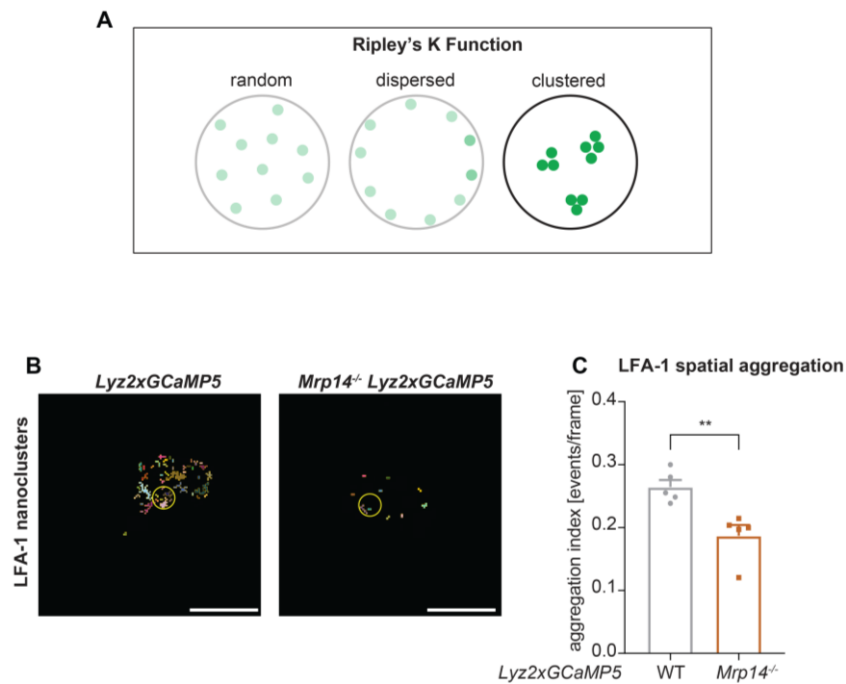
Figure 7.1.: Intracellular MRP8/14 induce LFA-1 spatial aggregation in crawling neutrophils. (**A**) Schematic representation of the Ripley's K statistics used to assess LFA-1 nanocluster spatial distribution. (**B**) Representative pictures of segmented LFA-1 nanoclusters in *Lyz2 GCaMP5* and *Mrp14$^{-/-}$ Lyz2 GCaMP5* neutrophils while crawling in E-selectin, ICAM-1, and CXCL1 coated flow chambers and (**C**) analysis of the LFA-1 spatial aggregation. [mean±SEM, *n*=5 mice per group, 56 (WT) and 54 (*Mrp14$^{-/-}$*) neutrophils, unpaired *t* test]. The results were obtained in collaboration with C. Marr and V. Lupperger from the Helmholtz Center, AI for Health, LMU Munich, Germany.

7.1.2 MRP8/14 deficiency leads to higher frequency but shorter duration of Ca^{2+} signals

To investigate a putative role for intracellular MRP8/14 in Ca^{2+} signaling regulation in the neutrophil cytosolic compartment, we studied Ca^{2+} signal frequencies. Semi-automatic single cell analysis with a custom-made pipeline was on previously generated movies of *Lyz2 GCaMP5* and *Mrp14$^{-/-}$ Lyz2 GCaMP5* crawling neutrophils. When frequency distribution was analyzed (Fig. A.2-A) we could detect higher frequencies in MRP8/14 deficient neutrophils (Fig. A.2-B). However, analyzing the distribution of the Ca^{2+} events (Fig. A.2-C) we observed shorter Ca^{2+} signals in the absence of MRP8/14 (Fig. A.2-D).
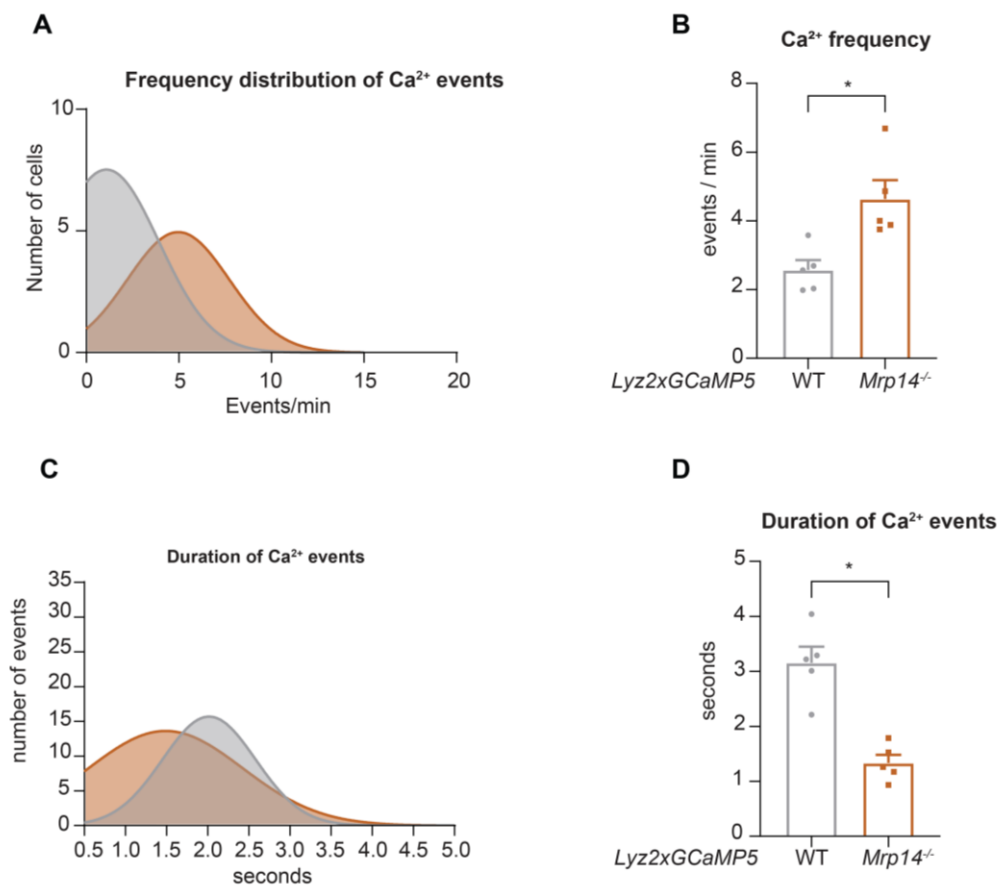
Figure 7.2.: MRP8/14 deficiency leads to higher frequency but shorter duration of Ca2+ signals. (**A**) Frequency distribution of Ca^{2+} events in *Lyz2 GCaMP5* and *Mrp14$^{-/-}$ Lyz2 GCaMP5* neutrophils while crawling in E-selectin, ICAM-1, and CXCL1 coated flow chambers and (**B**) analysis of the Ca^{2+} events/min [mean±SEM, *n*=5 mice per group, 56 (WT) and 54 (*Mrp14$^{-/-}$*) neutrophils, unpaired *t* test]. (**C**) Frequency distribution of Ca^{2+} event duration in *Lyz2 GCaMP5* and *Mrp14$^{-/-}$ Lyz2 GCaMP5* neutrophils while crawling in E-selectin, ICAM-1, and CXCL1 coated flow chambers and (**D**) analysis the Ca^{2+} event duration [mean±SEM, *n*=5 mice per group, 56 (WT) and 54 (*Mrp14$^{-/-}$*) neutrophils, unpaired *t* test]. The results were obtained in collaboration with M.S. Rupnik and J. Pfabe from the Medical University of Vienna, Wien, Austria.

Affidavit

Affidavit

Napoli, Matteo
_____
Surname, first name

Grosshaderner Strasse 9
_____
Street

82152, Munich, Germany
_____
Zip code, town, country

I hereby declare, that the submitted thesis entitled:

Myeloid-related protein 8/14 (MRP8/14) coordinates neutrophil recruitment through Ca^{2+} supply at LFA-1/F-actin adhesion clusters

is my own work. I have only used the sources indicated and have not made unauthorised use of services of a third party. Where the work of others has been quoted or reproduced, the source is always given.

I further declare that the dissertation presented here has not been submitted in the same or similar form to any other institution for the purpose of obtaining an academic degree.

Munich, 13/11/2023   Matteo Napoli
_____
place, date   Signature doctoral candidate

Confirmation of congruency

Confirmation of congruency between printed and electronic version of the doctoral thesis

Napoli, Matteo
_____
Surname, first name

Grosshaderner Strasse 9
_____
Street

82152, Munich, Germany
_____
Zip code, town, country

I hereby declare, that the submitted thesis entitled:

Myeloid-related protein 8/14 (MRP8/14) coordinates neutrophil recruitment through Ca^{2+} supply at LFA-1/F-actin adhesion clusters

is congruent with the printed version both in content and format.

Munich, 13/11/2023   Matteo Napoli
_____
place, date   Signature doctoral candidate

Publications

1. Pruenster Monika, Immler Roland, Roth Jonas, Kuchler Timon, Bromberger Thomas, Napoli Matteo, Nussbaumer Katrin, Rohwedder Ina, Wackerbarth Lou Martha, Piantoni Chiara, Hennis Konstantin, Fink Diana, Kallabis Sebastian, Schroll Tobias, Masgrau-Alsina Sergi, Budke Agnes, Liu Wang, Vestweber Dietmar, Wahl-Schott Christian, Roth Johannes, Meissner Felix, Moser Markus, Vogl Thomas, Hornung Veit, Broz Petr and Sperandio Markus. **E-selectin-mediated rapid NLRP3 inflammasome activation regulates S100A8/A9 release from neutrophils via transient gasdermin D pore formation**. Nat Immunol. 2023 Oct 30. doi: 10.1038/s41590-023-01656-1. Online ahead of print.

2. Aikaterini Gatsiou, Simon Tual-Chalot, Matteo Napoli, Almudena Ortega-Gomez, Tommy Regen, Rachit Badolia, Valeriana Cesarini, Claudia Garcia-Gonzalez, Raphael Chevre, Giorgia Ciliberti, Carlos Silvestre-Roig, Maurizio Martini, Jedrzej Hoffmann, Rana Hamouche, Joseph R Visker, Nikolaos Diakos, Astrid Wietelmann, Domenico Alessandro Silvestris, Georgios Georgiopoulos, Ali Moshfegh, Andre Schneider, Wei Chen, Stefan Guenther, Johannes Backs, Shin Kwak, Craig H Selzman, Kimon Stamatelopoulos, Stefan Rose-John, Christian Trautwein, Ioakim Spyridopoulos, Thomas Braun, Ari Waisman, Angela Gallo, Stavros G Drakos, Stefanie Dimmeler, Markus Sperandio, Oliver Soehnlein and Konstantinos Stellos. **The RNA editor ADAR2 promotes immune cell trafficking by enhancing endothelial responses to interleukin-6 during sterile inflammation.** Immunity. 2023 May 9;56(5):979-997.e11.doi: 10.1016/j.immuni.2023.03.021.Epub 2023 Apr 25.

3. Mehari Fitsumbirhan T., Miller Meike, Pick Robert, Bader Almke, Pekayvaz Kami, Napoli Matteo, Uhl Bernd, Reichel Christoph A., Sperandio Markus, Walzog Barbara, Schulz Christian, Massberg Steffen and Stark Konstantin. **Intravital calcium imaging in myeloid leukocytes identifies calcium frequency spectra as indicators of functional states.** Science Signaling. 26 Jul 2022, Vol 15, Issue 744, DOI: 10.1126/scisignal.abe6909

4. Qiuyue Ma, Roland Immler, Monika Pruenster, Markus Sellmayr, Chenyu Li, Albrecht von Brunn, Brigitte von Brunn, Rosina Ehmann, Roman Wölfel, Matteo Napoli, Qiubo Li, Paola Romagnani, Ralph Thomas Böttcher, Markus Sperandio, Hans-Joachim Anders and Stefanie Steiger. **Soluble uric acid inhibits β2 integrin-mediated neutrophil recruitment in innate immunity.** Blood. 2022 Jun 9;139(23):3402-3417.doi: 10.1182/blood.2021011234.

5. Roland Immler, Bärbel Lange-Sperandio, Tobias Steffen, Heike Beck, Ina Rohwedder, Jonas Roth, Matteo Napoli, Georg Hupel, Frederik Pfister, Bastian Popper, Bernd Uhl, Hanna Mannell, Christoph A Reichel, Volker Vielhauer, Jürgen Scherberich, Markus Sperandio and Monika Pruenster. **Extratubular Polymerized Uromodulin Induces Leukocyte Recruitment and Inflammation *In Vivo*.** Front Immunol. 2020 Dec 22;11:588245.doi: 10.3389/fimmu.2020.588245.eCollection 2020.